COHERENT STRUCTURES IN A BAROCLINIC ATMOSPHERE

by

PIERO MALGUZZI

B.Sc., Universita' di Bologna
(1978)

Submitted to the Department of Earth, Atmospheric and Planetary Sciences in Partial Fulfillment of the Requirements for the Degree of

DOCTOR OF PHILOSOPHY

in

METEOROLOGY

at the

MASSACHUSETTS INSTITUTE OF TECHNOLOGY

October 1984

Signature of Author _____
Center for Meteorology and Physical Oceanography
Department of Earth, Atmospheric and Planetary Sciences
October 18, 1984

Certified by _____
Paola Malanotte-Rizzoli
Thesis Supervisor

Accepted by _____
Theodore R. Madden
Chairman, Departmental Committee on Graduate Students

TABLE OF CONTENTS

COHERENT STRUCTURES IN A BAROCLINIC ATMOSPHERE

by

Piero Malguzzi

Submitted to the Department of Earth, Atmospheric and Planetary Sciences in October 18, 1984 in partial fulfillment of the requirements for the degree of Doctor of Philosophy in Meteorology.

ABSTRACT

In the present study we develop an analytical theory with solutions in the form of nonlinear, coherent structures superimposed on a mean, westerly wind. The model is the quasigeostrophic potential vorticity conservation equation in its baroclinic formulation; the mean wind profile we used is a model of the midlatitude jet stream in which we hypothesize the existence of two turning points (poleward and equatorward of the jet center) in order to confine the waves.

The coherent solution is an antisymmetric dipole with the anti-cyclone north of the cyclone, has an equivalent barotropic vertical structure, is meridionally as well as zonally trapped and obeys a nonlinear dynamics in the zonal wave guide. This pattern, even though idealized, exhibits a strong similarity and is consistent with observations of some Atlantic blocking patterns.

We present two derivations of the same solution. In the first derivation we specify the functional relationship between potential vorticity and streamfunction; the coherent structure is then found in the asymptotic limit of weak amplitude and weak dispersion (Long, 1964). In the second formulation we project the streamfunction onto the basis defined by the linear problem and, by suitably truncating the dynamical system obtained, an identical solution is recovered.

The validity of the truncation and the robustness of the coherent

structure to superimposed perturbations is assessed by numerical experiments. We find that the typical persistence time of our solution is, in realistic conditions, 10-to-12 days.

In order to determine the effects of transient eddies on the blocked pattern, the nonlinear interaction between a transient eddy and the vortex pair is analyzed, the underlying idea being that there exists an eddy vorticity forcing which tends to maintain the block against dissipation (Green, 1976). We find that short-scale eddies steepen the vortex-pair and push it westward. The effect of the forcing is parameterized in terms of the mean state. Numerical experiments and real data (Illari, 1982) are found to be consistent with our theoretical analysis.

We study the way coherent structures form in our model. Provided that the zonal wind field satisfies the above mentioned requirements, the pre-existence of a wave component with wavenumber one antisymmetric in the north-south direction with a large enough amplitude is a necessary and sufficient condition which leads to blocked configurations.

Finally, we give the physical interpretation of the important nonlinearity and we discuss the applicability of this theory to the real atmosphere.

Thesis Supervisor: Dr. Paola Malanotte Rizzoli
Assistant Professor
Center for Meteorology and Physical Oceanography

Acknowledgments

This research was carried out with the support of the National Science Foundation under Grant OCE-8118473.

I wish to thank Professors G. R. Flierl and P. Stone of the Massachusetts Institute of Technology and Professor Raymond Pierrehumbert of the Geophysical Fluid Dynamics Laboratory, Princeton University, for helpful discussions; in particular my advisor, Prof. Paola Malanotte-Rizzoli, was supportive of my efforts, providing also useful criticism.

My thanks also to Ms. Isabelle Kole for drafting the figures and to Joel Sloman for typing the manuscript.

Finally my friends, and especially Maribel Raventos to whom this thesis is dedicated, for making my Bostonian experience more enjoyable.

Introduction

In the last decade many theoretical and numerical studies have focused on finding solitary wave and coherent solutions to mathematical models describing geophysical flows. For the purposes of the present study "solitary wave" and "coherent structure" have the same meaning although, strictly speaking, the word "soliton" also implies survival in collision experiments between two such waves (see Scott et al., 1973). With the word "coherent structure" we refer to any nonsinusoidal solution to the governing equations that maintains its shape during translation. In a dispersionless medium coherent structures can be constructed simply by superimposing linear waves. However, when the linear waves are dispersive, the coherency of the solution can be maintained only when nonlinear interactions, which lead to phase locking of waves of different wavelength, balance linear dispersion.

Previously described solitary solutions to the quasigeostrophic equations have been of two types, which can be exemplified by the works of McWilliams (1980) and Long (1964).

The first kind of solution (which are referred to as "modons"), in their simplest form, consists of a vortex pair translating with constant phase speed. They are inviscid solutions of the barotropic (or equivalent barotropic) potential vorticity conservation equation which have a discontinuity in the functional relationship potential vorticity (q)-streamfunction (ψ) at a particular radius from the modon center--say, r = a, namely:

$$\begin{cases} q = K_1^2\psi & r \geq a \\ q = K_2^2\psi & r \leq a \\ \psi = 0 & r = a \end{cases} \qquad (1)$$

Modons require no upstream meridional shear, as is clear from the first equation of (1). McWilliams (1980) suggested that certain atmospheric features typically associated with Atlantic blocking can be modelled by the "equivalent modon," a particular nonlinear solution of the equivalent barotropic model which can be found in the presence of westerly zonal winds uniform in the north-south direction but with vertical structure. Equivalent modons, however, can exist only when a parametric relationship is satisfied (eq. 22 of McWilliams). McWilliams himself pointed out that this requirement is not satisfied with observed zonal wind vertical profiles. In other words, modons are structurally unstable.

The second type of solution requires a north-south shear field far upstream and is characterized by a single valued potential vorticity-streamfunction relationship. Long (1964) studied the problem of waves superimposed on a westerly current in a β-plane channel. He considered a current slightly varying with latitude (small constant shear) and found a mathematical solution bearing a resemblance to the solitary wave of Scott-Russell. Because of the weak upstream shear, the function $q = F(\psi)$ is quadratic in ψ, thus leading to a Korteweg-DeVries equation. In Long's original paper, the solitary wave was elongated in the x direction and the nonlinearity was weak. The assumption of weak nonlinearity was

dictated by reasons of mathematical convenience rather than physical realism; the long wave assumption was consequently needed if nonlinearity were to balance east-west dispersion. Up to now, to the author's knowledge, all solitary waves in geophysical flows have been derived within such limit.

The relevance of these ideas for geophysical flows relies, in part, on the supposition that in the atmosphere and in the oceans there exist localized features whose persistence and coherence calls for special explanations. Although it is easy to find examples of persistent features in oceans or in other planetary atmospheres (e.g., Jupiter's red spot), it is still a matter of debate whether atmospheric blocking, in general, shows unusual persistence.

However, sometimes blocking episodes are associated with typical patterns which show a marked local character. In particular, at least some blocking events consist of a vortex pair embedded in westerly winds. Examples are shown in Figure 1; the synoptic structure of these cases generally satisfies Rex's (1950,a) definition of blocking. According to Rex "a blocking case must exhibit the following characteristics:

a) the basic westerly current must split into two branches;

b) each branch current must transport an appreciable mass;

c) the double jet system must extend over at least 45° of longitude;

d) a sharp transition from zonal type flow upstream to meridional type downstream must be observed across the current split;

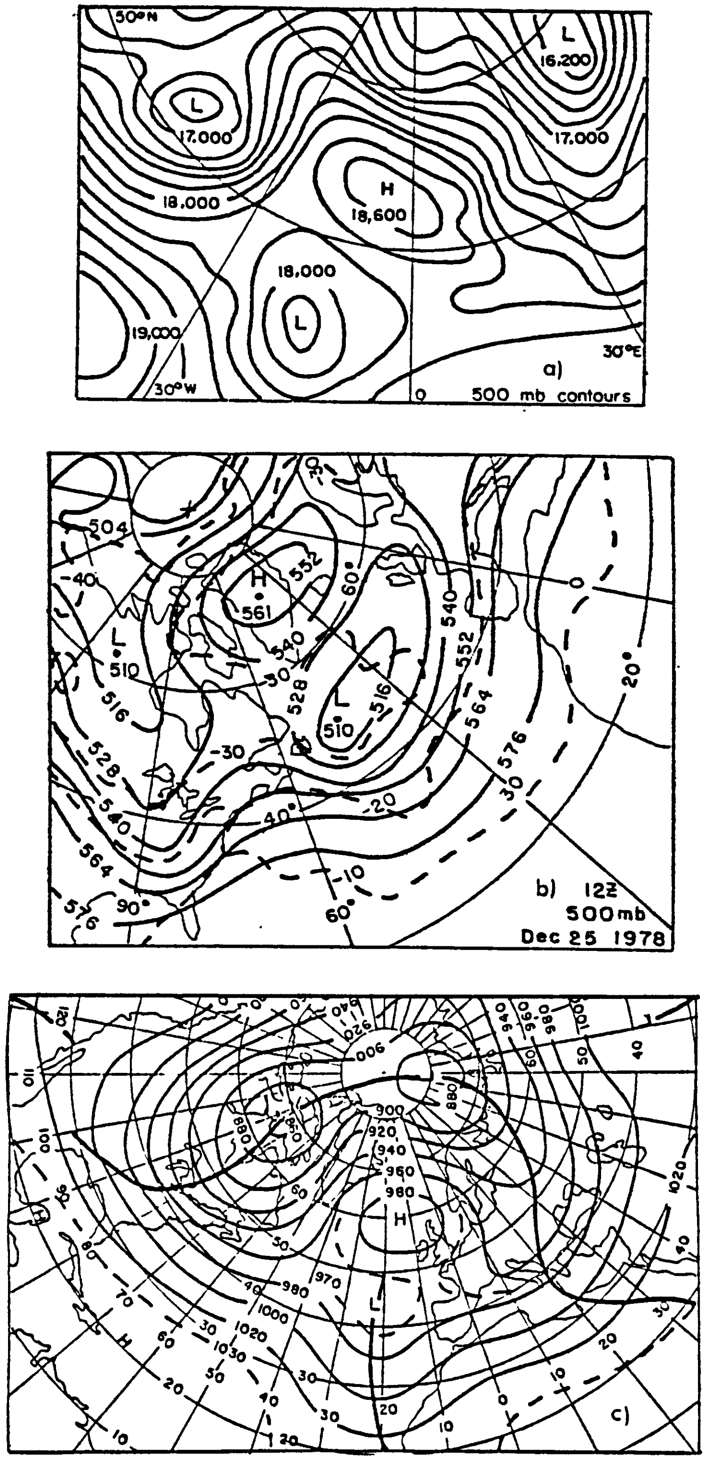
50°N
L
16,200
L
17,000
17,000
H
18,600
18,000
18,000
L
19,000
30°W
30°E
a)
0
500 mb contours
504
-40
H
561
552
60°
L
510
516
528
540
-30
L
510
516
540
552
564
576
30
-20
40°
564
576
90°
-10
60°
0
20°
b) 12Z
500mb
Dec 25 1978
900
920
940
960
980
H
970
980
1000
1020
L
1020
c)

Fig. 1

e) the pattern must persist with recognisable continuity for at least ten days."

Figure 1,a (after Sumner, 1954) is the 500 mb height contour observed during an Atlantic blocking case; Figure 1,b (after Hansen and Chen, 1982) is the 500 mb contour at 12Z of the 25 Dec. 1978 and Figure 1,c (after O'Conner, 1963) depicts the January 1963 average of the 700 mb geopotential height. In the cases shown the westerly current splits into two branches, each carrying a comparable amount of mass. The extension of the region interested by the split is very large, of the order of 60° of longitude or more. This particular kind of pattern is often observed over the eastern part of the Atlantic Ocean while it is less frequently observed over the Pacific Ocean.

In the present study the possibility that persistent patterns of the type shown in Figure 1 can be modelled by localized, coherent structures is explored again.

In Chapter I we look for localized solutions of the quasigeostrophic potential vorticity conservation equation in its inviscid and stationary formulation. It is shown that, in the long-wave and weakly nonlinear limit, solutions exist consisting of an isolated vortex pair, with the high center north of the low center, embedded in westerly zonal winds having vertical as well as horizontal shear.

In Chapter II the full time-dependent problem is analyzed by using a technique of truncated, orthonormal projection. The coherent structure found in Chapter I is now recovered by solving a severely truncated dynamical system. Because of the mathematical

approximations involved, this technique turns out to be more powerful than asymptotic expansion in the particular case at hand, since it permits us to treat the fully time-dependent and fully nonlinear case.

In Chapter III we show that the results obtained in Chapter II are not affected by the severe truncation employed. Also, by means of numerical experiments, we investigate the robustness of the coherent structure (in a baroclinically unstable environment) to superimposed perturbations. We find that the typical predictability time for our solution is 10 to 12 days.

In Chapter IV we introduce dissipation in the model. Since the coherent structure under consideration is an inviscid solution, any kind of friction will dissipate it. However, it is well know that short-scale transient eddies have a positive feedback on a split-flow (Hoskins et.al., 1983) in the sense that eddy flux of potential vorticity tends to maintain it against dissipation. The study of the interaction between a vortex pair and a monochromatic transient eddy shows that the latter tends to steepen the former,pushing it westward at the same time. The mechanism of eddy forcing is explained in terms of quasigeostrophic turbulence. In fact, the split flow, by stretching the eddy field, induces a cascade of enstrophy towards smaller scales which, in the quasigeostrophic dynamics, must be associated with an energy flux towards longer scales (Shutts, 1983). These characteristics are confirmed by numerical experiments.

Finally, in Chapter V, we show how, in our truncated model, the coherent structure form. We find that the pre-existence of a large amplitude wave component with wavenumber one antisymmetric in the north-south direction and trapped in the zonal wave guide defined by the turning points of the mean, zonal wind is a necessary and sufficient condition for the establishment of this blocking pattern. Also, the effect of nonlinearity upon different zonal scales is assessed.

Chapter I

Weakly Nonlinear Limit

Section (I,a). The model

Let us consider stationary flows governed by the quasi-geostrophic potential vorticity conservation equation in $z = H_0 \log (p_0/p)$ coordinates with H_0 the density height scale (Holton, 1972)

$$J(\psi,q) = 0 \qquad (I,1)$$

where $J(\ ,\ )$ is the Jacobian operator. The streamfunction ψ is decomposed into a zonal mean and a deviation from it:

$$\psi = \overline{\psi}(y,z) + \psi'(x,y,z) \qquad (I,2,a)$$

where

$$\lim_{|x|\to\infty} \psi' = 0 \qquad (I,2,b)$$

From now on, an overbar will denote zonal average and the prime the

deviation from it. In a finite domain of length L_x, the zonal mean would be defined as:

$$\overline{\psi} = 1/L_x \int_0^{L_x} \psi(x,y,z)dx \qquad (I,2,c)$$

Similarly, in dimensionless units (x and y scaled by the Rossby deformation radius L_r; z scaled by H_0), the potential vorticity is:

$$q = \overline{q} + q'$$
$$q' = \nabla^2\psi' + \psi'_{zz} - \psi'_z$$

where $\overline{q}$ corresponds to the upstream zonal wind $\overline{u} = \overline{u}(y,z) = -\overline{\psi}_y$ ($\overline{u} > 0$) and is given by:

$$\overline{q} = \overline{\psi}_{yy} + \overline{\psi}_{zz} - \overline{\psi}_z + \beta y$$

Subscripts denote partial derivatives and the Brunt-Väisälä frequency is assumed constant.

The general solution of equation (I,1) can be written in the form $q = F(\psi)$ where F is assumed to be an analytic function. A weakly nonlinear theory leading to permanent form

solutions is based upon the assumption that nonlinearity is a higher order effect and is balanced by some other physical process, in the present case dispersion (P. Malanotte-Rizzoli, 1982). There are two cases in which nonlinearity can be considered a higher order effect (see, for instance, Flierl, 1979):

a) the deviation ψ' from the mean flow is weak: $\psi' \ll 1$;

b) The mean flow has a weak meridional shear.

Cases (a) and (b) correspond to different expansions of the functional F in power series of its argument and we shall treat them separately.

Case a: $\psi' \ll 1$

Expanding F in power series around $\overline{\psi}$:

$$q = \overline{q} + q' = F(\overline{\psi} + \psi') = F(\overline{\psi}) + \frac{dF(\overline{\psi})}{d\overline{\psi}}\psi' + \frac{1}{2}\frac{d^2F(\overline{\psi})}{d\overline{\psi}^2}(\psi')^2 + \ldots \qquad (I,3)$$

The upstream boundary condition (I,2,b) implies:

$$\overline{q} = F(\overline{\psi}) \qquad (I,4)$$

and (I,3) becomes:

$$q' = \sum_{n=1}^{\infty} \frac{d^nF(\overline{\psi})}{d\overline{\psi}^n}\frac{(\psi')^n}{n!} \qquad (I,5)$$

The Taylor coefficients of F can be deduced by taking the y-derivative of both sides of (I,4):

$$\bar{q}_y = \frac{dF}{d\bar{\psi}} \bar{\psi}_y = -\bar{u} \frac{dF}{d\bar{\psi}}$$

so that

$$\frac{dF}{d\bar{\psi}} = -\frac{\bar{q}_y}{\bar{u}} = -\frac{\beta - \bar{u}_{yy} - \bar{u}_{zz} + \bar{u}_z}{\bar{u}} \qquad (I,6)$$

$\beta = \beta^* L_r^2/u_0$ is the dimensionless beta-parameter if β^* is the dimensional beta and u_0 the velocity scale, which will be set equal to the maximum wind speed of the $\bar{u}$ profile. Further differentiation of (I,6) with respect to y gives:

$$\frac{d^2F}{d\bar{\psi}^2} = -\frac{1}{\bar{u}} \frac{\partial}{\partial y} \left(\frac{1}{\bar{u}} \bar{q}_y\right)$$

$$\frac{d^nF}{d\bar{\psi}^n} = -\frac{1}{\bar{u}} \frac{\partial}{\partial y} \left(\frac{d^{n-1}F}{d\bar{\psi}^{n-1}}\right) = (-1)^n \left[\frac{1}{\bar{u}} \frac{\partial}{\partial y}\right] \cdots \left[\frac{1}{\bar{u}} \frac{\partial}{\partial y}\right] \bar{q}$$

Notice that $\frac{d^nF}{d\bar{\psi}^n}$ is zero for all $n > 1$ when the mean wind is a function of z alone.

Case b: Weak meridional shear.

Consider the following wind profile:

$$\bar{\psi} = -u(z)y + \varepsilon \bar{\psi}_1(y,z); \qquad \varepsilon \ll 1$$

From

$$\bar{q} = \bar{\psi}_{yy} + \bar{\psi}_{zz} - \bar{\psi}_z + \beta y = F(\bar{\psi}) = \sum_n a_n \bar{\psi}^n$$

with the previous wind profile one gets:

$$(\beta - u_{zz} + u_z)y + \varepsilon(\bar{\psi}_{1yy} + \bar{\psi}_{1zz} - \bar{\psi}_{1z}) = \Sigma\, a_n(-u(z)y + \varepsilon\bar{\psi}_1)^n$$

Once $\bar{\psi}_1$ has been specified, the coefficients a_n's can be evaluated by equating equal powers of y on both sides of the previous relation. If $\bar{\psi}_1 = y^3$ (weak parabolic shear) it is easy to show that $a_{2n+1} \approx \varepsilon^n$ and $a_{2n} = 0$. Thus, if $\bar{\psi}_1 = y^3$ and $\varepsilon \ll 1$:

$$q = F(\bar{\psi} + \psi') = a_1(\bar{\psi} + \psi') + \varepsilon a_3(\bar{\psi} + \psi')^3 + O(\varepsilon^2) \qquad (I,7)$$

The expansion leading to equation (I,7) is valid in the region where $\varepsilon y^2 \leq 1$.

Equations (I,5) and (I,7) clearly show that nonlinearity is an $O(\varepsilon)$ effect, ε being the weak amplitude of the perturbation ψ' [case (a)] or the weak shear of the mean flow [case (b)]. Cases (a) and (b) are the only cases for which a weak nonlinear theory can be formulated leading to coherent, localized analytic solutions. These are found solving the $O(\varepsilon)$ nonlinear problem and balancing nonlinearity with dispersion. The procedure to find the nonlinear solutions is completely analogous for cases (a) and (b). In the next section however we shall focus on case (a) as the one allowing use of realistic wind profiles.

It must be pointed out that the above approach is not valid in regions (if any) where the circulation is closed. In these regions, the functional relationship $q = F(\psi)$ need not be the same as determined from the upstream boundary condition. If $F(\psi)$ is

multi-valued, along each closed streamline $F(\psi)$ can be found from a balance between dissipation and vorticity sources (Pierrehumbert and Malguzzi, 1983). However, in a purely inviscid theory no information is available about the potential vorticity of such a closed streamline. Equations (I,5) [or (I,8)] are therefore assumed to be valid all over the domain, excluding the possibility for $F(\psi)$ to be multi-valued.

Section (I,b). The nonlinear problem

In this section we solve the nonlinear problem and find coherent, localized solutions for case (a) or Section 2. Case (a) in fact allows for the choice of mean wind profiles with a realistic horizontal shear. The mean wind profile chosen to model the mid-latitude jet stream is given by:

$$\overline{u}(y,z) = U(y)Z(z) \qquad (I,8,a)$$

with

$$U(y) = 1 - 2(1 - U_0)\frac{y^2}{y_0^2} + (1 - U_0)\frac{y^4}{y_0^4} \qquad (I,8,b)$$

where $2y_0$ is the overall width of the jet and U_0 the minimum of the wind speed. The meridional profile U(y) is shown in Fig.(I,1,a). Expression (I,8,b) is the Taylor series representation of a symmetric jet truncated after the fifth power of y. The requirements that the mean wind profile must satisfy will be discussed later. The vertical profile Z(z) is shown in Fig.(I,1,b). It was constructed point by point and is meant to model a characteristic mean profile observed at mid-latitudes. The numerical values chosen for the parameters will be discussed in the next section.

We seek solutions which are meridionally trapped in the zonal wave-guide defined by the two turning points of the U(y) profile. The solutions will be therefore insensitive to the details of the mean wind outside the interior jet region of width $2y_0$. The solutions are also vertically trapped as analogous considerations can be made for the vertical mean profile of Fig.(I,1,b). The problem is the two-dimensional, and weakly nonlinear, extension of the linear problem treated by Tung and Lindzen (1979b). Equation (I,5) of section (I,a) is the nonlinear model

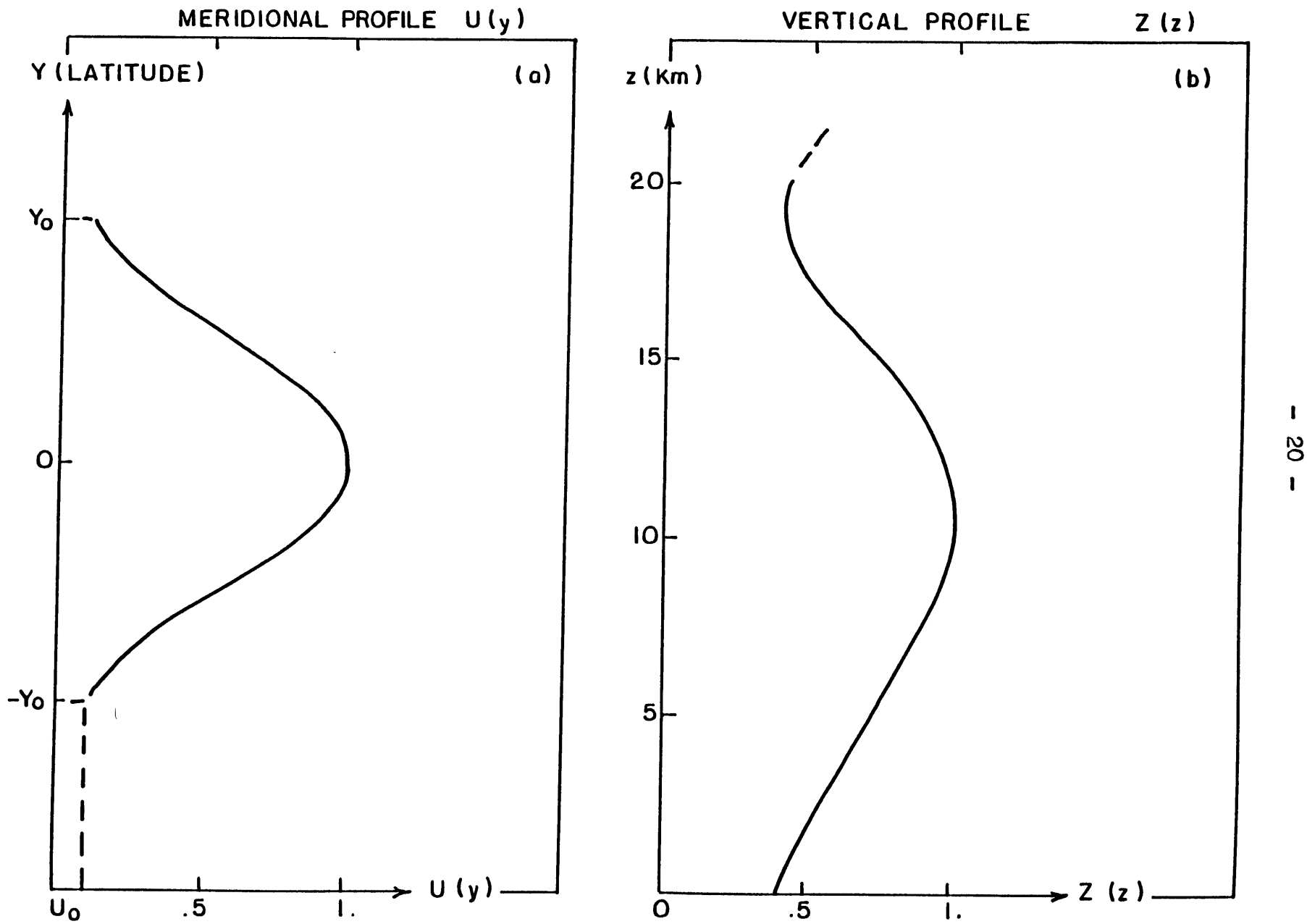
MERIDIONAL PROFILE U(y)
Y (LATITUDE)
(a)
Yo
0
-Yo
Uo
.5
1.
U (y)
VERTICAL PROFILE
Z (z)
z (Km)
(b)
20
15
10
5
0
.5
1.
Z (z)

Fig. (1,1)

for the case of finite horizontal shear in the zonal wind profile. From the results of Section (I,a), equation (I,5) can be written as:

$$\psi'_{xx} + \psi'_{yy} + \psi'_{zz} - \psi'_{z} = -\bar{q}_y\psi'/\bar{u} - [\partial_y(-\bar{q}_y/\bar{u})\psi'^2/2]/\bar{u} \qquad (I,9)$$
$$+O(\psi'^3)$$

As $\psi' \ll 1$, it is convenient to perform the substitution $\psi' \to \varepsilon\psi^* e^{z/2}$ with $\varepsilon \ll 1$ and $\psi^* = O(1)$. Then (I,9) becomes:

$$\psi^*_{xx} + \psi^*_{yy} + \psi^*_{zz} - V\psi^* = \frac{\varepsilon}{2} e^{z/2} \frac{1}{\bar{u}} \frac{\partial}{\partial y} (\frac{1}{\bar{u}} \bar{q}_y)\psi^{*2} + O(\varepsilon^2) \qquad (I,10)$$

where

$$V(y,z) = \frac{1}{4} - \frac{\bar{q}_y}{\bar{u}} = \frac{1}{4} - \frac{\beta - \bar{u}_{yy} - \bar{u}_{zz} + \bar{u}_z}{\bar{u}} \qquad (I,11)$$

The boundary conditions for equation (I,10) are: $\psi^*\big|_{|y|,z\to\infty} \to 0$. The lower boundary condition $w = 0$ at $z = 0$, where w is the vertical velocity, is derived in terms of ψ^* in appendix A. This is:

$$\psi^*_z = (\frac{\bar{u}_z(y,0)}{\bar{u}(y,0)} - \frac{1}{2})\psi^* \quad \text{at } z = 0 \qquad (I,12)$$

In equation (I,10) nonlinearity is an $O(\varepsilon)$ effect. We can expand ψ^* in the small parameter ε:

$$\psi^* = \psi^{(0)} + \varepsilon\,\psi^{(1)} + \ldots . \qquad (I,13)$$

and we require that east-west dispersion balances nonlinearity. The requirement for the dispersion to be $0(\varepsilon)$ is equivalent to introducing a long scale in x:

$$x = X/\sqrt{\varepsilon}, \text{ with } X = 0(1)$$

At the lowest order in ε, we would get

$$\psi_{yy}^{(0)} + \psi_{zz}^{(0)} - V\psi^{(0)} = 0$$

This is a homogeneous equation (with homogeneous boundary conditions) which is solvable only for particular choices of V or, in other words, particular choices of the basic state $\bar{u}$. Calling $V^{(0)}$ one of such functions, we can find a solution of (I,10) with weak dispersion if and only if V is "detuned" from $V^{(0)}$ by a small quantity (of order ε). Formally, the picture is identical to that encountered in a nonlinear pendulum (see Landau-Lifchitz) in which nonlinearity allows oscillation detuned from the linear frequency.

Hence, let $V = V^{(0)} + \varepsilon V^{(1)}$. The correct formulation of the zero-order problem is:

$$\psi^{(0)} = A(X)\phi(y,z)$$

$$\phi_{yy} + \phi_{zz} - V^{(0)}\phi = 0$$

There is a simple way to find $V^{(0)}$ and $V^{(1)}$. Let us consider the eigenvalue problem:

$$\phi_{yy} + \phi_{zz} - V\phi = -K\phi$$

$$\phi_z = \left(\frac{Z_z}{Z} - \frac{1}{2}\right)\phi, \quad z = 0 \qquad \text{(I,14)}$$

$$\phi \to 0 \qquad \text{as } |y|, \; z \to \infty$$

Thus, if the Schrödinger problem (I,14) has an eigenvalue of order ε [$K = \varepsilon K^{(1)}$, $K^{(1)} = O(1)$] then we may define

$$V^{(0)} = V - \varepsilon K^{(1)}$$
$$\text{(I,15)}$$
$$V^{(1)} = K^{(1)}$$

By using (I,15), the $O(\varepsilon)$ nonlinear problem is:

$$\phi A_{XX} - K^{(1)}\phi A + \psi^{(1)}_{yy} + \psi^{(1)}_{zz} - V^{(0)}\psi^{(1)} =$$

$$\frac{e^{z/2}}{2} \frac{1}{\underline{\underline{u}}} \frac{\partial}{\partial y} \left(\frac{1}{\underline{\underline{u}}} \bar{q}_y\right)\phi^2 A^2 \qquad \text{(I,16)}$$

The necessary (and sufficient) condition for the solvability of (I,16) requires multiplying (I,16) by ϕ and integrating over y and z. The contribution

$$\int_{-\infty}^{+\infty} dy \int_0^{+\infty} dz \; \phi[\psi^{(1)}{}_{yy} + \psi^{(1)}{}_{zz} - V^{(0)}\psi^{(1)}]$$

vanishes because of the zero-order eigenvalue problem (I,14) (as can be shown by integrating by parts). Thus (I,16) becomes:

$$A_{xx} - K^{(1)}A + \frac{\delta}{2} A^2 = 0 \qquad \text{(I,17)}$$

with

$$\delta = - \frac{\int_{-\infty}^{+\infty} dy \int_{0}^{+\infty} dz \; e^{z/2} \phi^3 [\frac{1}{\bar{u}} \frac{\partial}{\partial y} (\frac{1}{\bar{u}} \bar{q}_y)]}{\int_{-\infty}^{+\infty} dy \int_{0}^{+\infty} dz \; \phi^2} \qquad (I,17,a)$$

Equation (I,17) is the well-known Korteweg-de Vries (KdV) equation. When $K^{(1)}$ is positive, the solution to (I,17), localized in x, is:

$$A(X) = \frac{3K^{(1)}}{\delta} \operatorname{sech}^2 (\frac{\sqrt{K^{(1)}}}{2} X) \qquad (I,18)$$

The localized solutions given by (I,18) are long waves with north-south to east-west aspect ratio of $O(\sqrt{\varepsilon})$. It is natural to ask whether weakly nonlinear solutions can exist with x and y scales of the same magnitude. They can be found for case (b) of Section (I,a) (weak meridional shear in the mean wind profile) when the (x,y) scales are larger than the Rossby radius of deformation. In this scale range, in fact, dispersion becomes an $O(\varepsilon)$ effect. This problem was studied by Flierl (1979) assuming a small linear shear in a mean ocean current and by Malanotte-Rizzoli (1984) assuming a weak topography (equivalent to the weak shear). In this case, the zero-order problem giving the vertical structure is:

$$\phi^{(0)}_{zz}(z) + \frac{\beta - \bar{u}_{zz} + \bar{u}_z}{\bar{u}} \phi^{(0)}(z) = 0$$

where the y-dependence in the mean wind is $O(\varepsilon)$. It can be shown that the solutions to the above equation, weighted by $e^{-z/2}$, have zero vertical average. Thus, they are not suitable to represent the vertical structure of blocking (Dole,1982).

Section (I,c). Solutions on a mid-latitude jet

In Section (I,b) the weakly nonlinear problem was formally solved, leading to a coherent, localized solution given by:

$$\psi' = \frac{3K}{\delta}\phi(y,z)e^{z/2}\ \mathrm{sech}^2\left(\frac{\sqrt{K}}{2}x\right) \qquad (I,19)$$

with ϕ the eigensolution of the Schrödinger problem (I,14), K the corresponding eigenvalue and δ given by (I,17,a). For (I,19) to be a solution, $K > 0$ and $K = 0(\varepsilon)$.

In this section we evaluate the structure of the solution for the mean wind profile (I,8), shown in Fig. (I,1). The numerical values chosen for the parameters are typical of the atmosphere at mid-latitudes:

$\beta^* = 1.5 \times 10^{-11}$ sec^{-1} m^{-1} $\qquad$ $2y_0 = 5{,}500$ km

$L_r = 1{,}000$ km $\qquad$ $U_0 = 0.1$

$u_0 = 45$ m/sec

$H_0 = 8$ km

The meridional and vertical structure is given by the Schrödinger zero-order problem (I,14). (I,14) is the equation for the wave function of a quantum mechanical particle in the potential well V given by (I,11).

The structure of the V function [see Fig. (I,2)] is that of a potential well of finite depth. In general, there will be a finite number of bound states associated to eigenvalues K smaller than the limiting value given by the rim of the potential well, $K \approx 4$ in the present case. For

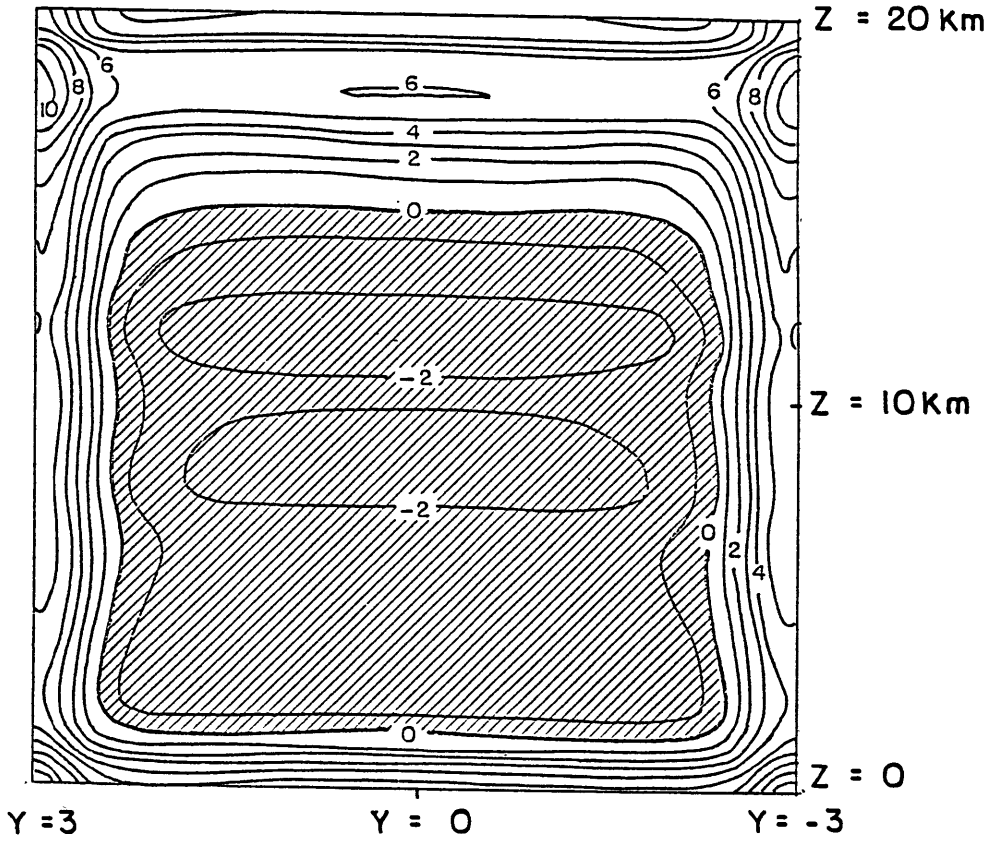

Fig. (I,2)

these bound states, the expression for K in terms of ϕ can be obtained by multiplying the Schrödinger equation (I,14) by $\bar{u}\, e^{-z/2}$, integrating over the meridional plane and using the boundary conditions on ϕ. The result is:

$$K = -\beta \frac{\int_{-\infty}^{+\infty} dy \int_{0}^{+\infty} dz [\phi e^{-z/2}]}{\int_{-\infty}^{+\infty} dy \int_{0}^{+\infty} dz [\bar{u}\phi e^{-z/2}]} \qquad \text{(I,20)}$$

In general, the eigenfunction ϕ_1 corresponding to the lowest eigenvalue K_1 has no nodal lines in both y and z. From (I,20), it follows that such eigenmode has $K = K_1 < 0$, as $\bar{u} > 0$ always and ϕ never changes sign ($\phi > 0$). Having $K_1 < 0$, the lowest bound state is not acceptable, as the solution given by (I,19) requires $K > 0$.(1) There is a further reason why the lowest bound state does not correspond to any localized structure. A general property in fact holds for localized solutions in incompressible, inviscid, stationary flows. This property states that the streamfunction weighted by the density must have zero average (Flierl et al., 1983). Only eigenmodes ϕ_n with one (or more) nodal lines in the meridional (y-z) plane can be associated with the zonal structure of the solution (I,19).

System (I,14) was solved numerically by means of an overrelaxation scheme. The eigenvalue was updated each iteration using expression (I,20). The structure of the potential well V is almost y-independent in great part of the domain. This suggests the choice of first guesses separable in y and z coordinates. Accordingly, the unidimensional eigenvalue problem

---

(1) Eigenfunctions of (I,14) with $K < 0$ give the meridional structure of linear Rossby waves with wavenumber $\sqrt{(-K)}$. Thus, they are acceptable solutions but do not correspond to a localized structure.

$$\phi_{zz} + [K - V(0,z)]\phi = 0 \qquad (I,21)$$

provides the first guess for the vertical structure, while the meridional structure is assumed sinusoidal. The unidimensional eigenvalue problem (I,21) is identical to the one analyzed by Tung and Lindzen (1979b) and can be solved with a finite difference scheme introduced by Lindzen (1971). The first guess so obtained was found to be very close to the final, relaxed solution.

The upper boundary condition in the numerical procedure, consistent with Lindzen's scheme, is the mixed Dirichlet-Von Neumann boundary condition

$$\phi_z = -[V - K]^{1/2}\phi \text{ as } z \to \infty$$

(Tung and Lindzen, 1979b, their equation 29). This ensures that the solution is in the exponentially decaying branch. This condition is accurate when V_z is small compared to V and ϕ_{yy} small compared to $V\phi$. The first requirement can be satisfied choosing the upper boundary condition at the level where V is maximum. The second approximation will introduce minor errors if the eigenmode is not too wiggled. Similar conditions and similar considerations apply laterally.

The second eigenmode ϕ_2 is the one with the desired vertical structure and corresponds to the eigenvalue $K_2 = .22$. Thus, it satisfies the requirements for the validity of (I,19). In (I,19) the coefficient δ was

evaluated numerically, using the zero-order pattern $\phi_2(y,z)$. Figure (I,3) shows the meridional structure associated to $\phi_2(y,z)$ multiplied by $e^{z/2}$. The correspondent anomaly pattern ψ', at the height of z = 5.6 km (500 mb), is shown in Figure (I,4) in dimensionless units. It is an antisymmetric dipole, with the anticyclone north of the cyclone. In dimensional units, the maximum geopotential height anomaly is $\approx$ 100 m, of the same order of magnitude as those actually observed (Dole, 1982). The pattern of Figure (I,4), even though idealized, exhibits some similarity to the blocking events of Fig. 1. Also, the vertical structure of $\phi_2 e^{z/2}$ shown in Figure (I,3) compares well with observations of atmospheric blocking (Dole, 1982).

In this chapter an attempt has been made to identify some blocking situation with stationary, nonlinear Rossby waves of localized character superimposed on a mean zonal wind with meridional and vertical shear. We have implicitly assumed that the energy is trapped in a region of horizontal and vertical finite extent and that no energy radiation occurs out of that region. These solutions are weakly nonlinear and weakly dispersive; they provide an alternative to the equivalent modon proposed by McWilliams (1980).

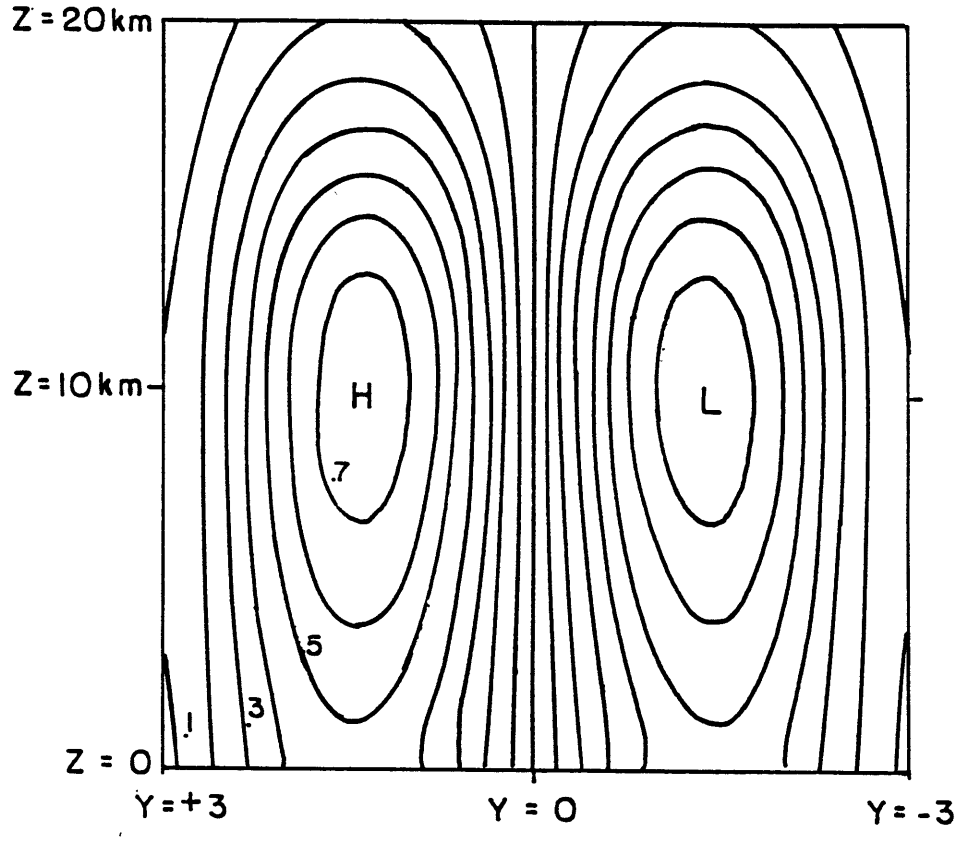

Fig. (I,3)

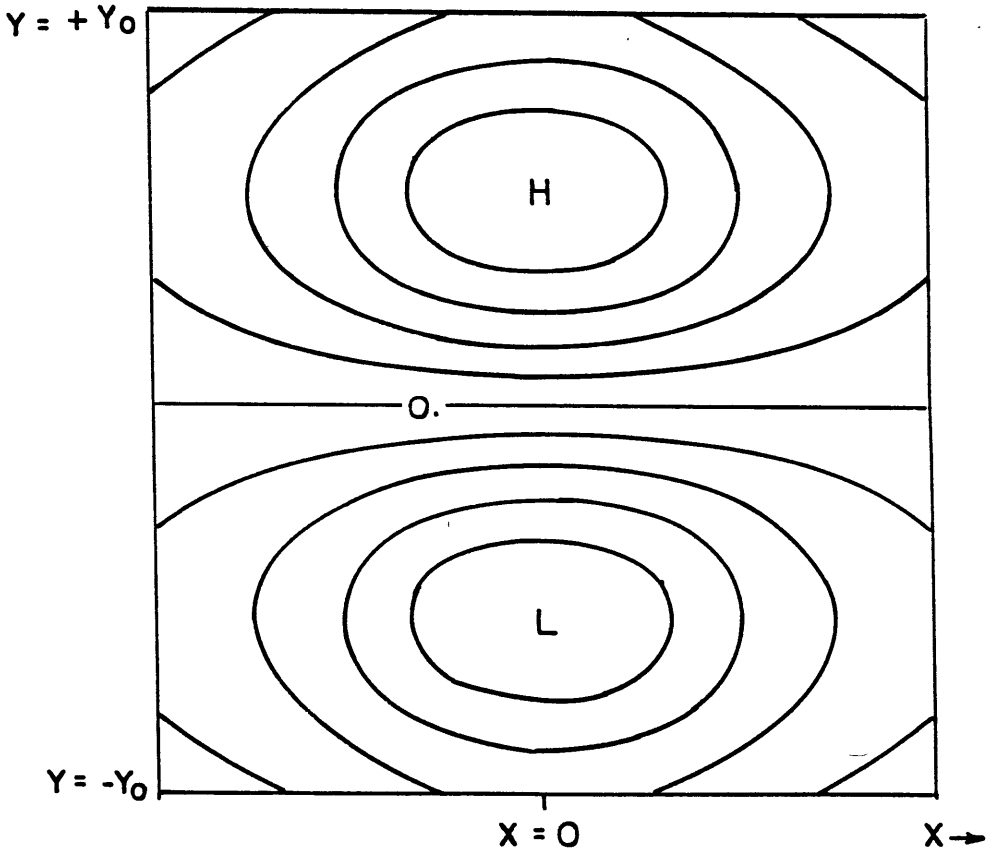

Fig. (I,4)

Chapter II

Finite Amplitude Solution

Section (II,a). Modal Model

In this chapter we study the solution described previously by using a different approach. The technique used in the previous chapter cannot be generalized to transient situations and is very difficult to extend to finite amplitude solutions. However, it turns out that, projecting the streamfunction over an appropriate set of modes and truncating after few terms, we can recover the same solution examined in the long wave limit and study its dynamics by analyzing a truncated dynamical system. It turns out that this technique is very powerful for the particular case under consideration.

We will project the streamfunction over the basis defined by the eigenfunctions of the linear problem (I,14) with $\overline{u}$ given by (I,8) and Figure (I,1).

The results of Chapter I suggest that the solutions of (I,14) form a "natural" set of eigenfunctions upon which to project the quasigeostrophic equations. Furthermore, we expect that the basis defined by (I,14) gives the best description of the particular solution we are interested in, because in the long wave, weakly nonlinear limit the meridional structure of this solution is given exactly by one of the eigenfunctions of (I,14).

Similar techniques are often used in studies about stratified oceans. In particular, Flierl (1978) has shown that in different physical situations two-mode models perform optimally if compared to two-layer models.

The eigenfunctions of the Schrödinger equation (I,14) form a complete, bidimensional set. Many of the arguments of the Sturm-Liouville theory can be carried over to the multi-dimensional case. In those cases where there is a lowest eigenvalue, where there is no upper bound for the eigenvalues, and where there is a variational equation for the eigenfunctions, the arguments set forth in the Sturm-Liouville theory can be utilized to prove that these more general eigenfunctions form a complete set which can represent any piecewise continuous function inside the boundaries in terms of a series.

The eigenfunctions of (I,14) that correspond to different eigenvalues are orthogonal. Let ϕ_m, ϕ_n denote two eigenfunctions with $K_n \neq K_m$. Then:

$$\phi_{n_{yy}} + \phi_{n_{zz}} + (K_n - V)\phi_n = 0 \qquad \text{(II,1)}$$

$$\phi_{m_{yy}} + \phi_{m_{zz}} + (K_m - V)\phi_m = 0 \qquad \text{(II,2)}$$

We multiply (II,1) by ϕ_m, (II,2) by ϕ_n and integrate over y and z after having subtracted member by member:[1]

$$\langle \phi_m(\phi_{n_{yy}} - \phi_{n_{zz}}) - \phi_n(\phi_{m_{yy}} - \phi_{m_{zz}})\rangle + (K_n - K_m)\langle \phi_n\phi_m\rangle = 0$$

Integrating by parts:

$$\langle \phi_m\phi_{n_{yy}}\rangle = [\int_0^\infty \phi_m\phi_{n_y}dz]_{-\infty}^{+\infty} - \langle \phi_{m_y}\phi_{n_y}\rangle =$$

$$= [\int_0^\infty \phi_m\phi_{n_y}dz]_{-\infty}^{+\infty} - [\int_0^\infty \phi_{m_y}\phi_n dz]_{-\infty}^{+\infty} + \langle \phi_{m_{yy}}\phi_n\rangle$$

Similarly

$$\langle \phi_m\phi_{n_{zz}}\rangle = [\int_{-\infty}^{+\infty}dy\phi_m\phi_{n_z}]_0^\infty - [\int_{-\infty}^{+\infty}dy\phi_{m_z}\phi_n]_0^\infty + \langle \phi_{m_{zz}}\phi_n\rangle$$

---

[1] From now on, the integral over y and z will be denoted by the symbol "< >".

With the assumption that ϕ_n, $\phi_m \to 0$ as $|y|$, $z \to \infty$ all the boundary terms computed at infinity vanish. The boundary terms at $z = 0$ also vanish because of (I,12) and we are left with:

$$\langle \phi_m, \phi_n \rangle = 0 \quad \text{if} \quad K_n \neq K_m \tag{II,3}$$

In general, the Schrödinger equation (I,14) has at most a finite number of bound states (K_n, $n = 1, 2, \ldots, N$) and a continuum spectrum for $K > K_N$. Since we shall truncate the representation of ψ' after the first few terms, we will neglect the continuous part of the spectrum. In other words, our model is going to describe a flow motion internally trapped in the waveguide defined by the two turning points of the mean zonal wind $\bar{u}$.

Let:

$$\psi' e^{-z/2} = A_n(x,t)\phi_n(y,z) \tag{II,4}$$

where the factor $e^{-z/2}$ has been shown explicitly for reasons of mathematical convenience. We use the convention that repeated indices are contracted when they appear in only one side of the equations. In order to close the system, the zonal wind has to be projected onto the same basis. The instantaneous zonal wind is denoted by $u(y,z,t)$. It is convenient to introduce the time deviation from the mean zonal wind $\bar{u}(y,z)$ which was used to compute the basis eigenfunctions. Let

$$u(y,z,t) = \bar{u}(y,z) + u''(y,z,t) \tag{II,5}$$

where two primes denote transient quantities. The components of u, $\overline{u}$, and u" in the basis $\{\phi_n\}$ will be denoted respectively by u_n, $\overline{u}_n$, and $u"_n$. Thus:

$$ue^{-z/2} = u_n\phi_n$$

$$\overline{u}e^{-z/2} = \overline{u}_n\phi_n$$

$$u"e^{-z/2} = u"_n\phi_n$$

$$u_n(t) = \overline{u}_n + u"_n(t) \qquad n = 1, \ldots, N$$

Note that $\overline{u}_n$ can be easily computed by multiplying (I,14) by $\overline{u}$ and subsequently integrating twice by parts. The result is

$$\overline{u}_n = -\frac{\beta}{K_n} < \phi_n e^{z/2} > \qquad \text{(II,6)}$$

The time-dependent version of the quasigeostrophic potential vorticity equation (I,1), separated off into zonal mean and deviation from it becomes:

$$\partial_t q' + J(\psi',q') + \partial_x(uq' + \overline{q}_y\psi') - \partial_y\overline{(\psi'_x q')} = 0 \qquad \text{(II,7)}$$

$$\partial_t\overline{q} = -\partial_y\overline{(\psi'_x q')} \qquad \text{(II,8)}$$

Taking the y-derivative of (II,8) we get:

$$\dot{u}_{yy} + \dot{u}_{zz} - \dot{u}_z = \partial_{yy}\overline{(\psi'_x q')} \qquad \text{(II,9)}$$

where the dot stands for time derivative. In deriving (II,9) the definition of $\overline{q}_y (= - u_{yy} - u_{zz} + u_z + \beta)$ has been used.(1)

---

(1) To avoid confusion, we stress that the zonal average is denoted by an overbar. However, we keep the symbol $\overline{u}$ to indicate the zonal wind used to compute the basis eigenfunctions.

The lower boundary condition is vertical velocity equal to zero ($\psi_z = 0$) at z =0. A vertical velocity different from zero at the bottom would be inconsistent with the lower boundary condition on ϕ_n. However, topography, Ekman friction and surface heating could be incorporated as well in the present model even if each normal mode satisfies w = 0 at z = 0; series (II,4) would still be convergent at any interior point except that at the lower boundary (Gibbs phenonemon). More details on this point can be found in Flierl (1978); throughout the present study we will stick with w = 0 at the ground.

The projection of all the terms appearing in (II,7) and (II,9) upon the basis $\{\phi_n\}$ is presented in appendix B; here we report in detail only the spectral decomposition of $\partial_x(\overline{u}q' - q_y\psi')$. From the definition of $\overline{q}_y$ and (II,5) it follows that

$$u\partial_x q' - \partial_x \overline{q}_y \psi'_n = \overline{u}\,\partial_x\left(\psi'_{xx} + \psi'_{yy} + \psi'_{zz} - \psi'_z + \frac{\beta - \overline{u}_{yy} - \overline{u}_{zz} + \overline{u}_z}{\overline{u}}\psi'\right)$$

$$+ u''\partial_x(\psi'_{xx} + \psi'_{yy} + \psi'_{zz} - \psi'_z) + \psi'_x(-u''_{yy} - u''_{zz} + u''_z)$$

Making use of (II,4) and analogous expressions for $\overline{u}$ and u", the right-hand side of the previous relation becomes:

$$e^z\,\overline{u}_n\phi_n\partial_x[A_{m_{xx}}\phi_m - K_m A_m\phi_m] + e^z u''_n\phi_n[A_{m_{xxx}}\phi_m + A_{m_x}(\phi_{m_{yy}} + \phi_{m_{zz}})]$$

$$- e^z A_{m_x}\phi_m[u''_n(\phi_{n_{yy}} + \phi_{n_{zz}})]$$

where (I,14) has been used. Using again the definition of the eigenfunctions ϕ_n and ϕ_m given by (II,1) and (II,2) we can rearrange the previous expression in the form:

$$e^z u_n \phi_n \phi_m [A_{m_{xxx}} - K_m A_{m_x}] + e^z A_{m_x} u''_n K_n \phi_n \phi_m$$

The i^{th} component in the base $\{\phi_n\}$ is then obtained by taking the scalar product with ϕ_i:

$$e^{z/2}[\varepsilon_{inm} u_n (A_{m_{xxx}} - K_m A_{m_x}) + \varepsilon_{inm} u''_n K_n A_{m_x}] \qquad \text{(II,10)}$$

where the tensor ε_{inm} is defined as

$$\varepsilon_{inm} = \langle e^{z/2} \phi_i \phi_n \phi_m \rangle \qquad \text{(II,11)}$$

ε_{imn} is a completely symmetric tensor, namely

$$\varepsilon_{inm} = \varepsilon_{imn} = \varepsilon_{mni} \qquad \text{(II,12)}$$

Equations (II,7) and (II,9), written in the basis $\{\phi_n\}$ read:

$$\dot{A}_{i_{xx}} + (\alpha_{in} - \zeta_{in})\dot{A}_n + \varepsilon_{inm} u_n (A_{m_{xxx}} - K_m A_{m_x}) + \varepsilon_{inm}(u_n - \overline{u_n}) K_n A_{m_x}$$

$$+ \gamma_{nmi}(A_n A_{m_{xxx}} - A_{m_x} A_{n_{xx}}) + \gamma_{mni} A_{n_x} A_m (K_m - K_n) + \delta_{inm} A_{n_x} A_m$$

$$+ \gamma_{inm} K_m \overline{A_{n_x} A_m} = 0 \qquad \text{(II,13)}$$

$$(\zeta_{in} - \alpha_{in})\dot{u}_n + \varepsilon'_{inm} K_n \overline{A_{n_x} A_m} = 0 \qquad \text{(II,14)}$$

(For the definitions of tensors γ, δ, ζ, α, and ε' see appendix B.)

Equations (II,13) and (II,14) will be referred to as "modal equations." They describe the time evolution of the Fourier coefficients A_n, u_n representing respectively the projection of the streamfunction

and of the zonal wind upon the normal mode ϕ_n. Equation (II,13) is a system of nonlinear, partial differential equations; it can be reduced to a dynamical system by further decomposing A_n onto an orthonormal, unidimensional basis and by suitably truncating it. The term, radically new, which is not present in other classical, normal mode decomposition is

$$\delta_{inm} A_{n_x} A_m$$

where the completely symmetric tensor δ_{inm} is defined as

$$\delta_{inm} = \langle e^{z/2} V_y \phi_i \phi_n \phi_m \rangle \qquad \text{(II,15)}$$

Basically, the tensor δ_{inm} contains all the information about the presence of the mean shear $\bar{u}(y,z)$. In particular, when $\bar{u}$ has no meridional shear, all the elements of such tensors vanish.

Before analyzing some particular stationary solutions (fixed point) of equations (II,13) and (II,14), we compute the eigenfunctions and the eigenvalues of (I,14) by specifying a particular zonal wind $\bar{u}$. We choose the zonal wind shown in Figure (I,1) to which corresponds the potential V depicted in Figure (I,2). The first three eigenfunctions are shown in Figure (II,1); ϕ_1 has no nodal lines in the y,z domain while ϕ_2 and ϕ_3 have one nodal line respectively at y = 0 and at z ≈ 7 km. All the normal modes other than ϕ_1, ϕ_2, and ϕ_3 have at least two nodal lines in the y,z domain. Mode ϕ_2, multiplied by $e^{z/2}$, gives the meridional structure of the coherent solution examined in Chapter I. We will refer to ϕ_3 as the first baroclinic eigenmode.

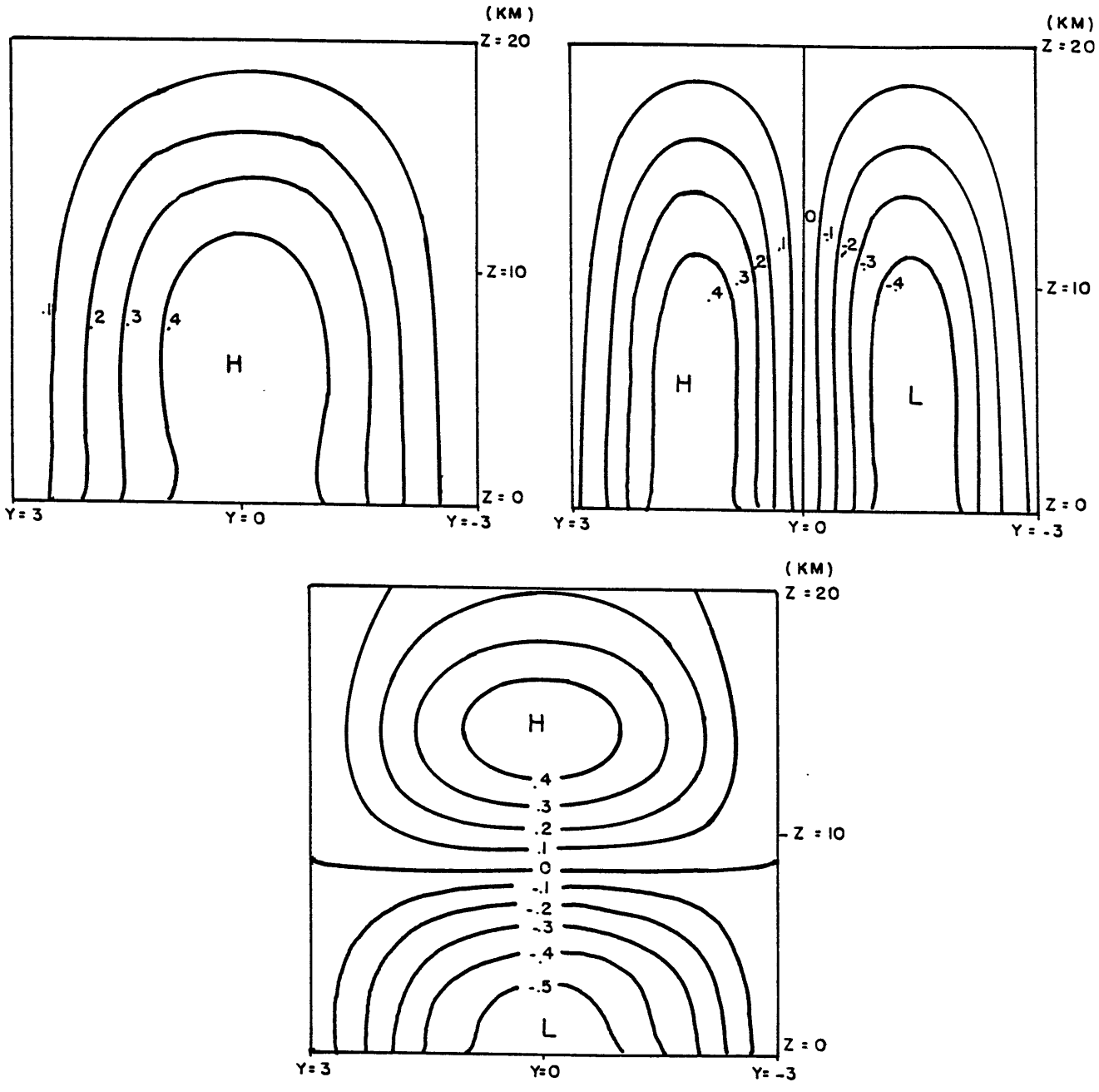
(KM)
Z = 20
Z = 10
Z = 0
Y = 3
Y = 0
Y = -3
H
.1
.2
.3
.4
(KM)
Z = 20
Z = 10
Z = 0
Y = 3
Y = 0
Y = -3
H
L
.1
.2
.3
.4
0
-.1
-.2
-.3
-.4
(KM)
Z = 20
Z = 10
Z = 0
Y = 3
Y = 0
Y = -3
H
L
.4
.3
.2
.1
0
-.1
-.2
-.3
-.4
-.5

Fig. (II,1)

Release of available potential energy of the mean wind can be obtained by suitably combining modes ϕ_1 and ϕ_3. The energy equation, obtained by multiplying (II,13) by A_i and by averaging over the zonal domain, is:

$$\frac{d}{dt}\{\langle KE\rangle + \langle AE\rangle\} = \langle CE\rangle$$

where

$$\langle KE\rangle = \frac{1}{2}(\overline{A_{i_x}A_{i_x}} + \zeta_{in}\overline{A_iA_n})$$

is the eddy kinetic energy,

$$\langle AE\rangle = -\frac{1}{2}\alpha_{in}\overline{A_iA_n}$$

is the eddy available potential energy, and

$$\langle CE\rangle = \varepsilon_{inm}u_nK_m\overline{A_{i_x}A_m} \qquad \text{(II,16)}$$

is the total, zonal-to-eddy energy conversion.

Summing over indices 1 and 3 only, (II,16) becomes

$$\langle CE\rangle_{1,3} = (\varepsilon_{133}u_3 + \varepsilon_{113}u_1)(K_3 - K_1)\overline{A_{1_x}A_3} \approx \varepsilon_{133}u_3(K_3 - K_1)\overline{A_{1_x}A_3} \qquad \text{(II,17)}$$

where $\varepsilon_{113}u_1$ is negligible compared to $\varepsilon_{133}u_3$ (see appendix C). We will refer to u_3 as the "shear" component of the zonal wind. If the shear is positive, then zonal energy will be released whenever A_{1_x} and A_3 are positively correlated. Assuming a sinusoidal profile for A_1 and A_3, maximum correlation is attained when A_3 lags A_1 by $\pi/2$. In more synoptic

terms, maximum conversion of zonal energy occurs when the thickness is out of phase of $\pi/2$ with the mean geopotential height. It is easy to show graphically that, in this circumstance, the phase lines in the x-z plane tilt westward with increasing height.

The suitable way of ordering a bidimensional set is by nodal lines. The diagram (II,2) illustrates schematically the position of ϕ_1, ϕ_2, and ϕ_3 in such ordering.

With this scheme in mind, we will refer to the system truncated after the first three modes as the "first triangular truncation." In appendix C the values of the tensor δ_{ijm}, γ_{ijm}, ε_{ijm}, ε'_{ijm}, ζ_{ij} and α_{ij} truncated at $i = j = m = 3$ are reported. These values were computed numerically from the normal modes shown in Figure (II,1).

Section (II,b). Coherent structure

In this section we examine a particular solution of the first triangular truncation of equations (II,13) and (II,14).

It is very easy to show that, if A_1 and A_3 are zero initially, they will remain zero at any time. Furthermore, since $\overline{A_{n_x} A_m}$ vanishes in

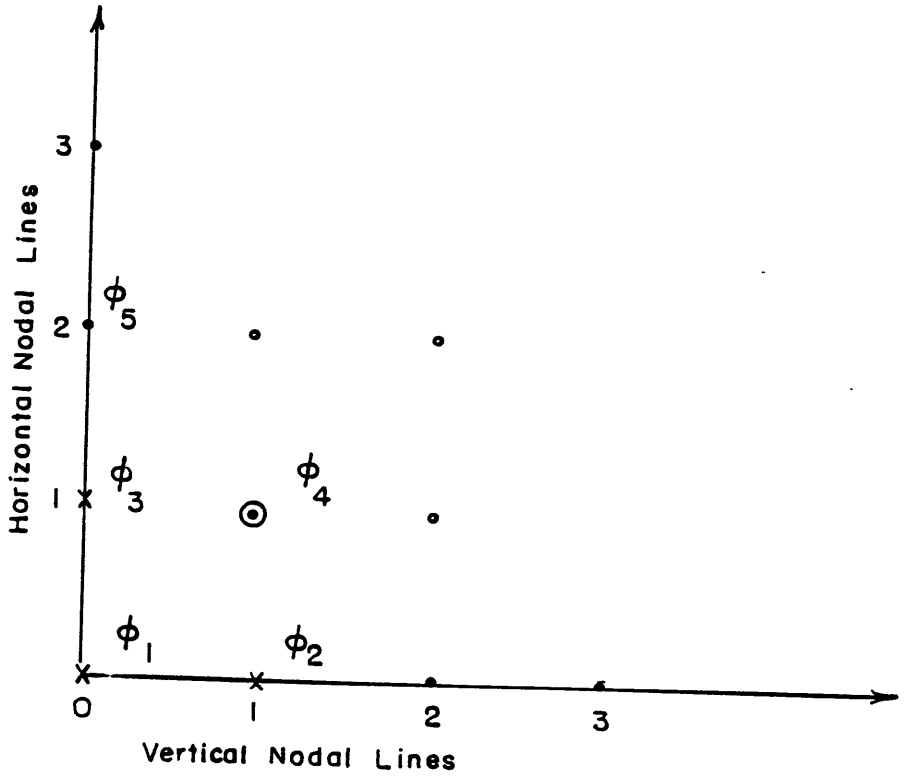
Horizontal Nodal Lines
3
2
1
0
ϕ_5
ϕ_3
ϕ_4
ϕ_1
ϕ_2
1
2
3
Vertical Nodal Lines

Fig. (II,2)

this case, from (II,14) follows that $u_n(t) = u_n(0)$. Thus, the modal equations reduce to

$$\dot{A}_{2_{xx}} + (\alpha_{22} - \zeta_{22})\dot{A}_2 + \varepsilon_{2n2}u_n(A_{2_{xxx}} - K_2A_{2_x}) + \varepsilon_{2n2}(u_n - \bar{u}_n)K_nA_{2_x} + \\ +\delta_{222}A_{2_x}A_2 = 0 \qquad \text{(II,18)}$$

$$u_n = \text{constant}$$

We look for solutions having the form of propagating waves:

$$A_2 = A_2(x - ct)$$

Hence, (II,18) becomes:

$$A_{2_{xx}} - \Omega A_2 + \delta A_2^2/2 = c_1 \qquad \text{(II,19)}$$

where c_1 = constant

$$\delta = \delta_{222} \; / \; (\varepsilon_{2n2}u_n - c)$$

$$\Omega = - \frac{\varepsilon_{2n2}(u_n - \bar{u}_n)K_n - \varepsilon_{2n2}u_nK_2 - c(\alpha_{22} - \zeta_{22})}{\varepsilon_{2n2}u_n - c} \qquad \text{(II,19,a)}$$

Equation (II,19) is a KdV equation in the amplitude of mode ϕ_2. In an infinite longitudinal domain, the upstream boundary condition $A_{2\ x \to -\infty} \to 0$ implies $c_1 = 0$; in a finite, periodic domain of length L_x, c_1 is computed using definitions (I,2,a) and (I,2,c). In the former case, the solution of (II,19) is

$$A_2 = P_\infty \operatorname{sech}^2 Q_\infty x$$

$$Q_\infty = \frac{\sqrt{\Omega}}{2} \qquad \text{(II,20)}$$

$$P_\infty = \frac{3\Omega}{\delta}$$

In the latter case, an excellent approximation of the solution of (II,19) can be written in the form:

$$A_2 = P \operatorname{sech}^2 Qx + c_2 \qquad \text{(II,21)}$$

The condition $\int_{-L_x/2}^{L_x/2} A_2 dx = 0$ implies:

$$\int_{-L_x/2}^{L_x/2} P \operatorname{sech}^2 Qx \, dx + L_x c_2 \approx P \int_{-\infty}^{+\infty} \operatorname{sech}^2 Qx + c_2 L_x = 0$$

Thus, $c_2 = -2P/L_xQ$. Substituting the expression of c_2 and (II,21) into (II,19) we get:

$$Q = \frac{3}{L_x} + \left(\frac{9}{L_x^2} + \frac{\Omega}{4}\right)^{1/2}$$

$$P = 12Q^2/\delta \qquad \text{(II,22)}$$

Let us suppose now that $c = 0$ (stationary solution) and that $u_n = \bar{u}_n$. Thus, Ω reduces to K_2, the eigenvalue corresponding to the eigenmode ϕ_2. Hence, in an infinite domain, (II,19) becomes identical to equation (I,17) found in Chapter I. In particular, the coefficient of the nonlinear term in equation (II,19)

$$\delta = \frac{\langle e^{z/2} v_y \phi_2^3 \rangle}{\varepsilon_{2n2} u_n} \qquad \text{(II,23)}$$

corresponds to $\langle e^{z/2} v_y \phi_2^3 / \bar{u} \rangle$ in equation (I,17) (note that the sum $\varepsilon_{2n2} u_n$ in (II,23) is the mean value of $\bar{u}$ weighted by ϕ_2^2). Thus, (II,19) and (II,20) are the finite amplitude correspondents (in the truncated system) of the solution examined in the first chapter.

In the following we will refer to solutions (II,20) and (II,21) as the "coherent structure" or "vortex pair."

Figure (II,3) shows the total streamfunction pattern and the anomaly pattern at 500 mb given by (II,21) computed with $c = 0$ and $L_x = 30$ (30,000 km). The similarity with the blocking cases shown in Figure 1 is self evident. In diagram (II,4) the phase speed as function of the amplitude P is plotted for the infinite and periodic domain. In the case of periodic domain the amplitude of the stationary coherent structure is higher. In both cases the phase speed decreases as the amplitude increases; this is because more intense vortices advect each other against the mean wind with greater strength. Another important characteristic is that the phase speed is very small for a wide range of amplitudes, supporting the claim that certain kinds of blocking may be modelled by these solutions.

In concluding this chapter we make a last important remark. The

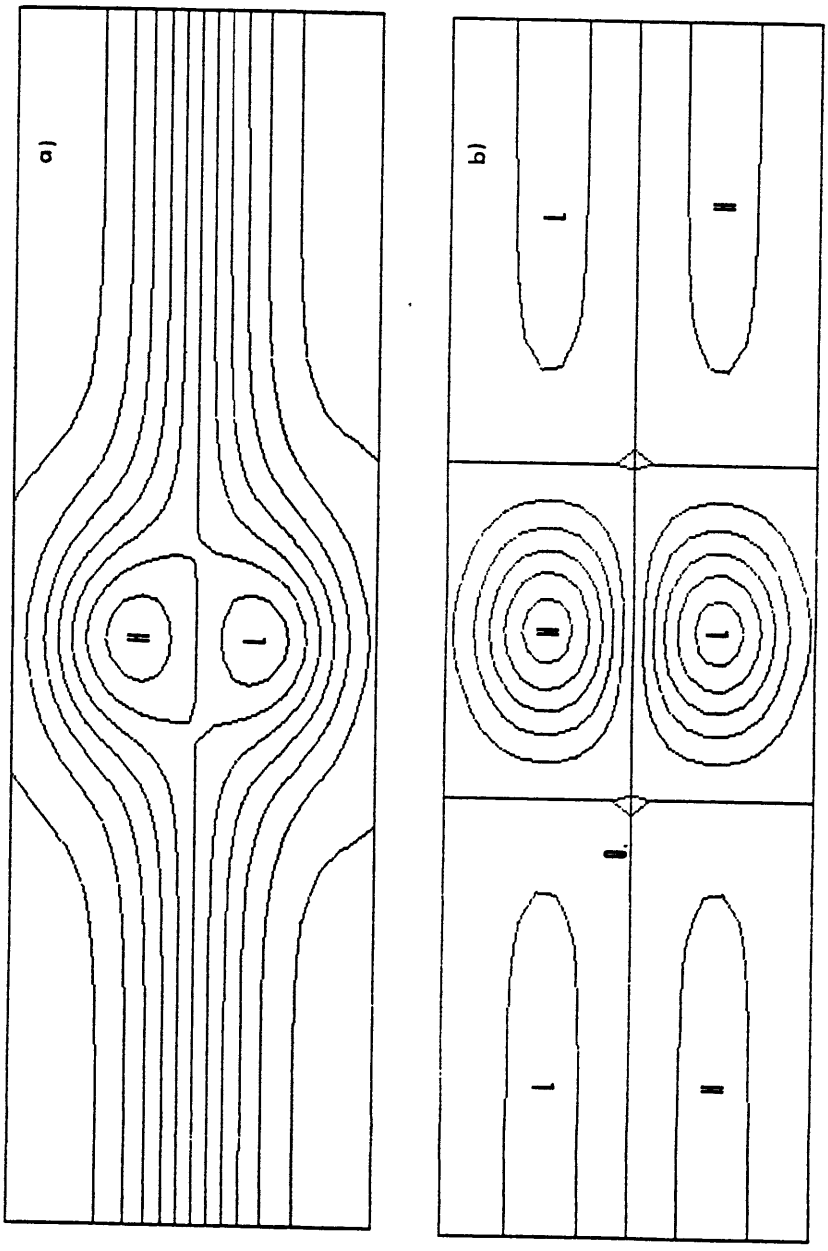

Fig. (II,3)

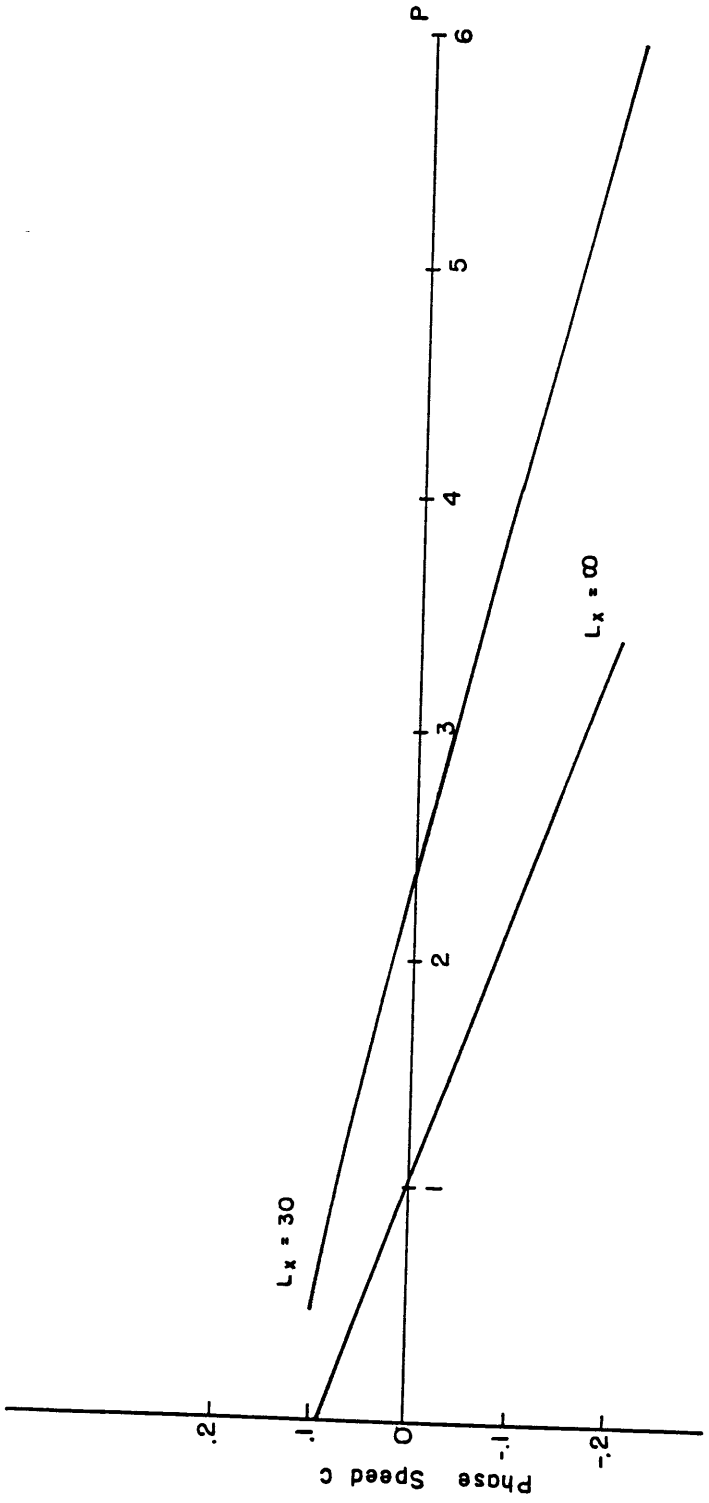

Fig. (II,4)

sech^2 solution of (II,19) exists only under certain conditions. Necessary and sufficient condition for the existence of (II,20) is that Ω be positive ($q/L_x^2 + \Omega/4 > 0$ if $L_x < +\infty$). Provided the phase speed is small and the time fluctuations of $u(y,z,t)$ are negligible, Ω is positive when K_2 is positive [see (II,19,a)]. If the zonal wind were to change in time in such a way that Ω became negative, then (II,20) would no longer be a solution of the truncated system. There is a subtle difference between the derivation presented in this chapter and the derivation of Chapter I. In Chapter I, the requirement $K_2 > 0$ was necessary in order to satisfy the upstream boundary condition (I,2,b). Here, (I,2,b) is replaced by the weaker condition

$$\int_0^{L_x} \psi' \, dx \, / L_x = 0$$

which follows from definitions (I,2,a) and (I,2,c). One of the consequences is that solutions of equation (II,19) can be written in terms of elliptic integrals even if $\Omega < 0$ (or $K_2 < 0$). These solutions are not formed by a single pulse as in the case $K_2 > 0$: they consist of an infinite train of nonlinear waves (cnoidal waves). In Fig. (II,5) an example of a cnoidal wave solution of (II,19) is presented for the case $\Omega = -.2$; it can be noticed that the wave becomes very steep near the crest so that the split flow is associated with intense meridional motion.

In this chapter we have recovered the coherent structure found in Chapter I by solving a severely truncated dynamical system. Solution (II,20) [or (II,21)] is the generalization to finite amplitude and finite dispersion of the well-known solitary wave (Long, 1964; Patoine and Warn, 1983; etc.). It consists of a vortex pair translating with small phase speed resembling certain atmospheric patterns typically associated with Atlantic blocking.

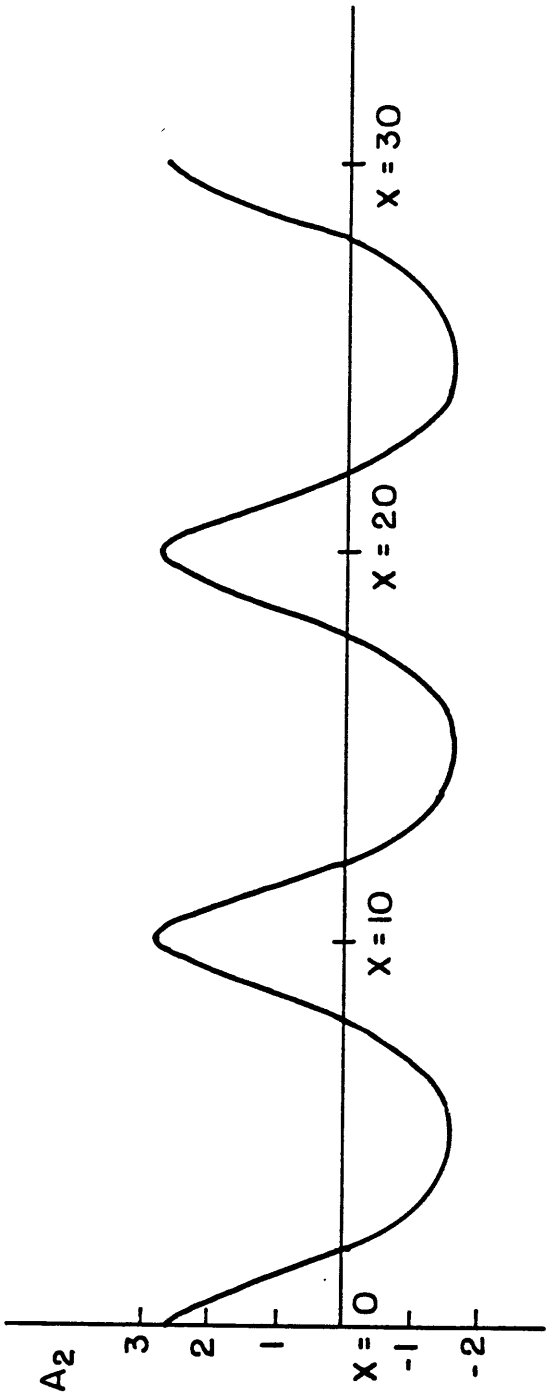

Fig. (II,5)

Chapter III

Stability

Section (III,a). Convergence

To see the effect that severe truncation has on the coherent structure we examined in Chapter II, the following procedure has been devised.

A new eigenmode with two nodal lines has been added to the three modes already considered. The new eigenmode, shown in Figure (III,1), has the same symmetry as ϕ_2 and is denoted by the index 4. The reason why this eigenmode is selected among all the remaining ones is because ϕ_4 is the only eigenmode with two nodal lines having the same symmetry as the coherent structure. In fact, the coherent structure does not project over symmetric (around y = 0) modes and the Fourier coefficients of higher, antisymmetric eigenmodes are likely to be smaller.

In the system truncated after 4 modes, A_1, A_3, u_2, and u_4 are zero at all times provided they were zero initially. However, in the remaining equations, A_2 and A_4 are coupled in a complicated fashion so that a simple analytic solution is no longer possible. The simplest way to determine how the sech^2 solution is modified by the introduction of the fourth mode is to initialize the 4-mode system with (II,21) and integrate forward for a sufficient period of time. If (II,21) is close to a fixed point of the new system, and if the fixed point is stable, then only small transients will be observed in the time evolution.

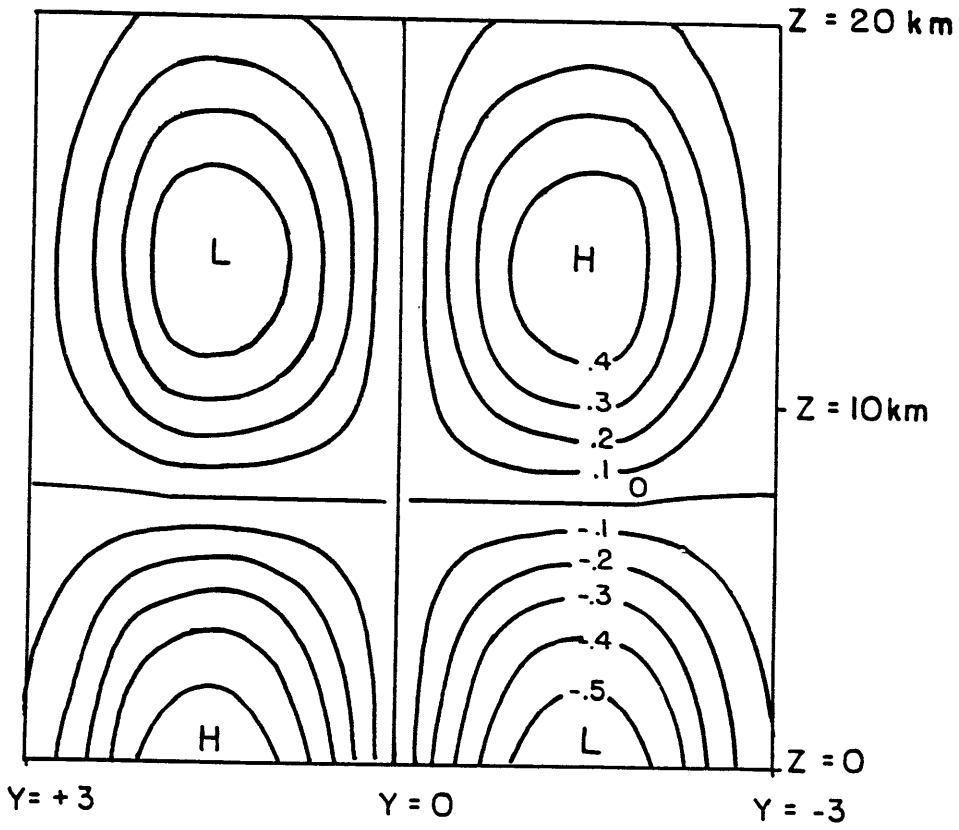

Fig. (III,1)

The problem of stability deserves further consideration. The zonal wind over which the coherent structure is superimposed can be baroclinically unstable. Let us truncate (II,13) after the four modes ϕ_1, ϕ_2, ϕ_3, and ϕ_4 shown in diagram (II,2) and let us linearize around the zonal wind

$$(u_1,0,u_3,0) \qquad \text{(III,1)}$$

The first component of the zonal wind, u_1, can be set equal to $\bar{u}_1$ for the purposes of the following discussion. Small perturbations around the basic state (III,1) can take the form $(0,A_2,0,A_4)$ or $(A_1,0,A_3,0)$[1]. In the former case (II,13) reduces to:

$$\begin{aligned}
&\dot{A}_{2_{xx}} + (\alpha_{22} - \zeta_{22})\dot{A}_2 + (\alpha_{24} - \zeta_{24})\dot{A}_4 + \varepsilon_{2n2}u_n(A_{2_{xxx}} - K_2A_{2_x}) + \\
&+ \varepsilon_{2n4}u_n(A_{4_{xxx}} - K_4A_{4_x}) + K_3(u_3 - \bar{u}_3)(\varepsilon_{232}A_{2_x} + \varepsilon_{234}A_{4_x}) = 0 \qquad \text{(III,2)} \\
&\dot{A}_{4_{xx}} + (\alpha_{44} - \zeta_{44})\dot{A}_4 + (\alpha_{24} - \zeta_{24})\dot{A}_2 + \varepsilon_{4n2}u_n(A_{2_{xxx}} - K_2A_{2_x}) + \\
&+ \varepsilon_{4n4}u_n(A_{4_{xxx}} - K_4A_{4_x}) + K_3(u_3 - \bar{u}_3)(\varepsilon_{432}A_{2_x} + \varepsilon_{434}A_{4_x}) = 0
\end{aligned}$$

(The feedback over the mean wind is neglected.) The solution of (III,2) can be written as:

---

[1] Larger growth rates would be obtained by introducing a second baroclinic eigenmode with two horizontal nodal lines. Its effect will be discussed later.

$$A_{2,4} = a_{2,4} e^{iK(x - ct)} \qquad \text{(III,3)}$$

where $a_{2,4}$ and c are complex quantities. After substituting (III,3) into (III,2) a linear and homogeneous system determining a_2 and a_4 is obtained. The necessary and sufficient condition for the solvability of the system gives the following condition on c:

$$\begin{aligned} & c^2[K_2^2K_4^2 - (\alpha_{24} - \zeta_{24})^2] + c\{K_2^2[U_4^*K_3 - U_4(K + K_4) + K_4^2[U_2^*K_3 - \\ & - U_2(K^2 + K_2)] + (\alpha_{24} - \zeta_{24})[2U_{24}^*K_3 - U_{24}(2K^2 + K_2 + K_4)]\} + \\ & + [U_4^*K_3 - U_4(K^2 + K_4)] \cdot [K_3U_2^* - U_2(K^2 + K_2)] - [U_{24}^*K_3 - \\ & -U_{24}(K^2 + K_4)][U_{24}^*K_3 - U_{24}(K^2 + K_2)] = 0 \end{aligned} \qquad \text{(III,4)}$$

where

$$K_2^2 = K^2 + \zeta_{22} - \alpha_{22}$$

$$K_4^2 = K^2 + \zeta_{44} - \alpha_{44}$$

$$U_2 = \varepsilon_{2n2}u_n$$

$$U_4 = \varepsilon_{4n4}u_n$$

$$U_{24} = \varepsilon_{2n4}u_n$$

$$U_2^* = \varepsilon_{232}(u_3 - \bar{u}_3)$$

$$U_4^* = \varepsilon_{434}(u_3 - \bar{u}_3)$$

$$U_{24}^* = \varepsilon_{234}(u_3 - \bar{u}_3)$$

The dispersion relation (III,4) admits, under certain conditions, complex conjugate roots. The imaginary part of c as a function of u_3 and K^2 is plotted in diagram (III,2). Similarly to the two-layer model case, there is a critical value of the vertical shear above which instability occurs (note that the long wave cutoff and the critical shear are the consequence of the 2-mode truncation). The position of the wavenumber corresponding to 5, 6, and 7 wavelengths in the latitude circle is indicated by an arrow on the x-axis. Figure (III,3) shows the real part of c, that is the phase speed of baroclinic waves.

Similar considerations apply to perturbations having the form (A_1, 0, A_3, 0). In this case (diagrams (III,4) and (III,5) show respectively the growth rate and the phase speed) the growth rates are bigger than in the previous case. In fact, it is a feature common to all baroclinic instability theories that the growth rate decreases as the meridional wavelength of the disturbance gets smaller.

Another source of instability can come from the coherent structure itself. Rossby wave motion in the atmosphere may suffer from <u>barotropic</u> instability (Lorenz, 1971) especially when the waves are sufficiently strong or the wavenumber is sufficiently high. It is not clear how Lorenz's results concerning Rossby wave motion can apply to this particular case; the solution examined here has a sinusoidal y-dependence and decays exponentially as x goes to $\mp\infty$. We have shown that, in the long-wave and weakly nonlinear limit, (II,21) becomes an asymptotic solution of the quasigeostrophic equations. <u>In such a limit</u>, the wave motion reduces to a zonal flow which is <u>not</u> unstable by resonant interaction (Gill, 1974). More generally, there are indications that, as long as the coherent

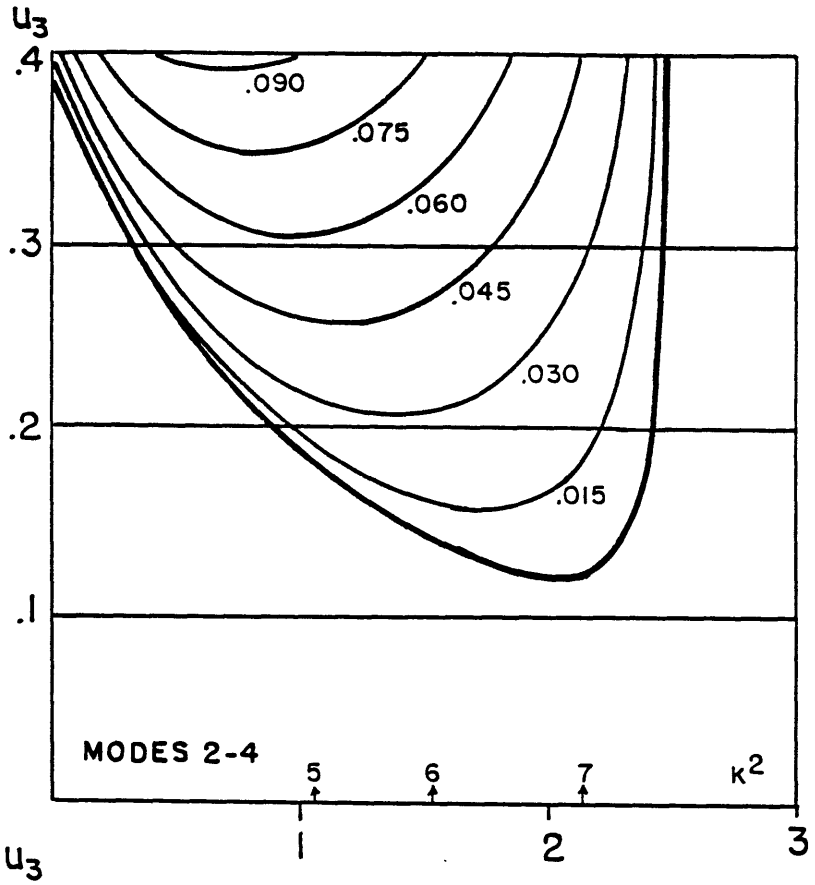

Fig. (III,2)

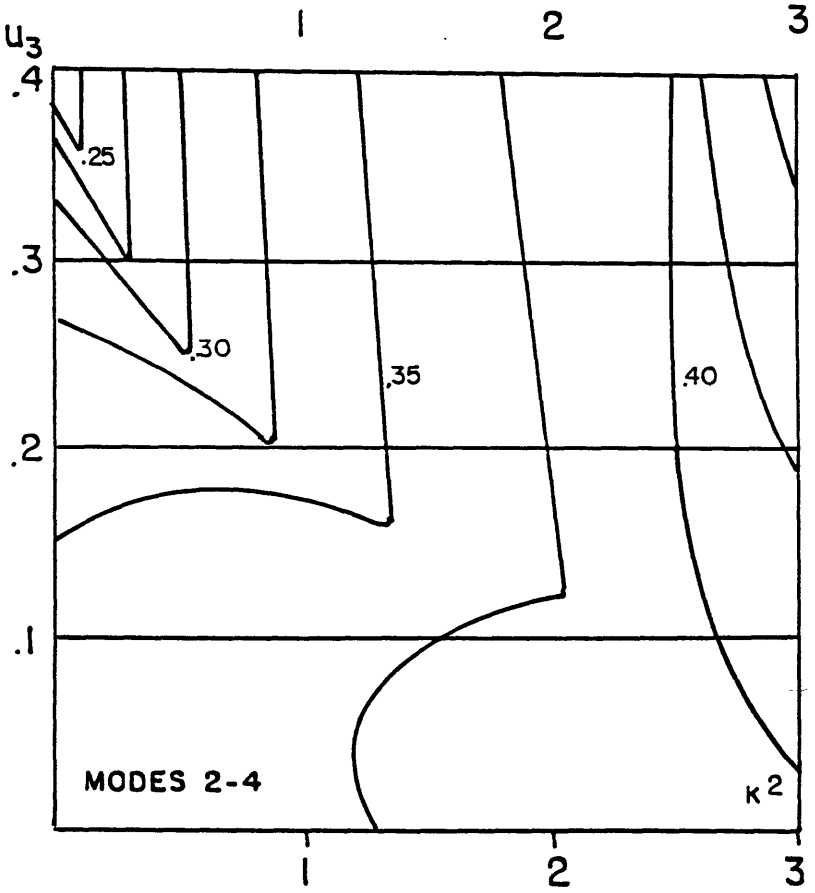

Fig. (III,3)

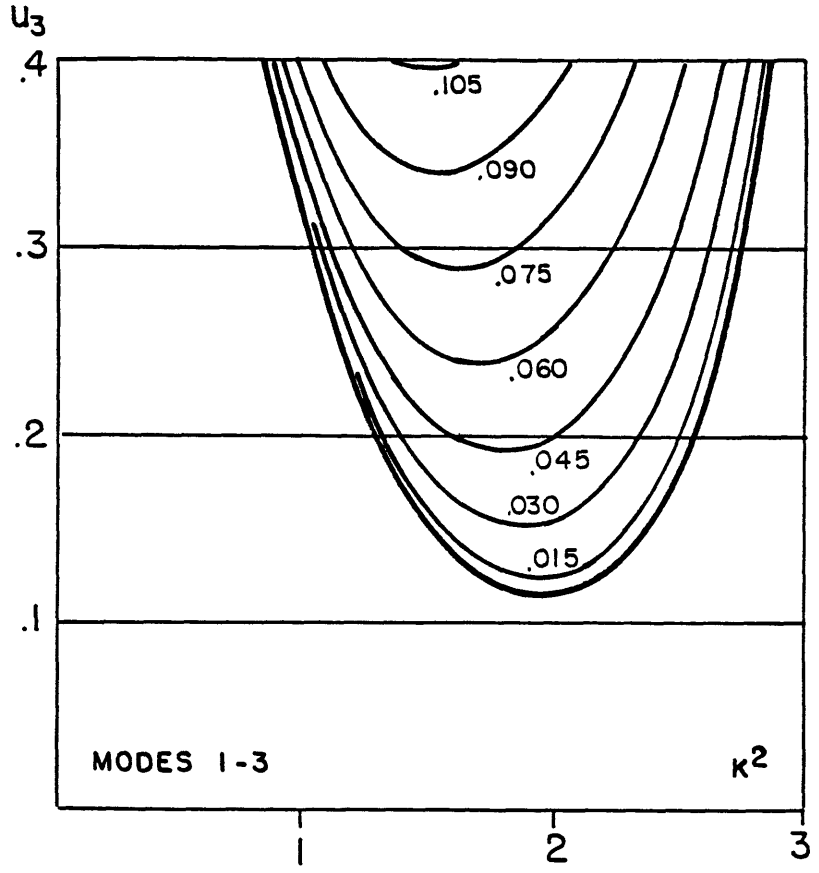

Fig. (III,4)

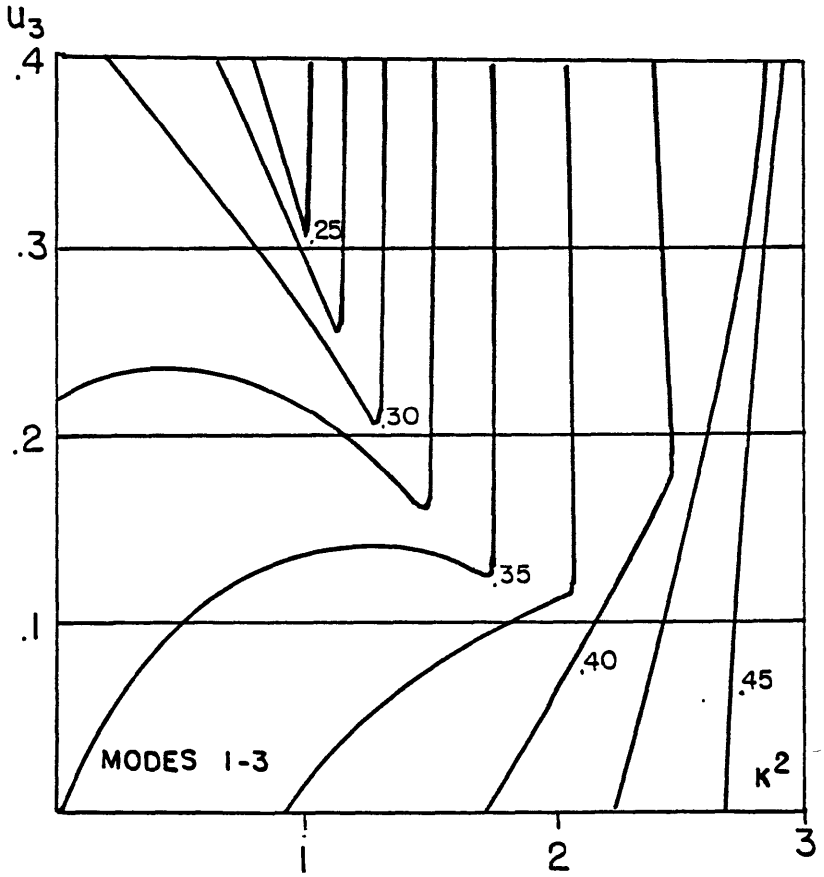

Fig. (III,5)

structure follows a KdV dynamics, an enhanced stability has to be expected in the region occupied by it. A sufficient condition for the stability of quasigeostrophic flow can be obtained generalizing a method presented by Arnold (1965), which is based on a variational principle. For flows such that $q = F(\psi)$ it can be shown (Blumen, 1968) that a sufficient condition for stability is that $[dF/d\psi]_{\psi=\psi_s} > 0$ everywhere in the domain (here ψ_s is the fixed point whose stability is to be determined). From the previous sections:

$$F(\psi) = F(\bar{\psi}) + \left.\frac{dF}{d\psi}\right|_{\psi=\bar{\psi}} \psi' + \frac{1}{2}\left.\frac{d^2F}{d\psi^2}\right|_{\psi=\bar{\psi}} \psi'^2 + \ldots$$

Since

$$\frac{dF}{d\psi'} = \frac{dF}{d\psi}\frac{d\psi}{d\psi'} = \frac{dF}{d\psi}$$

we get

$$\left.\frac{dF}{d\psi}\right|_{\psi=\psi_s} = \left.\frac{dF}{d\psi'}\right|_{\psi'=\psi'_s} = \left.\frac{dF}{d\psi}\right|_{\psi=\bar{\psi}} + \left.\frac{d^2F}{d\psi^2}\right|_{\psi=\bar{\psi}} \psi_s' + \ldots$$

$$\simeq -\frac{\beta + V_y\psi'_s - \bar{u}_{yy} - \bar{u}_{zz} + \bar{u}_z}{\bar{u}}$$

where (I,6) and (I,6,a) have been used. For the stationary solution under consideration, the term $V_y\psi'_s$ is positive in most of the domain. Its effect is to increase locally the β term, thus giving a stabilizing contribution. This argument, although not precise, indicates that the region of space occupied by the stationary solution which satisfies the KdV dynamics (quadratic nonlinearity) is going to have enhanced stability

properties if compared to the remainder of the domain. The argument breaks down when higher order terms in the Taylor expansion of $F(\psi)$ have to be considered; this happens when the amplitude of the stationary solution is high.

Returning to the effect that the truncation of the series (II,4) has on the coherent solution (II,21), two numerical computations are performed. In the first experiment the 4-mode model is initialized with (II,21) superimposed to a zonal wind having $u_3 = .1$, that is, in the stable region of the phase space. The integration is carried on for 30 days. A brief description of the numerical model is given in appendix D. Figure (III,6) shows the time evolution of the total streamfunction at 500 mb. The smallness of the transients observed indicates that the initial condition is very close to a fixed point of the new system, and that such equilibrium is stable. Since we are dealing with a conservative system, the situation is identical, at least conceptually, to a frictionless pendulum slightly displaced from its stable equilibrium. The second numerical calculation is initialized with $u_3 = .2$, that is, in the unstable region of the phase space [see diagram (III,2)], and is carried out for 30 days. Figure (III,7) shows the new time evolution at 500 mb. After the initial period of apparent stationarity, departures from the initial condition are observed. However, the coherent structure is found to persist in its original position despite the instability of the mean wind. Thus, a clear statement about the robustness of (II,21) can still be stated.

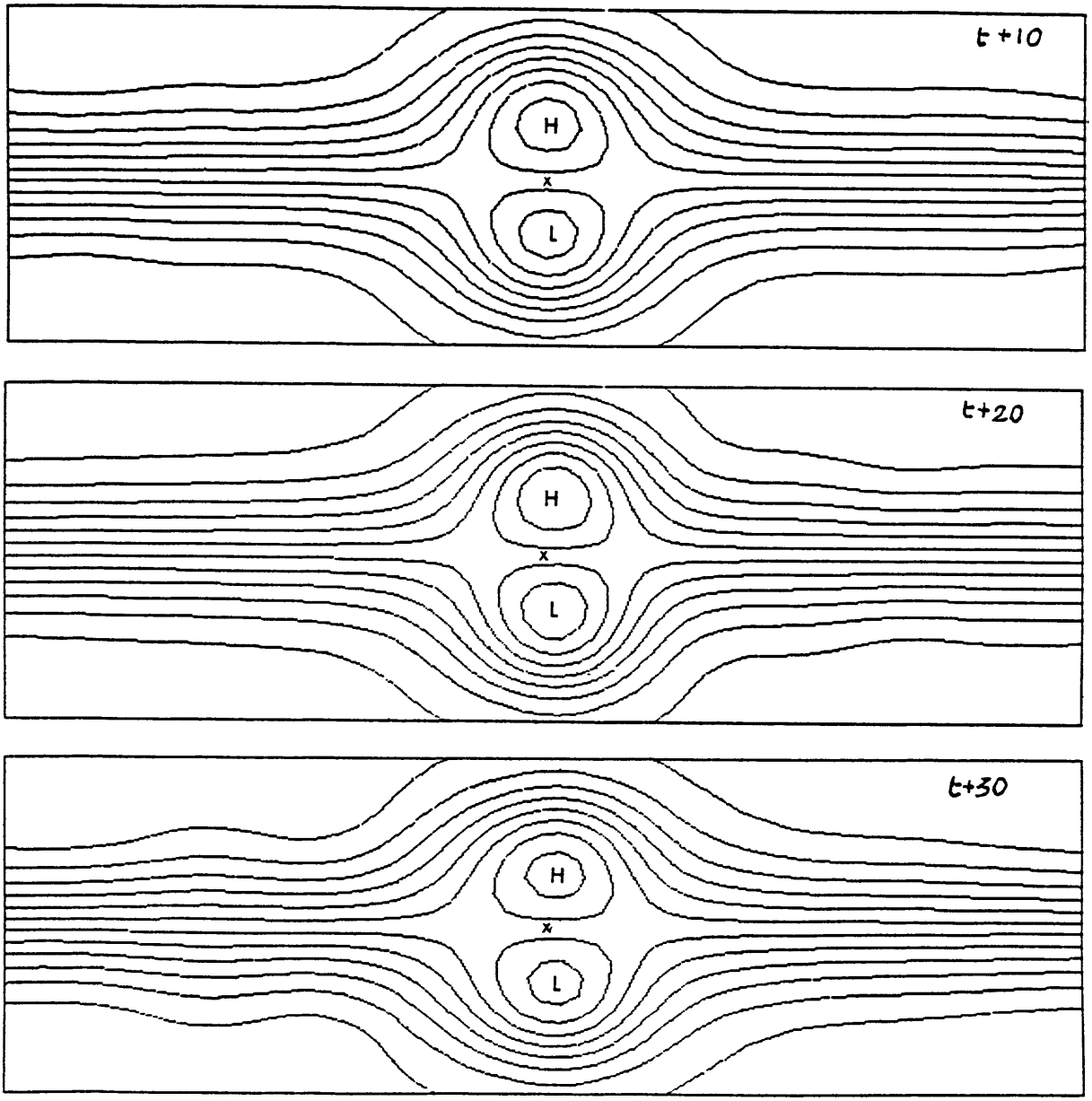

Fig. (III,6)

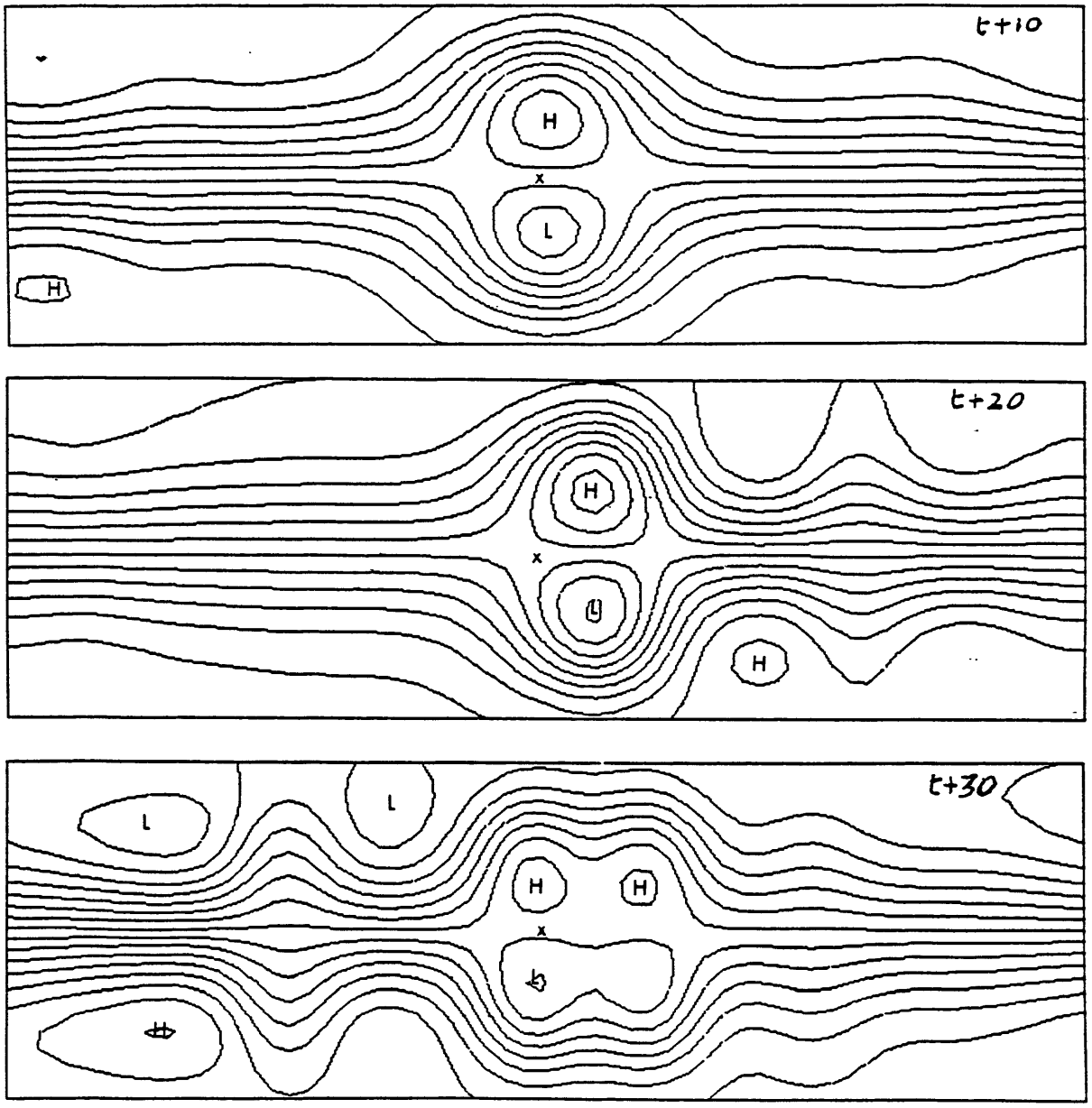

Fig. (III,7)

Section (III,b). Stability experiments

Still, it remains a possibility that (II,21) is "unstable" when small perturbations in other directions of the phase space are superimposed to it or for finite amplitude perturbations. The word "unstable" must be intended in the following sense: how long is the coherent structure going to maintain its identity when finite amplitude disturbances coexist with it in a baroclinically unstable atmosphere? In other words, how robust is solution (II,21)? If it happens that, within an environment as turbulent as the real atmosphere, the coherent solution is destroyed after a few days, then (II,21) is not an acceptable model of blocking.

The following numerical computations are thus meant to determine the robustness of (II,21). An initial perturbation, to be added to the coherent structure, satisfying the constraints of the quasigeostrophic turbulence (Charney, 1971) is defined using a computer random number generator. The n^{th} Fourier component of A_i, randomly generated, is divided by

$$\left(\frac{4\pi^2 n^2}{L_x^2} + \zeta_{ii} - \alpha_{ii} \right)^{1/2}$$

for $n < 6$ and by

$$\left(\frac{4\pi^2 n^2}{L_x^2} + \zeta_{ii} - \alpha_{ii} \right)^{5/4}$$

for $n \geq 6$; this implies a constant energy spectrum for $n < 6$ and a K^{-3} low for $n > 6$ (see Figure 1 of Julian et al., 1970). Also, the equipartition of energy between the two components of the kinetic energy and the available potential energy turns out to be satisfied quite well. Figure (III,8) shows the energy spectrum of the perturbation and, for comparison, the mean spectrum for all blocking days during the 1978-1979 winter season (after Hansen and Sutera, 1983).

In order to determine the effect of the zonal wind instability on the predictability of (II,21), several initial conditions are chosen deeper and deeper inside the unstable lobe of diagrams (III,2) and (III,4). All the numerical integrations are carried on for 15 days using the four-mode truncation previously described.

The last two columns of Table (III,I) indicate respectively the initial vertical shear and e-folding time (in days) of the most unstable zonal wavenumber (indicated in parentheses) which are obtained from diagram (III,2). In the last two rows of Table (III,I) we report respectively the dimensionless (E_0) kinetic energy of the initial perturbation and the kinetic energy of the initial perturbation plus coherent structure, measured in Joule/m^2. These values are relative to the area-average, vertical integral of the eddy kinetic energy; typical December values of this quantity for the atmosphere are between 1.0 and 1.4 $\times$ $10^6 J/m^2$ (Hansen and Chen, 1982). In the remaining part of Table (III,I) the circled numbers are the corresponding "persistence time", defined as the instant at which the coherent structure breaks down under the effect of the perturbation. To give an idea of the amount of turbulence present in each

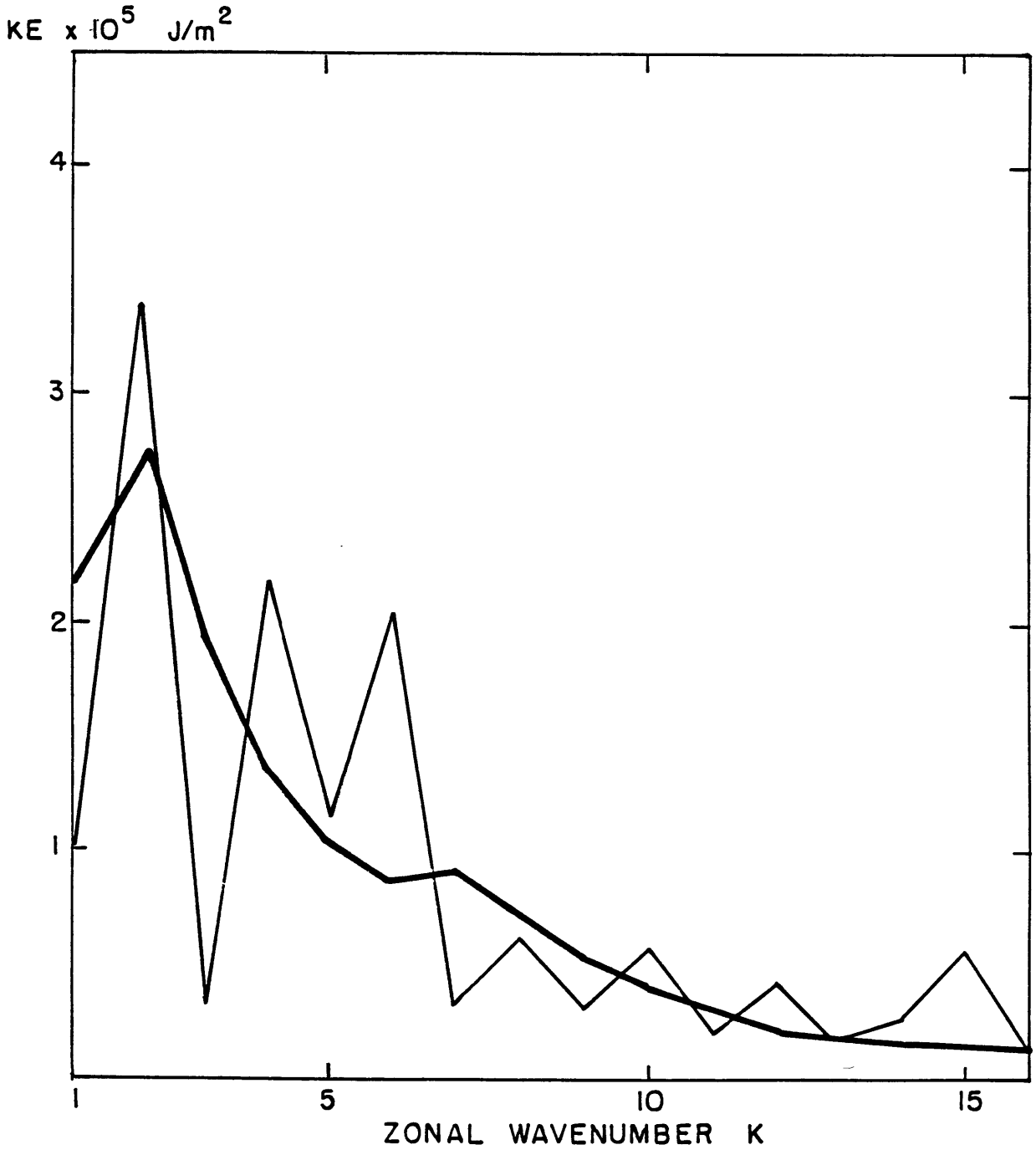

Fig. (III,8)

Table (III,1)

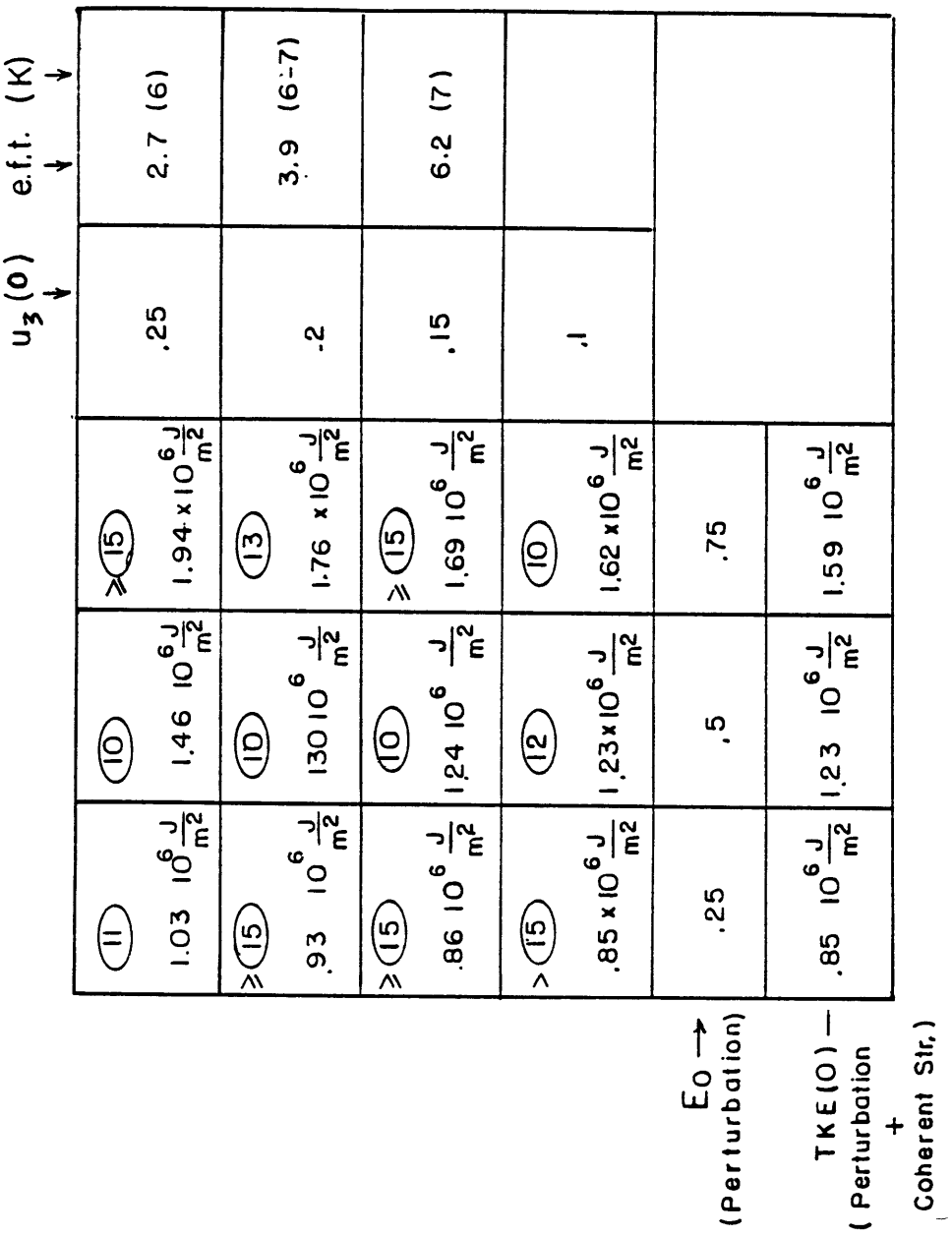
$u_3(0)$ ↓
e.f.t. (K) ↓
.25
2.7 (6)
.2
3.9 (6-7)
.15
6.2 (7)
.1
(11) $1.03\ 10^6 \frac{J}{m^2}$
(10) $1.46\ 10^6 \frac{J}{m^2}$
≥(15) $1.94 \times 10^6 \frac{J}{m^2}$
≥(15) $.93\ 10^6 \frac{J}{m^2}$
(10) $1301 0^6 \frac{J}{m^2}$
(13) $1.76 \times 10^6 \frac{J}{m^2}$
≥(15) $.86\ 10^6 \frac{J}{m^2}$
(10) $1.24\ 10^6 \frac{J}{m^2}$
≥(15) $1.69\ 10^6 \frac{J}{m^2}$
>(15) $.85 \times 10^6 \frac{J}{m^2}$
(12) $1.23 \times 10^6 \frac{J}{m^2}$
(10) $1.62 \times 10^6 \frac{J}{m^2}$
E_0 → (Perturbation)
.25
.5
.75
TKE(0) — (Perturbation + Coherent Str.)
$.85\ 10^6 \frac{J}{m^2}$
$1.23\ 10^6 \frac{J}{m^2}$
$1.59\ 10^6 \frac{J}{m^2}$

experiment, the eddy kinetic energy averaged over the coherent structure lifetime is also reported. It can be noticed that in none of the cases examined is the persistence time less than 10 days. Indeed, 10 to 12 days seems to be the typical lifetime that is to be expected in realistic conditions. No evident correlation between the persistence time and the initial mean vertical shear can be observed; the initial perturbation is of finite amplitude and consequently the linear baroclinic instability of the mean flow has no effect. More surprising is the increased persistence within more turbulent environments. A possible explanation may lie in a systematic interaction between coherent structure and turbulent flows; such interaction will be the subject of the next chapter.

The time evolution shown in figures (III,9) and (III,10) is typical of the instability process that the coherent structure undergoes in its evolution. The sequences go from day 5 to day 8 of the experiment with $E_0 = .5$, $u_3 = .2$; Figure (III,9) shows the time evolution of the streamfunction field at 500 mb projected upon the normal mode ϕ_2 (which is the subspace where the soliton projects upon) while the total field during the same time sequence is shown in Figure (III,10).

Initially, the interaction with the perturbation goes in such a way that vorticity is accumulated into the vortex pair; at this point (day 5) the dynamics of the vortex pair is not of a KdV type any more; an instability sets in and in two days most of the vorticity is radiated away by means of a barotropic Rossby wave [see Figure (III,10)]. In the case shown here this barotropic instability is a particularly nasty one that ultimately leads to the complete destruction of the coherent structure

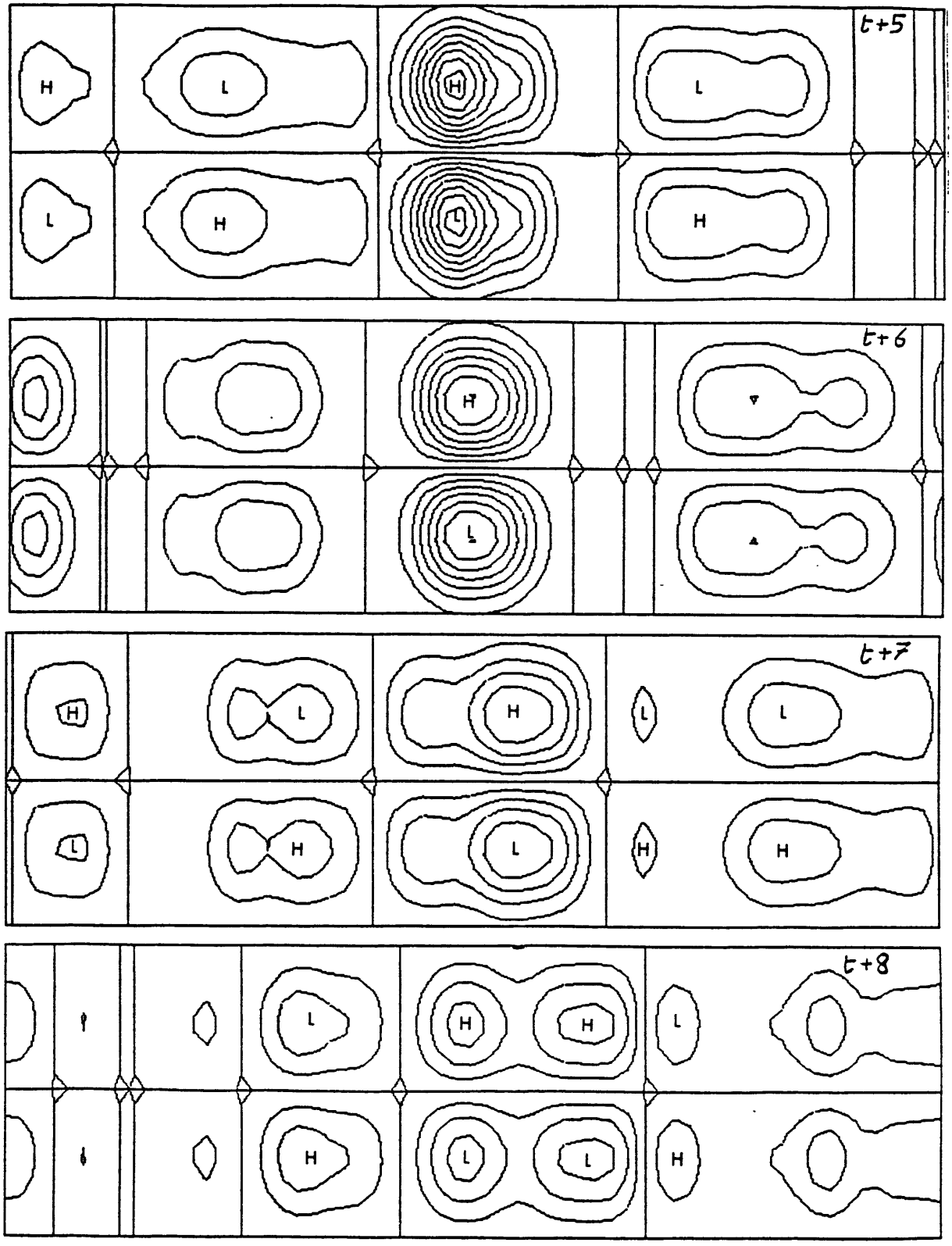

Fig. (III,9)

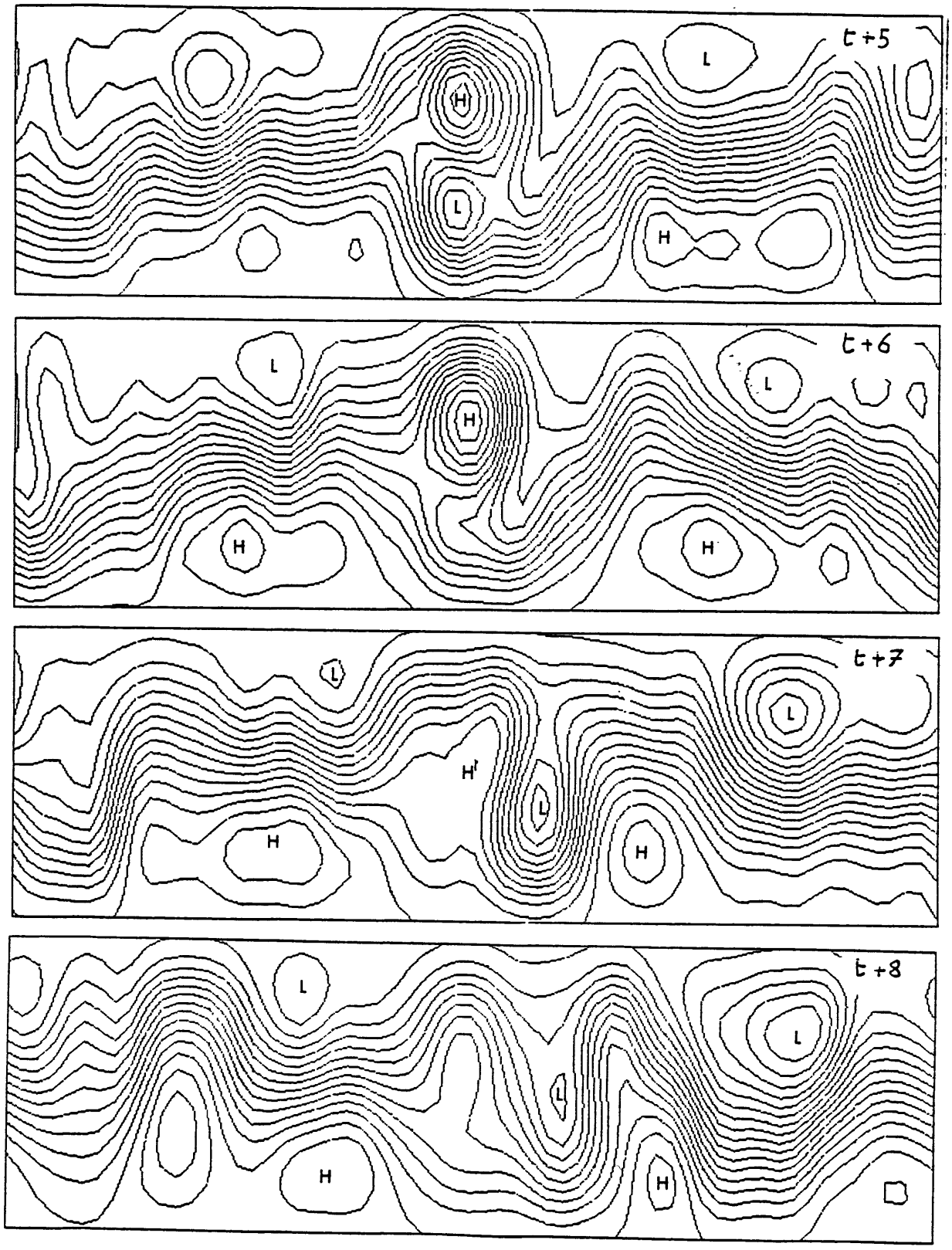

Fig. (III,10)

after day 10. Very often, in the experiments performed, we noticed that the vortex pair survived the instability process in a less intense form. Also, in the experiments with a lot of turbulence present, the vortex pair underwent the same process twice; that is, after the instability set in once, vorticity was again accumulated in a structure that soon became as intense as it was originally: at this point the instability set in a second time. Basically, in qualitative terms, the instability process removes the excess of vorticity that was accumulated throughout the nonlinear interaction between coherent structure and perturbation. Instability experiments along the same lines were also performed using a different truncation, namely, inserting the second baroclinic eigenmode ϕ_5 instead of ϕ_4 [see diagram (II,2)]. In fact, the growth rates (not shown) of baroclinic instability with modes ϕ_1, ϕ_3, and ϕ_5 are significantly higher than those computed with ϕ_1 and ϕ_3 alone. However, the persistence of the coherent structure was not affected by its introduction.

The 10-to-12 days estimate as the predictability of the coherent structure, although consistent with Rex's definition, is not a very long time. To determine whether this persistence time is significant for our model, we have to show that other features exist which are, under the same circumstances, less predictable. Thus, we performed the stability

analysis of the Rossby wave $\phi_1 e^{z/2}\sin(Kx)$ with zonal wavenumber 4 which is almost stationary (period ≈ 60 days). Figure (III,11) shows the time evolution of the modulus when the Rossby wave is unperturbed (solid line) and when randomly generated perturbations of the kind previously described with kinetic energy E_0 = .25, .5, and .75 are superimposed. Note that the amplitude of the unperturbed wave is not constant in time; this is because the Jacobian $J(\phi_1 , \nabla^2\phi_1 + \phi_{1_{zz}} - \phi_{1_z})$ is not identically zero as it would be if ϕ_1 were a pure sinusoidal, Fourier component. The initial kinetic energy of the Rossby wave, in dimensionless units, is .21 and corresponds to unitary amplitude. The persistence of this "quasi-stationary" Rossby motion is less than 4 days for those cases in which the initial perturbation has realistic energy levels.

To conclude this section we describe the method that was used to determine the final instant of the coherent structure life. We found that looking at the time evolution of the streamfunction pattern in the real space gave, in many cases, a rather subjective estimate of the "last day of blocking." A more objective criterion can be obtained by constructing a phase diagram of the most energetic components of the coherent structure (see Rizzoli, 1980). One complication is introduced by the fact that the coherent structure, weakened by the nonlinear interaction with the components of the perturbation, may show some eastward motion before disappearing.

Let's consider a propagating wave f(x - ct) translating without changing its shape. If we Fourier decompose it we get

$$f = \sum_n f_n e^{ik_n(x-ct)} = \sum_n f_n e^{-ick_nt} e^{ik_nx} , \ f_n \text{ complex}$$

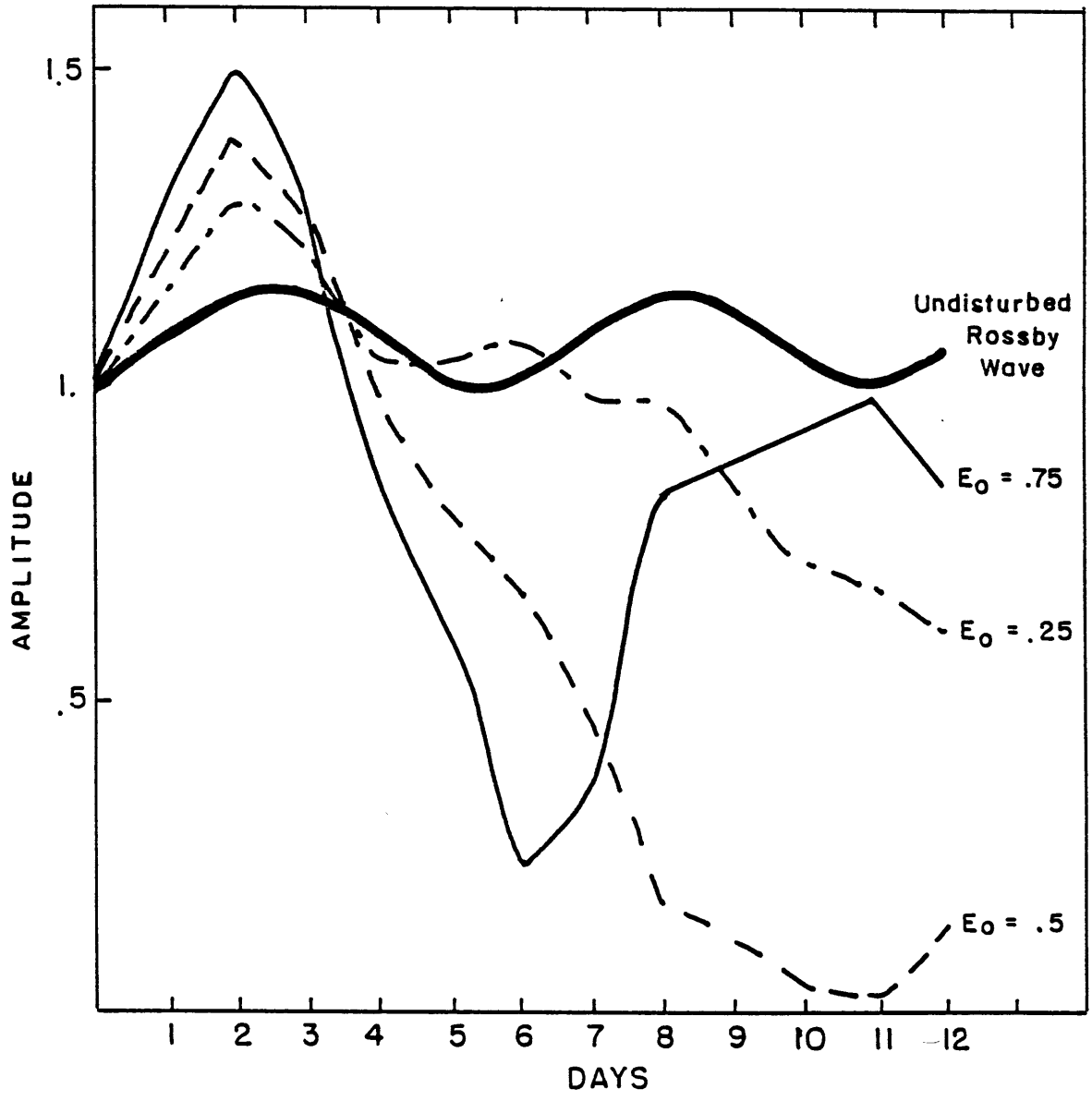
1.5
1.
.5
AMPLITUDE
Undisturbed
Rossby
Wave
E_o = .75
E_o = .25
E_o = .5
1 2 3 4 5 6 7 8 9 10 11 12
DAYS

Fig. (III,11)

Thus, the phase of the n^{th} Fourier coefficient of a shape-preserving envelope moving with phase speed c will evolve according to the linear law.

$$\theta_n = \theta_0 - k_n ct = \theta_0 - \frac{2\pi nct}{L_x} \qquad \text{(III,5)}$$

where θ_0 is the initial phase.

In diagrams (III,12) and (III,13) the phase of the first three Fourier coefficients of A_2 are plotted versus time respectively for cases $u_3(0) = .25$, $E_0 = .5$ and $u_3(0) = .25$, $E_0 = .75$. The thin, sloping lines are given by equation (III,5) with c = .1, that, is the maximum phase speed that the coherent structure can attain [see fig.(II,4)]. It can be noticed that, in case $E_0 = .5$, after 10 days of integration the second and third components run away much faster than the limiting phase speed allowed by the dispersion relation (II,22), while in case $E_0 = .75$ all the components are locked according to (III,5) with c = .1.

The criterion here presented, used together with streamfunction observations in the real space, allowed us to pinpoint more precisely the persistence time for each experiment.

Fig. (III,12)

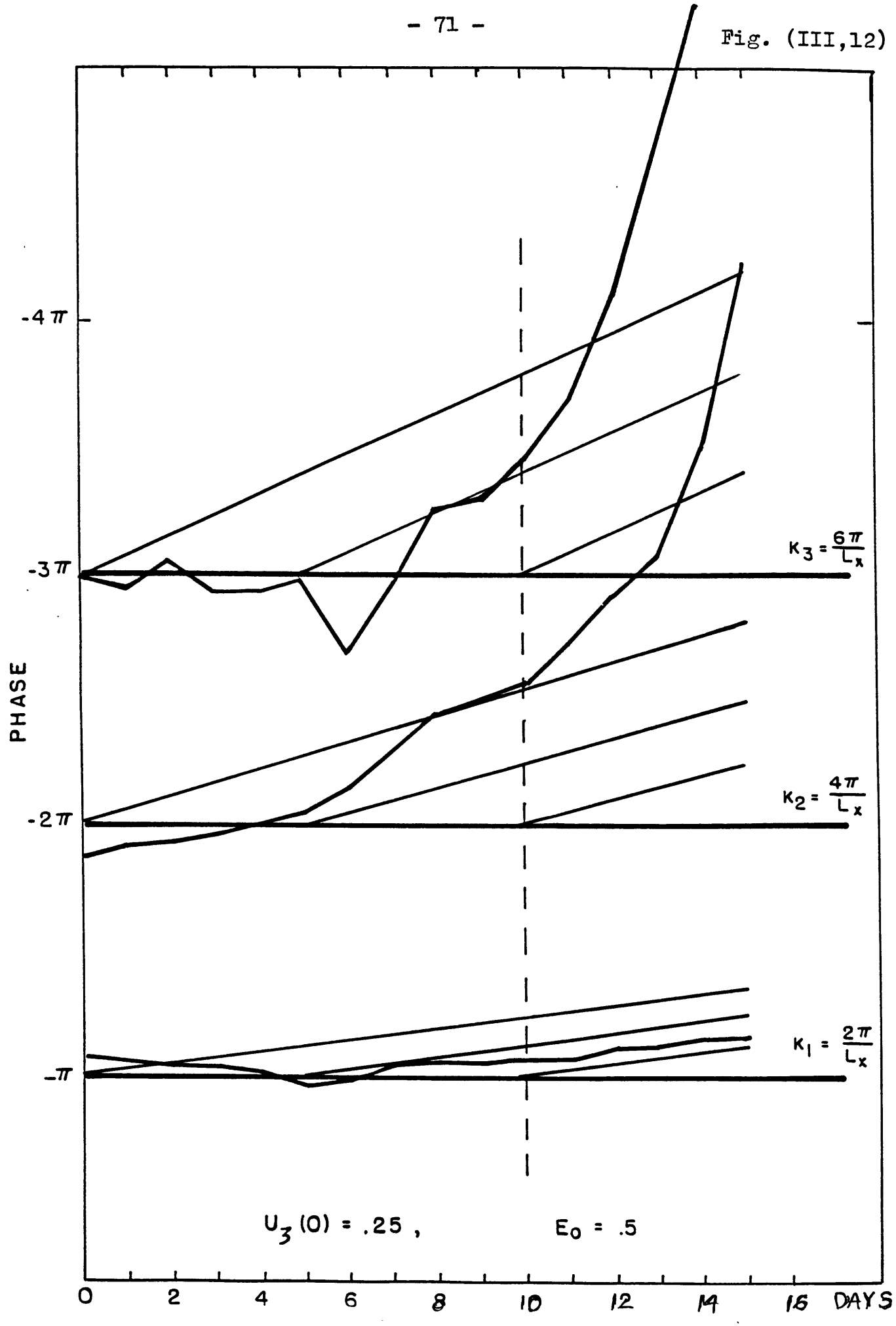
-4π
-3π
-2π
-π
PHASE
$K_3 = \frac{6\pi}{L_x}$
$K_2 = \frac{4\pi}{L_x}$
$K_1 = \frac{2\pi}{L_x}$
$U_3(0) = .25$,
$E_0 = .5$
0
2
4
6
8
10
12
14
16
DAYS

Fig. (III,13)

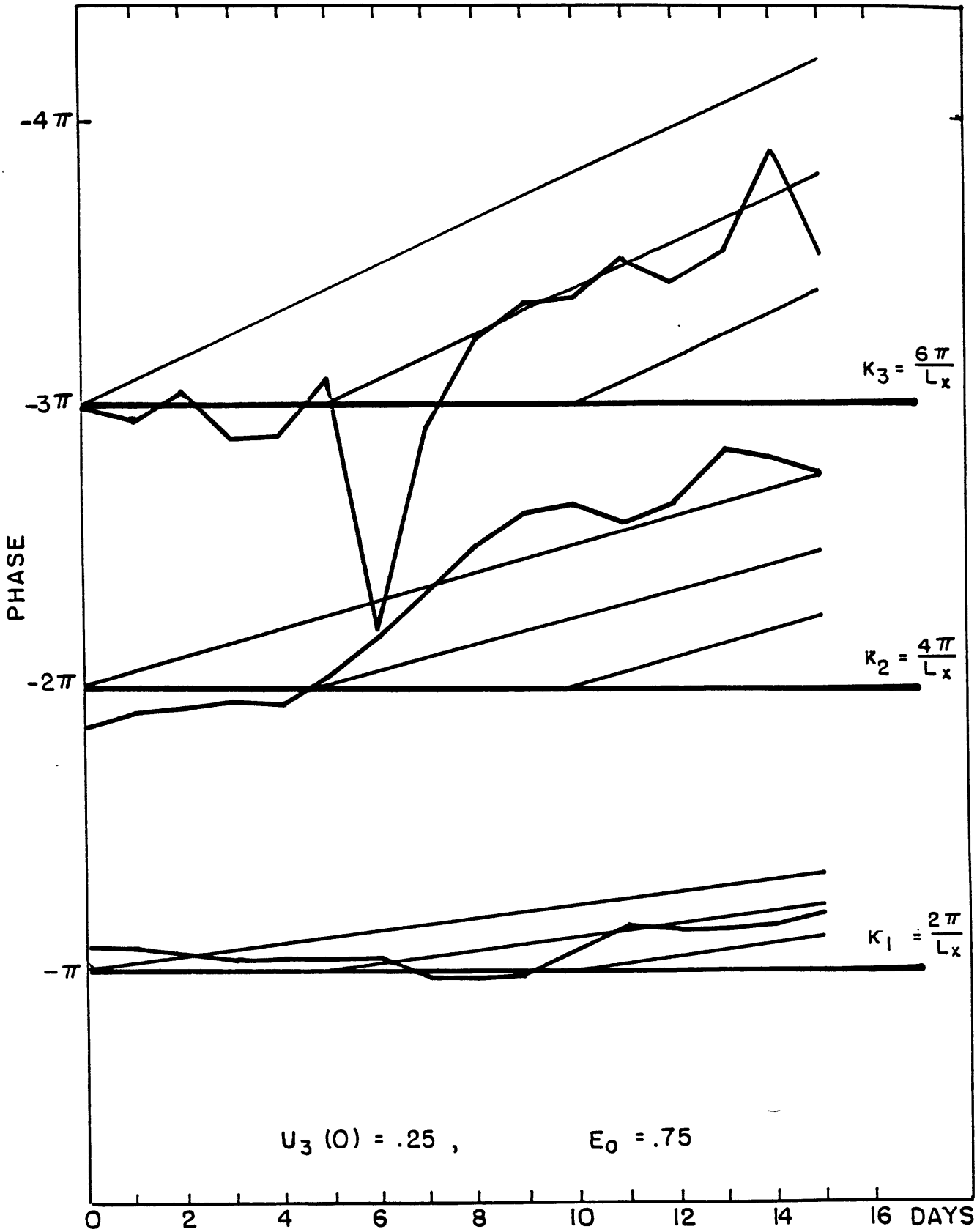
-4π
-3π
-2π
-π
PHASE
$K_3 = \frac{6\pi}{L_x}$
$K_2 = \frac{4\pi}{L_x}$
$K_1 = \frac{2\pi}{L_x}$
$U_3(0) = .25$,
$E_0 = .75$
0
2
4
6
8
10
12
14
16 DAYS

Chapter IV

Vortex-Wave Interaction

Section (IV,a). The effect of viscosity

In this chapter we will examine the effects of transient eddies and friction upon the coherent solution (II,20-21). We introduce two kinds of dissipation into the modal model previously described: linear drag and Newtonian cooling.

In the basis $\{\phi_n\}$, the two kinds of friction take the form:

Newtonian cooling $\quad \partial_t A_{i_{xx}} + \ldots = -\mu\alpha_{in}A_n$

Linear drag $\quad \partial_t A_{i_{xx}} + \ldots = -\nu(A_{i_{xx}} - \zeta_{in}A_n)$

The Newtonian cooling penalizes long scales more than shorter scales and baroclinic eigenmodes more than barotropic ones; linear drag is not scale selective.

The effect of the two kinds of dissipations upon the coherent solution (II,20) is illustrated in diagram (IV,1). Curve I represents the time evolution of the kinetic energy of (II,21) when acted upon by Newtonian cooling; curve II gives the kinetic energy decay when the same solution is acted upon by linear drag. The coefficients μ and ν are set equal to $(14 \text{ days})^{-1}$. The linear drag is more efficient than Newtonian cooling in dissipating the coherent structure.

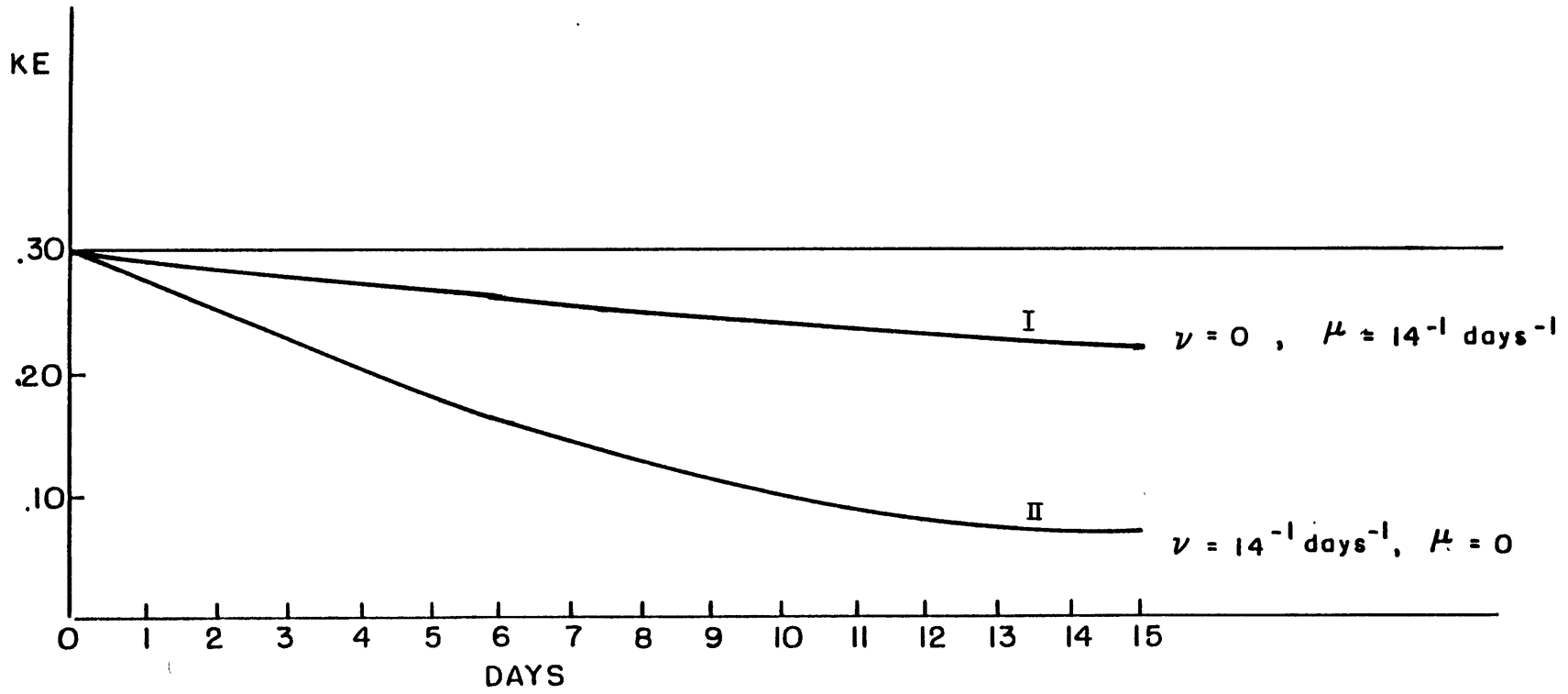
KE
.30
.20
.10
I
$\nu = 0$, $\mu = 14^{-1}$ days^{-1}
II
$\nu = 14^{-1}$ days^{-1}, $\mu = 0$
0 1 2 3 4 5 6 7 8 9 10 11 12 13 14 15
DAYS

Fig. (IV,1)

Green (1976) suggested that the persistence of the 1976 block over the British Isles could be accounted for by eddy flux of westerly momentum out of the blocked region, flux accomplished by transient eddies moving along the branches of the split flow. Later, Illari (1980) computed the eddy forcing of potential vorticity during the above-mentioned episode. She found that the intensity of the eddy forcing was quite strong and out of phase by $\pi/2$ with respect to the time-mean circulation.

The effect of transient eddies of different scales on the time-mean flow was also investigated by Hoskins et al. (1983). The mean flow forcing by high-pass eddies and by low-pass eddies is well approximated by the meridional derivative of the horizontal divergence of the vector

$$E = (\widehat{v''^2} - \widehat{u''^2},\ -\widehat{u''v''})$$

where, from now on, the "hat" stands for time average. In particular, data from one blocking episode (26 November - 7 December 1981) gave an indication of a positive feedback of the synoptic eddies onto the mean blocking flow.

Section (IV,b). Vortex-wave interaction; eddy forcing

These and other works on the feedback of transient eddies on the time-mean circulation motivated the following theoretical analysis. Using the modal model introduced in Chapter II, we will study the nonlinear interaction between a transient wave and a stationary vortex pair.

Let us consider the barotropic version of (II,13) ($A_3 \equiv A_4 = 0$):

$$\left\{\begin{array}{l} \partial_t(A_{1xx} - \ell_1^2 A_1) + U_1(A_{1xxx} - K_1 A_{1x}) + \gamma_{121}(A_1 A_{2xxx} - A_{2x} A_{1xx}) + \\ + \gamma_{121} A_{2x} A_1 (K_1 - K_2) - 2\gamma_{121}(A_2 A_{1xxx} - A_{1x} A_{2xx}) - 2\gamma_{121} A_{1x} A_2 (K_2 - K_1) \\ + \delta_{121}(A_1 A_2)_x/2 = (K_2 - K_1)\gamma_{121}\overline{A_1 A_{2x}} \\ \\ \partial_t(A_{2xx} - \ell_2^2 A_2) + U_2(A_{2xxx} - K_2 A_{2x}) + \gamma_{121}(A_{1xxx} A_1 - A_{1x} A_{1xx}) + \\ + \delta_{222}(A_2^2)_x/2 + \delta_{211}(A_1^2)_x/2 = 0 \end{array}\right.$$

where $U_1 = \varepsilon_{111}\bar{u}_1$, $\quad [\bar{u} = (\bar{u}_1, 0)]$,

$U_2 = \varepsilon_{122}\bar{u}_1$,

$\ell_i^2 = \zeta_{ii} - \alpha_{ii}$,

and where the feedback over the mean wind has been neglected. Furthermore, let $\delta_{211}/2 \simeq 0$ (see appendix C), and let's define $\delta_{222}/2 \equiv \delta$, $\gamma_{121} \equiv \gamma$. The previous system reduces to

$$\begin{cases} \partial_t(A_{1xx} - \ell_1^2 A_1) + U_1(A_{1xxx} - K_1 A_{1x}) = \gamma\{A_{2x}A_{1xx} - A_1 A_{2xxx} + \\ +2A_2 A_{1xxx} - 2A_{1x}A_{2xx} + (K_2 - K_1)(2A_{1x}A_2 + A_{2x}A_1 - \overline{A_{1x}A_2})\} \end{cases} \quad (IV,1)$$

$$\partial_t(A_{2xx} - \ell_2^2 A_2) + U_2(A_{2xxx} - K_2 A_{2x}) + \delta(A_2^2)_x = \gamma(A_{1x}A_{1xx} - A_1 A_{1xxx}) \quad (IV,2)$$

γ (=.2) is the vortex-wave interaction coefficent. In fact, if γ were zero (IV,1) and (IV,2) would reduce to:

$$\begin{cases} \partial_t(A_{1xx}^{(0)} - \ell_1^2 A_1^{(0)}) + U_1(A_{1xxx}^{(0)} - K_1 A_{1x}^{(0)}) = 0 \quad (IV,3) \\ \partial_t(A_{2xx}^{(0)} - \ell_2^2 A_2^{(0)}) + U_2(A_{2xxx}^{(0)} - K_2 A_{2x}^{(0)}) + \delta(A_2^2)_x = 0 \quad (IV,4) \end{cases}$$

that is, a linear Rossby wave and a solitary wave (obeying the KdV dynamics) without mutual interaction. Next, suppose that γ is small but different from zero. Then equations (IV,3) and (IV,4) give the zero-order approximation of the streamfunction in power series of the interaction coefficient:

$$A_1 = A_1^{(0)} + \gamma A_1^{(1)} + \gamma^2 A_1^{(2)} + \ldots$$

$$A_2 = A_2^{(0)} + \gamma A_2^{(1)} + \gamma^2 A_2^{(2)} + \ldots$$

The solution of (IV,3), (IV,4) is:

$$\begin{cases} A_2^{(0)} = P\ \mathrm{sech}^2\ Qx & P = 3K_2U_2/(2\delta) \\ & Q = \sqrt{K_2/2} \end{cases}$$

$$A_1^{(0)} = a\ \sin(\Omega_1 x - \omega t), \quad \omega = U_1\Omega_1\frac{\Omega_1^2 + K_1}{\Omega_1^2 + \ell_1^2} \quad \text{or} \quad c = U_1 - \frac{(\ell_1^2 - K_1)U_1}{\Omega_1^2 + \ell^2}$$

At the first order:

$$\begin{aligned} &\partial_t(A_{1xx}^{(1)} - \ell_1^2 A_1^{(1)}) + U_1(A_{1xxx}^{(1)} - K_1 A_{1x}^{(1)}) = \{A_{2x}^{(0)}A_{1xx}^{(0)} - A_1^{(0)}A_{2xxx}^{(0)} + \\ &+ 2A_2^{(0)}A_{1xxx}^{(0)} - 2A_{1x}^{(0)}A_{2xx}^{(0)} + (K_2 - K_1)(2A_{1x}^{(0)}A_2^{(0)} - A_{2x}^{(0)}A_1^{(0)} - \\ &- \overline{A_{1x}^{(0)}A_2^{(0)}})\} \end{aligned} \tag{IV,5}$$

$$\begin{aligned} &\partial_t(A_{2xx}^{(1)} - \ell_2^2 A_2^{(1)}) + U_2(A_{2xxx}^{(1)} - K_2 A_{2x}^{(1)}) + 2\delta(A_2^{(0)}A_2^{(1)})_x = \\ &= A_{1x}^{(0)}A_{1xx}^{(0)} - A_1^{(0)}A_{1xxx}^{(0)} = 0 \end{aligned} \tag{IV,6}$$

The forcing in equation (IV,6) turns out to be zero. Thus, at the first-order in γ, the vortex is not yet affected by the wave. We are left with the linear equation (IV,5) forced by a complicated function of the zero-order solution. The quantity we are interested in is the eddy vorticity forcing $J(\psi'',q'')$ averaged in time. If we start off with a stationary vortex, the transients up to order γ have projection on the

first normal mode ϕ_1 alone. The Jacobian of such streamfunction has projection on the second mode, that is:

$$J(A_1\phi_1 e^{z/2},\ \nabla^2(A_1\phi_1 e^{z/2}) + A_1(\phi_{1_{zz}} - \tfrac{1}{4}\phi_1)e^{z/2}) = \tag{IV,7}$$

$$= \gamma_{121}(A_1 A_{1_{xxx}} - A_{1_x}A_{1_{xx}})\phi_2\ e^{z/2}$$

From the expansion of A_1 in power series of γ we get

$$\gamma(A_1 A_{1_{xxx}} - A_{1_x}A_{1_{xx}}) = \gamma(A_1^{(0)}A_{1_{xxx}}^{(0)} - A_{1_x}^{(0)}A_{1_{xx}}^{(0)}) + \gamma^2(A_1^{(0)}A_{1_{xxx}}^{(1)} +$$

$$+ A_1^{(1)}A_{1_{xxx}}^{(0)} - A_{1_x}^{(0)}A_{1_{xx}}^{(1)} - A_{1_x}^{(1)}A_{1_{xx}}^{(0)}) \quad + \ O(\gamma^3)$$

Again, from the expression of $A_1^{(0)}$ we see that the order γ forcing is zero, consistently with the fact that the correction to A_2 is order γ^2. Thus, in the limit of weak vortex-wave interaction, the divergence of the eddy flux of potential vorticity is given by:

$$\gamma^2(\widehat{A_1^{(0)}A_{1_{xxx}}^{(1)}} + \widehat{A_1^{(1)}A_{1_{xxx}}^{(0)}} - \widehat{A_{1_x}^{(0)}A_{1_{xx}}^{(1)}} - \widehat{A_{1_x}^{(1)}A_{1_{xx}}^{(0)}})\phi_2\ e^{z/2} \tag{IV,8}$$

where the time average is taken over a period of the transient Rossby wave.

We seek solutions of (IV,5) in the form:

$$A_1^{(1)} = S(x)\ \sin\ (\Omega_1 x - \omega t) + C(x)\ \cos\ (\Omega_1 x - \omega t) \tag{IV,9}$$

The right-hand side of (IV,5) can be further simplified assuming L_x very large or infinite. In this case

$$\overline{A_{1_x}^{(0)} A_2^{(0)}} = \frac{1}{L_x} \int_0^{L_x} A_{1_x}^{(0)} A_2^{(0)} \, dx \quad \to \quad 0 \qquad \text{(IV,10)}$$

Hence, the right-hand side of (IV,5) becomes:

$$\begin{aligned} \text{r.h.s.} = a \sin(\Omega_1 x - \omega t)\{(K_2 - K_1)A_{2_x}^{(0)} - A_{2_{xxx}}^{(0)} - \Omega_1{}^2 A_{2_x}^{(0)}\} \\ + a \cos(\Omega_1 x - \omega t)\{2(K_2 - K_1)\Omega_1 A_2^{(0)} - 2\Omega_1{}^3 A_2^{(0)}\} \end{aligned} \qquad \text{(IV,11)}$$

Substituting (IV,9) and (IV,11) into (IV,5) and defining the new constants

$$\begin{aligned} \sigma &= \omega - 3U_1\Omega_1 \\ \rho &= 2\Omega_1\omega - 3\Omega_1{}^2 U_1 - K_1 U_1 \\ \eta &= K_2 - K_1 - \Omega_1{}^2 \end{aligned} \qquad \text{(IV,12)}$$

we obtain the following system determining S and C:

$$\begin{cases} U_1 S_{xxx} + \sigma C_{xx} + \rho S_x = a(\eta A_{2_x}^{(0)} - A_{2_{xxx}}^{(0)}) \\ U_1 C_{xxx} - \sigma S_{xx} + \rho C_x = 2a\Omega_1 \eta A_2^{(0)} \end{cases} \qquad \text{(IV,13)}$$

Equation (IV,13) can be solved expanding $A_2^{(0)}$ in Fourier series. Strictly speaking, in a domain of finite length L_x, the term $\overline{A_{1_x}^{(0)} A_2^{(0)}}$ should be considered in the r.h.s. of (IV,5). This time-dependent forcing introduces a new term in (IV,9) which is a function of t alone. The eddy forcing associated with it is, however, independent of x. Let

$$\operatorname{sech}^2 Qx = \sum_n \alpha_n \cos k_n x \ , \qquad k_n = \frac{2\pi n}{L_x}$$

and $S = \Sigma\, S_n \cos k_n x$, $C = \Sigma\, C_n \sin k_n x$, where the properties of symmetry around x = 0 of sech^2 have been used. Then:

$$\begin{cases} S_n(U_1 k_n^3 - \rho k_n) + C_n(-k_n^2 \sigma) = aPk_n \alpha_n (k_n^2 - \eta) \\ S_n(\sigma k_n^2) + C_n(\rho k_n - U_1 k_n^3) = 2a\Omega_1 \eta P \alpha_n \end{cases} \qquad \text{(IV,14)}$$

Note that a resonance occurs when

$$-k_n^2(U_1 k_n^2 - \rho) + (k_n^2 \sigma)^2 = 0$$

If one of the allowed wavelengths satisfies the dispersion relation of the homogeneous problem, then it is reasonable to expect that the vortex interacts strongly with the incident wave or, in other words, that the vortex is "unstable" for such scales (at resonance, however, the expansion breaks down).

By using (IV,9) and the expression of $A_1^{(0)}$, the eddy forcing (IV,8) becomes:

$$\widehat{J(\psi'',q'')} = \gamma^2\phi_2 e^{z/2} a\{(S_{xxx} - 3\Omega_1 C_{xx} - 2\Omega_1^2 S_x)\ \widehat{\sin^2}(\Omega_1 x-\omega t) -$$

$$- \Omega_1(2S_x\Omega_1 + C_{xx})\ \widehat{\cos^2}(\Omega_1 x-\omega t)\}$$

$$= \gamma^2 a\phi_2 e^{z/2}\{S_{xxx} - 4\Omega_1 C_{xx} - 4\Omega_1^2 S_x\}/2 \qquad \text{(IV,15)}$$

The previous relation, expressed in terms of the C_ns and S_ns, takes the form

$$\gamma^2 \frac{a^2}{2} P\phi_2 e^{z/2} \sum_n (S_n k_n^3 + 4\Omega_1 C_n k_n^2 + 4\Omega_1^2 k_n S_n) \sin k_n x \qquad \text{(IV,16)}$$

that is, antisymmetric around the axes x = 0 and y = 0. The forcing is also independent of the phase of the incident Rossby wave.

Figure (IV,2) shows the eddy forcing obtained with incident Rossby waves having wavenumbers $2\pi n/L_x$, n = 1, . . ., 5. Only the first half of the zonal domain is shown; the complete pattern is antisymmetric around x = 0. Apart from a small near-field response, the eddy forcing is basically monochromatic. This is because of the resonant nature of the left-hand side of equation (IV,14). This is especially the case with incident Rossby waves having wavenumbers 2 and 5; they excite a resonant response at wavenumber 7. We stress that these results apply to a single incident wave; because of the nonlinear nature of the problem, the effect due to eddies that are not monochromatic is not the sum of the effects caused by each single incident transient wave.

Fig. (IV,2)

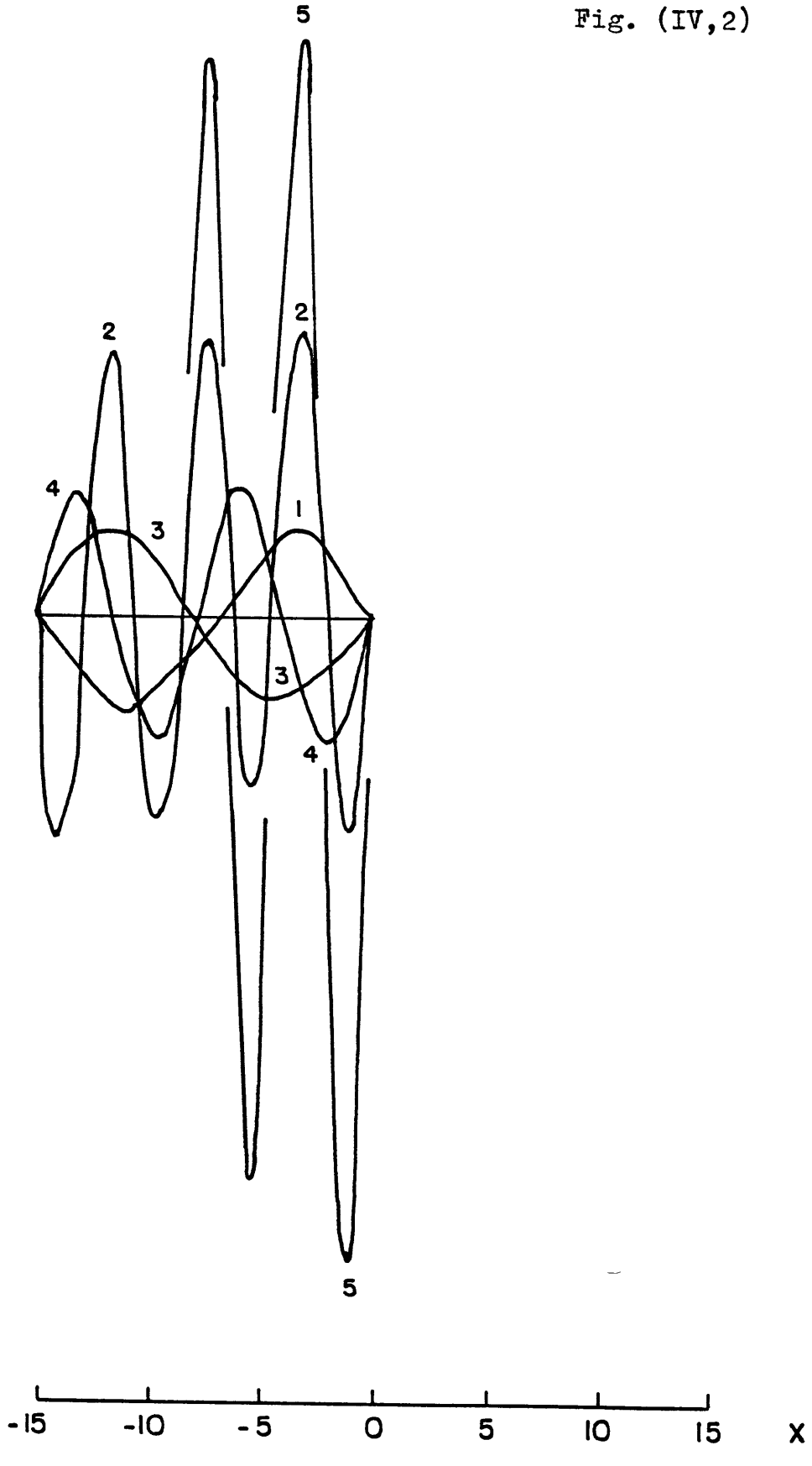

The picture for shorter incident waves is completely different. Figure (IV,3,a) shows the eddy forcing due to eddies with wavenumbers between 6 and 16. The forcing is now localized against the vortex pair and especially strong at higher wavenumbers. The effect of very short eddies is thus systematic and consistent with a westward motion of the blocking pattern [see Figure (IV,3,b)]. Intuitively, the reason for this completely different behavior is not difficult to grasp if one thinks of the analogy of an electromagnetic wave entering a medium with a different diffraction index. Shorter scale incident waves make several oscillations within the region of the larger scale, straining flow (the blocking pattern) so that they can feel its effect systematically (Shutts,1983). For incident waves with scales longer than, or comparable to, the scale of the block this is not possible. The analogy is thus the geometrical and physical optics; the phenomenology of these two limiting cases is completely different.

The fact that eddy forcing is so neat at short scales is encouraging for the parameterization of its effect over the mean state $A_2^{(0)}$. The effect of short scales is, in fact, the one that needs to be parameterized in any model in which the resolution is a limiting factor.

In the limit of $\Omega_1 \to \infty$ [1], the constants in (IV,12) tend to

$$\begin{aligned} \omega &\to U_1\Omega_1 \\ \sigma &\to -2\Omega_1 U_1 \\ \rho &\to -\Omega_1^2 U_1 \\ \eta &\to -\Omega_1^2 \end{aligned} \qquad \text{(IV,17)}$$

---

[1] Consistency requires $\gamma\Omega_1 \ll 1$.

Fig. (IV,3)

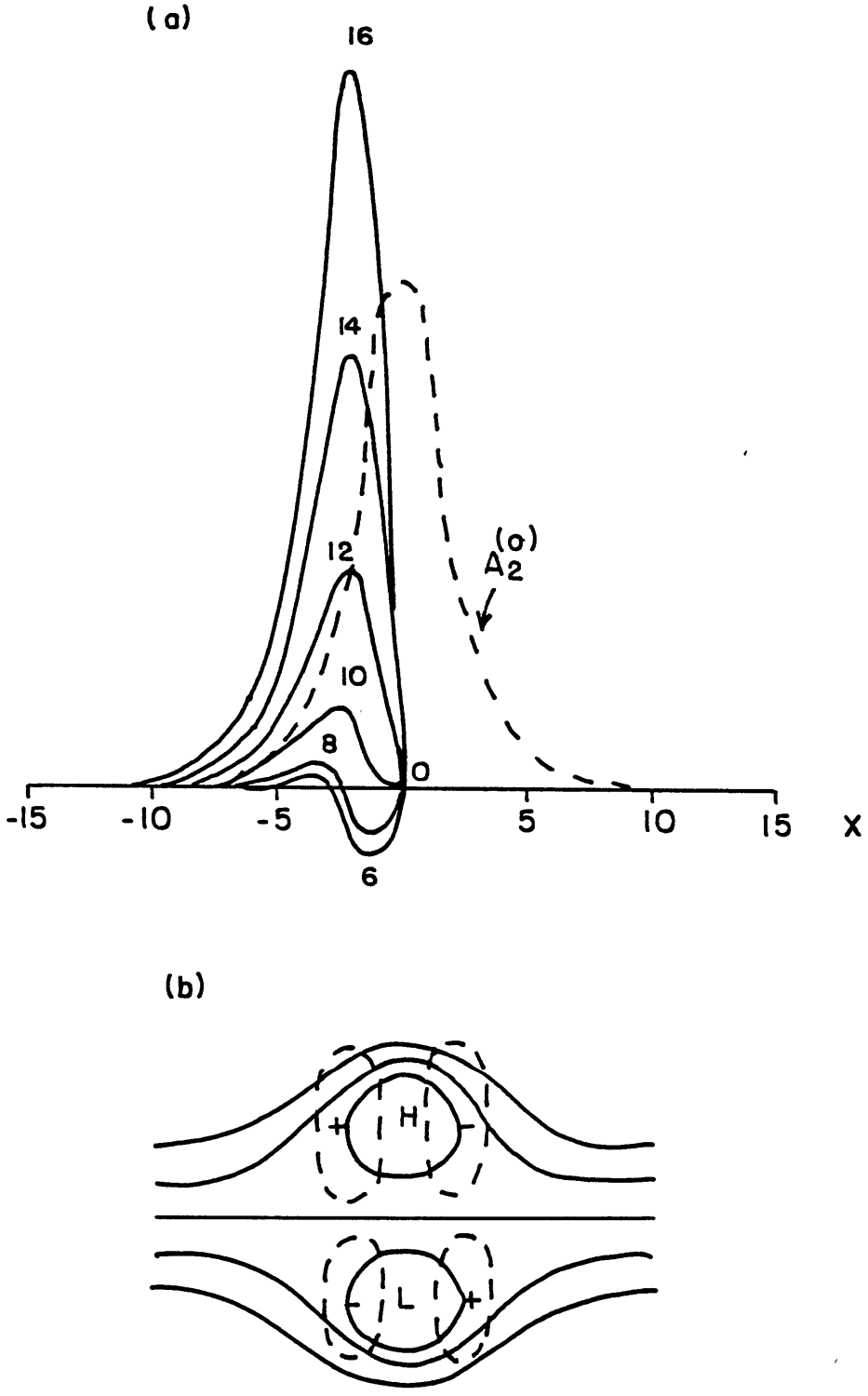

Consequently, the behavior of the leading terms of C and S for large Ω_1 is [after (IV,13)]:

$$S \approx -3A_2^{(0)} \frac{a}{U_1}$$

$$C \approx 2a\,\Omega_1 \left(\int_{-\infty}^{x} A_2^{(0)}\, dx \right)/U_1 \qquad \text{(IV,18)}$$

Hence, in the limit of large Ω_1, the eddy forcing (IV,15) becomes

$$\widehat{J(\psi'',q'')} \approx 2\gamma^2 \frac{a^2\Omega_1{}^2}{U_1} \widehat{\psi}_x \qquad \text{(IV,19)}$$

Expression (IV,19) is the parameterization of the forcing due to short eddies in terms of the mean state $A_2^{(0)}\phi_2\, e^{z/2}$ (note that this forcing is energetically neutral since this analytic analysis is inviscid). Its magnitude is proportional to the energy density of the incoming eddy and to the meridional velocity of the mean state divided by the phase speed of the incident wave, which gives a measure of the distortion exerted on the eddy field by the larger-scale mean flow.

Section (IV,c). Feedback on the mean state

At the second order in γ we get the equation governing the "modified flow" $A_2^{(2)}$. The equation is:

$$-c^{(2)}[A_{2xx}^{(0)} - \ell_2^2 A_2^{(0)}]_x + U_2(A_{2xxx}^{(2)} - K_2 A_{2x}^{(2)}) + 2\delta(A_2^{(0)} A_2^{(2)})_x = \quad \text{(IV,20)}$$

$$= - \text{ eddy forcing}$$

where the eddy forcing is given by the term between parentheses in (IV,8). In writing this equation we assumed that the vortex pair varies on the long time scale $\tau = \gamma^2 t$ like $A_2 = A_2(x - c^{(2)}\tau)$. The introduction of the long time scale is necessary because, as we shall see shortly, a secularity arises in equation (IV,20). In more physical terms, the pattern of eddy forcing shown in Figure (IV,3,b) is pushing the vortex pair upstream; since such forcing is an order γ^2 quantity, its effect is such that the vortex pair will move with an $O(\gamma^2)$ phase speed.

Taking the time average of (IV,20) over a period of the Rossby wave we get:

$$-c^{(2)}[A_{2xx}^{(0)} - \ell_2^2 A_2^{(0)}]_x + U_2(\widehat{A_{2xxx}^{(2)}} - K_2 \widehat{A_{2x}^{(2)}}) + 2\delta(A_2^{(0)} \widehat{A_2^{(2)}})_x = \quad \text{(IV,21)}$$

$$= - \frac{a}{2}\{S_{xxx} - 4\Omega_1 C_{xx} - 4\Omega_1^2 S_x\}$$

where expression (IV,15) has been used. Eq. (IV,21) can be integrated once in x:

$$\widehat{A_{2_{xx}}^{(2)}} - (K_2 - \frac{2\delta}{U_2} A_2^{(0)})\widehat{A_2^{(2)}} = -\frac{a}{2U_2}\{S_{xx} - 4\Omega_1 C_x - 4\Omega_1{}^2 S\} + \qquad \text{(IV,22)}$$

$$+ c^{(2)} \; [A_{2_{xx}}^{(0)} - \ell_2{}^2 A_2^{(0)}]/U_2$$

For very short incident waves, the right-hand side of (IV,22) becomes:

$$\text{r.h.s.} = -\frac{2a^2\Omega_1{}^2}{U_1 U_2} A_2^{(0)} + \frac{c^{(2)}}{U_2}(A_{2_{xx}}^{(0)} - \ell_2{}^2 A_2^{(0)}) \qquad \text{(IV,23)}$$

where expression (IV,19) has been used.

We shall solve (IV,22) and (IV,23) in an infinite domain. When x goes to $\pm\infty$ there is a secularity to be removed. In such limit, (IV,23) reduces to

$$\text{r.h.s.} = -\frac{2a^2\Omega_1{}^2}{U_1 U_2} 4P \; e^{\mp\sqrt{K_2}\, x} + \frac{c^{(2)}}{U_2} \; 4P \; (K_2 - \ell_2{}^2) \; e^{\mp\sqrt{K_2}\, x} \qquad \text{(IV,24)}$$

Since $e^{\mp\sqrt{K_2}\,x}$ identically satisfies the left-hand side of (IV,22), expression (IV,24) must be identically zero. This implies:

$$c^{(2)} = -\frac{2a^2\Omega_1{}^2}{U_1[\ell_2{}^2 - K_2]} < 0 \qquad \text{(IV,25)}$$

that is, the vortex pair moves upstream with phase speed proportional to the energy density of the eddy. Thus, substituting back (IV,25) into (IV,23), and using the expression for the zero-order solution $A_2{}^{(0)}$ equation (IV,22) finally reduces to:

$$\widehat{A_2^{(2)}}_{xx} - K_2\widehat{A_2^{(2)}} + \frac{2\delta P}{U_2}\,\mathrm{sech}^2\left(\frac{\sqrt{K_2}}{2}x\right)\widehat{A_2^{(2)}} = \frac{3a^2\Omega_1{}^2PK_2}{U_1U_2(\ell_2{}^2 - K_2)}\,\mathrm{sech}^4\left(\frac{\sqrt{K_2}}{2}x\right) \qquad \text{(IV,26)}$$

This equation can be solved analytically. For $\widehat{A_2^{(2)}}$, we seek a solution in the form:

$$\widehat{A_2^{(2)}} = \frac{3a^2\Omega_1{}^2P}{U_1U_2(\ell_2{}^2 - K_2)}\sum_{n=1}^{\infty} c_n\,\mathrm{sech}^{2n}\left(\frac{\sqrt{K_2}}{2}x\right) \qquad \text{(IV,27)}$$

By using the relation

$$\frac{d^2}{dx^2}\,\mathrm{sech}^{2n}\left(\frac{\sqrt{K_2}}{2}x\right) = n^2K_2\,\mathrm{sech}^{2n}\left(\frac{\sqrt{K_2}}{2}x\right) - \frac{n}{2}K_2(2n+1)\,\mathrm{sech}^{2n+2}\left(\frac{\sqrt{K_2}}{2}x\right),$$

The following recurrence relations are obtained:

$$c_1 = 0$$

$$c_2 = \frac{1}{3}$$

$$(n^2 - 1)c_n = [n^2 - \frac{3}{2}n - \frac{5}{2}]c_{n-1}, \quad n \geq 3$$

Since (Gauss test)

$$\frac{c_{n-1}}{c_n} = 1 + \frac{1.5}{n} + 0(\frac{1}{n^2})$$

series (IV,27) is convergent for all x. The modified flow $\widehat{A_2}^{(2)}$ is shown in Figure (IV,4) where it is normalized to 1 in order to compare it with the zero-order solution. The effect of short wave eddies is to push the vortex pair westward and to steepen it.

Fig. (IV,4)

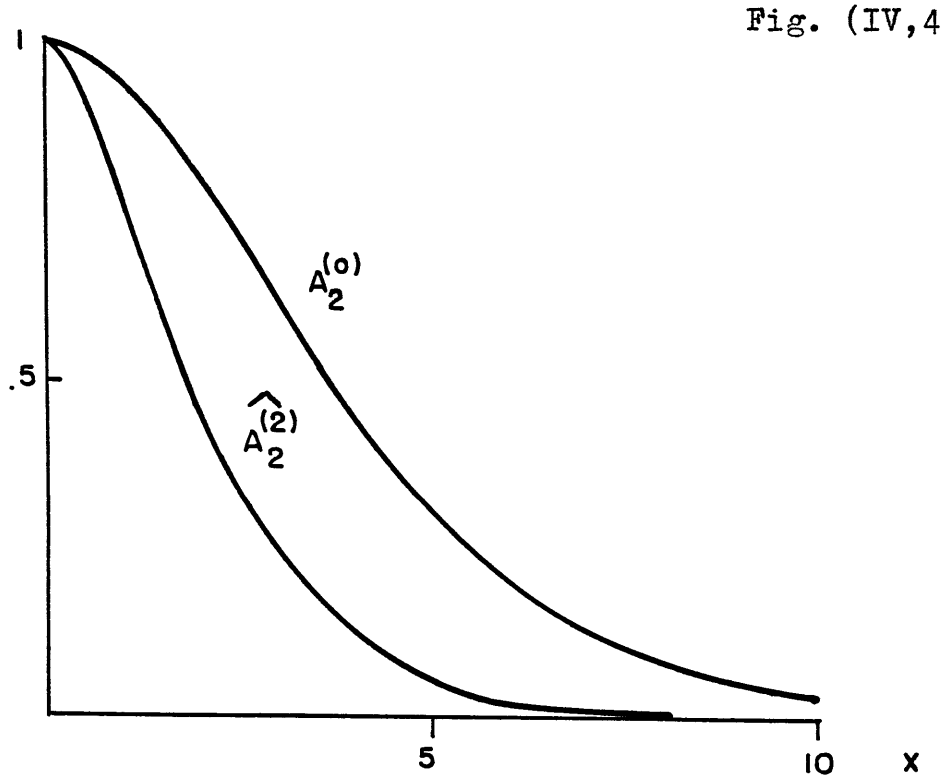

Section (IV,d). Feedback over the transient

A better physical insight into the interaction between the vortex pair and the eddy can be obtained looking at the first-order correction to $A_1^{(0)}$.

Up to order γ^2, the incident Rossby wave is:

$$A_1 = a \sin(\Omega_1 x - \omega t) + \gamma S(x) \sin(\Omega_1 x - \omega t) + \gamma C(x) \cos(\Omega_1 x - \omega t) \quad \text{(IV,28)}$$

In the limit of short incident Rossby waves we have already shown that [see (IV,18)]

$$\omega \to U_1 \Omega_1$$

$$S \to -3\frac{a}{U_1} A_2^{(0)}$$

$$C \to 2a \frac{\Omega_1}{U_1} \int_{-\infty}^{x} A_2^{(0)} dx$$

Thus, equation (IV,28) can be written as:

$$A_1 = M(x)\ \sin[\Omega_1(x - U_1 t) + \theta(x)] \qquad \text{(IV,29)}$$

where

$$M \cos\theta = a + \gamma S$$

$$M \sin\theta = \gamma C$$

and

$$\tan\theta = \frac{\gamma C}{a + \gamma S} \approx \frac{\gamma C}{a}$$

Hence, at the leading order in γ:

$$\theta \approx \frac{\gamma C}{a} = 2\gamma \frac{\Omega_1}{U_1} \int_{-\infty}^{x} A_2^{(0)} dx$$

$$M \approx a$$

(IV,29) becomes:

$$A_1 \approx a\ \sin[\Omega_1 (x - U_1 t + \frac{2\gamma}{U_1} \int_{-\infty}^{x} A_2^{(0)} dx)]$$

A local wavenumber can be defined in a W.K.B. sense:

$$\Omega_1 [1 + \frac{2\gamma}{U_1} A_2^{(0)}(x)] > \Omega_1 \qquad \text{(IV,30)}$$

What expression (IV,30) tells us is basically that the incident Rossby wave gets shorter and shorter as it interacts with the vortex pair, and resumes its original wavelength after the interaction is over. In more physical terms, eddies propagating into a split jetstream suffer an east-west compression and north-south extension of their vorticity fields. If this process is viewed in the sense of an initial value problem, local enstrophy cascade is associated with energy transmission to the straining flow (i.e., the blocking pattern). In fact, eddies embedded within the deformation fields of larger scale flows are, on average, strained into filaments so that the constraint of energy and enstrophy conservation demands that energy should appear at progressively larger scales. We stress that these considerations apply to the time-dependent process that corresponds to the straining of eddies by the larger scale motion; the analytical model presented before is relative to an equilibrium configuration in which energy fluxes are zero. It is during the transients which ultimately lead to such equilibrium configuration that energy is exchanged between the strained eddies and the straining flow. Such interesting problems, as well as the effect of friction within the theoretical picture presented here is, however, a much harder problem to solve. Nevertheless, as we shall see, the simple equilibrium theory presented here captures many of the effects that short scale eddies induce on blocking patterns (see, for instance, the numerical computations carried out by Shutts, 1983) and we leave more elaborate theories to future research.

In summary, in Sections (IV,b), (IV,c) and (IV,d) we have analyzed the nonlinear interaction between a barotropic, monochromatic Rossby wave and

the stationary coherent structure. The result of the interaction strongly depends on the wavelength of the incident eddy. Short eddies produce an eddy potential vorticity forcing that pushes the blocking pattern westward and steepens it. We showed that its effect can be parameterized in terms of the meridional velocity of the straining, larger-scale mean flow.

The interaction with longer eddies (zonal wavenumber ≤ 5) produces a strong eddy forcing basically monochromatic whose sign near the vortex center is generally opposite to that of the forcing due to short eddies.

We also looked at how high wavenumber eddies are modified during the interaction; the wavelength of the incident wave becomes shorter owing to the straining effect of the larger-scale flow.

Section (IV,e): Numerical verification

In this section we will see whether the arguments put forward in the previous sections will hold in a less idealized case in which all wavelengths are simultaneously present and when long scale eddies interact with the vortex pair. We will also obtain indications whether the steepening caused by interaction with short waves and the westward correction to the phase speed of the coherent structure can balance the effect of friction.

In order to find answers to these questions we conceived the following experiment.

We initialize the 4-mode model already used in the previous chapter using the stationary solution (II,21). At $t = 0$ we superimpose on it a randomly generated perturbation having the same form as the one used previously with $E_0 = .75$. Dissipation and forcing are added as well. Following several authors (Charney et al, 1981; Shutts, 1983) we chose the relaxation time of the linear drag to be 14 days (the Newtonian cooling relaxation time is also set equal to 14 days). The value of u_3^h (see appendix D), the vertical shear forcing due to differential heating, is set equal to 0.8. Basically, we want to obtain an energy cycle in which the eddy kinetic energy destroyed by friction is substituted by eddy energy converted via the baroclinic instability of the mean wind. If the forcing u_3^h is too small, the system will fall into the Hadley regime (lorenz, 1965). Hence, before initiating the actual experiment, we performed several tests by integrating the model for a long time. In this way we were able to determine the value of u_3^h capable of mantaining a realistic

amount of eddy kinetic energy in the model.

Since one of the purposes of this experiment is to compare the phase speed of the coherent structure embedded in a viscous and turbulent environment with the phase speed that the same structure would have if acted upon only by friction, we neglected the feedback over the mean wind component u_1. In other words, we chose the momentum driving u_1^d in such a way to give exactly zero tendency, that is $\dot{u}_1 = 0$. In this way we make sure that variations in the phase speed of the vortex pair are not caused by variations in the advecting mean wind u_1 (note that the phase speed of (II,21) depends only on u_1).

Figure (IV,5,a) shows the streamfunction at 500 mb after 10 days of integration. For comparison, the state that the coherent structure would reach at the same instant if eddies were not present is plotted in figure (IV,5,b). It can be noticed that, apart from a certain degree of deformation, the coherent structure appears steeper and displaced westward ($\approx$ 1,000 km) when compared to the control, purely dissipative experiment.

Figure (IV,6,a) shows the time-mean of the 500 mb streamfunction computed from day 3 to day 10 (1). We note that a stationary Rossby wave trails the vortex pair. This feature, that is not predicted by the theory of the previous section, incidentally makes the time-mean look much more realistic than the stationary solution (II,21) (compare with Figure (IV,6,b). In particular, the phase of the Rossby wave is such that it enhances the high center while weakening the low center, conferring at the same time a realistic east-west tilt to the blocking structure.

---

(1) A longer averaging period could not be taken because the coherent structure disappeared at t = 12 days.

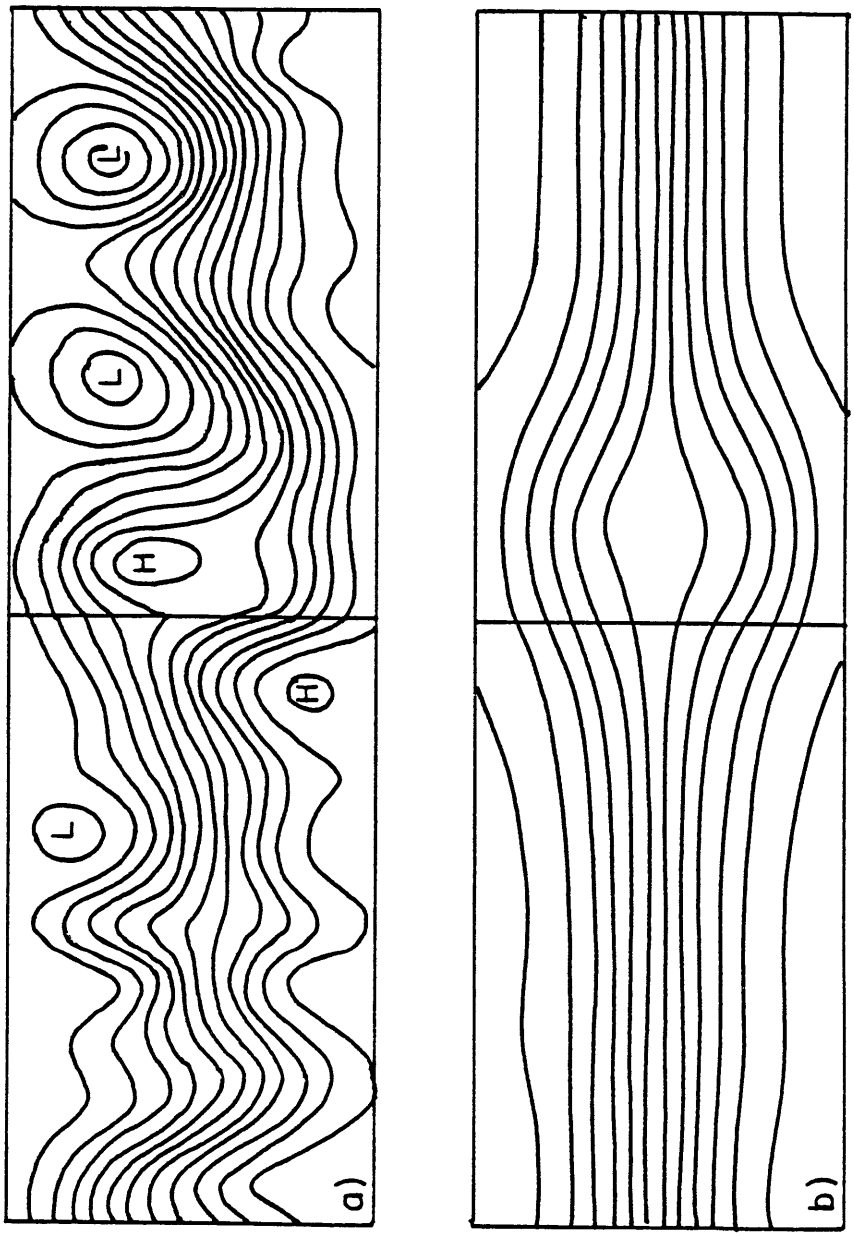

Fig. (IV,5)

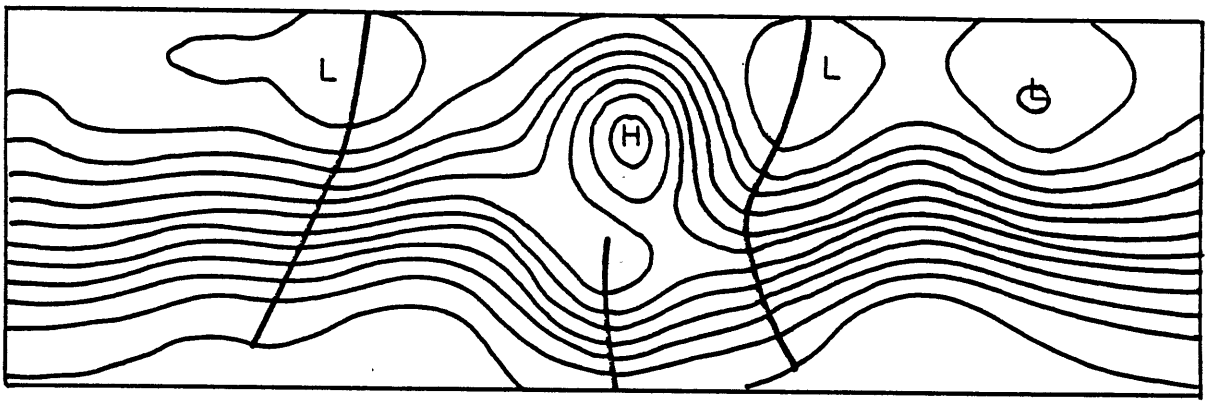

a)

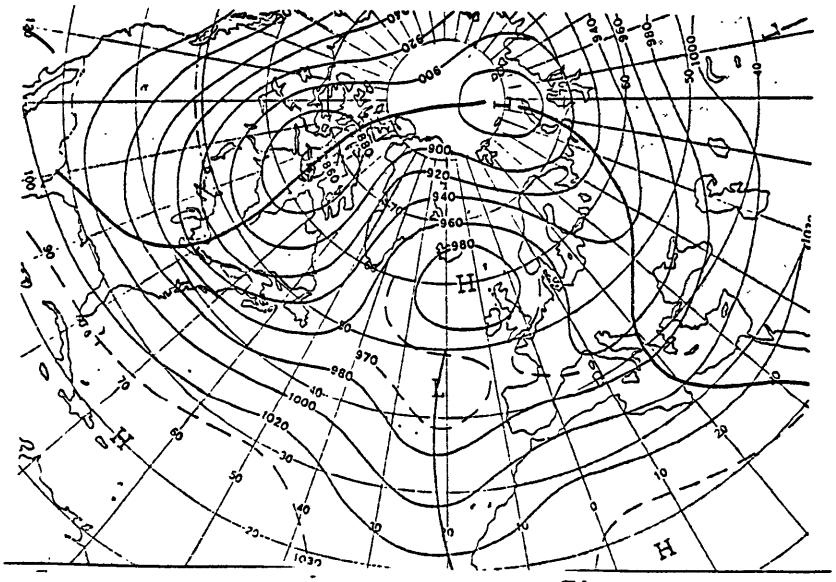

b) JANUARY 1963

Fig. (IV,6)

Figure (IV,7,a) shows the eddy forcing $\widehat{J(\psi'',q'')}$ superimposed on the time-mean potential vorticity at 250 mb,a level at which the forcing is particularly strong. Positive maxima are observed upstream the low center and downstream the high center while negative minima are located upstream the high center and downstream from the low center. Basically, the structure is consistent with the one predicted (see Figure (IV,3)) but a strong north-south asymmetry is again observed. The pattern of eddy forcing shown in Figure (IV,7,a) is typical of all the numerical experiments performed. In particular, it does not depend on the truncation chosen and on the parameterization of the friction.

For comparison, the eddy forcing of potential vorticity computed during the July 1976 drought over the British Isles is reported in Figure (IV,7,b) (after Illari, 1982). We stress the following points:

a) the magnitude of the observed eddy forcing is similar to the one computed in the experiment;

b) positive eddy forcing is observed upstream time-mean potential vorticity minima while negative forcing is observed downstream. In general, the observed forcing pattern is consistent with a westward tendency of the time-mean potential vorticity.

c) in the real case analyzed, the eddy forcing is almost exactly balanced by the mean advection $J(\hat{\psi},\hat{q})$, the frictional term being a negligible residue. The same balance holds in our numerical experiments;

d) the observed eddy vorticity forcing has an equivalent barotropic structure with a strong maximum at $\approx$ 300 mb.

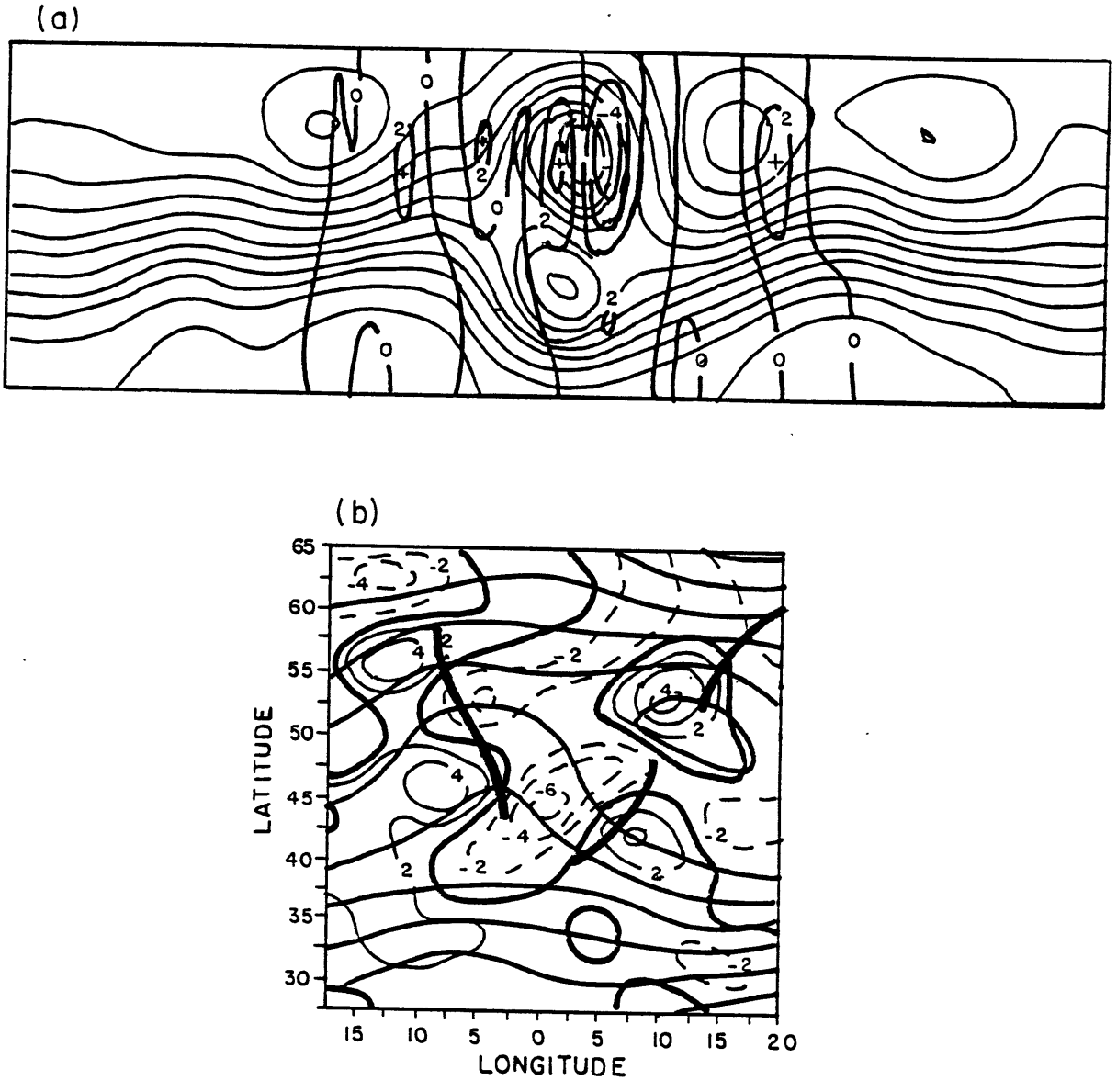

Fig. (IV,7)

The numerical experiment described above suggests that the feedback of short scale transient eddies over the time-mean geopotential field is such that it maintains the time-mean field against mean advection, consistently with Illari's (1982) results. Such positive feedback is also responsible for the steepening and deepening of larger-scale, stationary features of the atmospheric circulation (Shutts, 1983). In particular, there are indications [see Figure (IV,5)] that the eddy forcing can counteract, up to a certain point, the effect of dissipation.

The simple analytical theory presented in this chapter (even though relative to an equilibrium configuration) qualitatively accounts for the above-mentioned effects.

Chapter V

The Formation of the Coherent Structure

In all the numerical experiments analyzed so far, we integrated the modal equations forward in time, starting from an initial condition containing the stationary coherent structure. The subject of this final chapter will be the growth and formation of the coherent structure starting from more general initial conditions.

The basic question we want to address is: which kind of situations will evolve, within the dynamics of our truncated model, into the vortex pair (II, 20)? In other words, we want to define, at least in qualitative terms, the basin of attraction in our phase space of solution (II, 20).

We have seen that the coherent structure projects only upon the normal mode ϕ_2 and that its dynamics is basically of a KdV type. In fact, the coupling between mode ϕ_2 and the modes next to it (mode ϕ_4 in particular) does not make significant modifications in the dynamics, as is clear from the numerical integration represented in Fig. (III,6).

A distinctive feature of the KdV dynamics is the evolution of a sinusoidal initial condition into solitons (Zabusky and Kruskal, 1965). Inspired by this result, we initialized our model (truncated after ϕ_1, ϕ_2, ϕ_3, and ϕ_4) with the initial condition

$$\psi' \Big|_{t=0} = -\phi_2 e^{z/2} \cos \frac{2\pi x}{L_x} \qquad (V,1)$$

that is, with a sinusoidal wave of wavenumber one in the east-west direction and antisymmetric around y = 0. Figure (V,1) shows the time evolution observed; the 500 mb streamfunction pattern is plotted at t = 0, 3, 6, 9, 12, and 15 days, respectively. The initial condition was normalized to one.

The evolution observed can be described in terms of three time intervals. Initially, the tendency of A_2 and the nonlinearity $A_{2_x}A_2$ dominate and the classical overtaking phenomenon occurs: A_2 steepens where it has positive derivatives (see, for instance, Courant and Friedrichs, p. 96). After A_2 has steepened enough, the dispersion ($A_{2_{xxx}}$) becomes important and prevents the formation of a discontinuity. Oscillations of shorter wavelength develop on the right to the shock front and their amplitude increases until each oscillation assumes a shape almost identical to that of an individual coherent structure. Finally, each pulse begins to move uniformly according to the dispersion relation (II,21,a). In Fig.(V,1) at t=15 days three pulses of decreasing amplitudes can be recognized. After a very long time all the pulses merge to the same point (they "pass through" on another without losing their identity); at this point the initial state is almost reconstructed through the nonlinear interaction.

The same behavior is also observed when the initial condition is not a pure ϕ_2 mode. In the experiment shown in Figure (V,2) the initial condition is the sum of (V,1) and of a wave having the meridional structure of mode ϕ_1 and east-west wavenumber 6. It can be noticed that the KdV dynamics of the mode ϕ_2 is not affected by

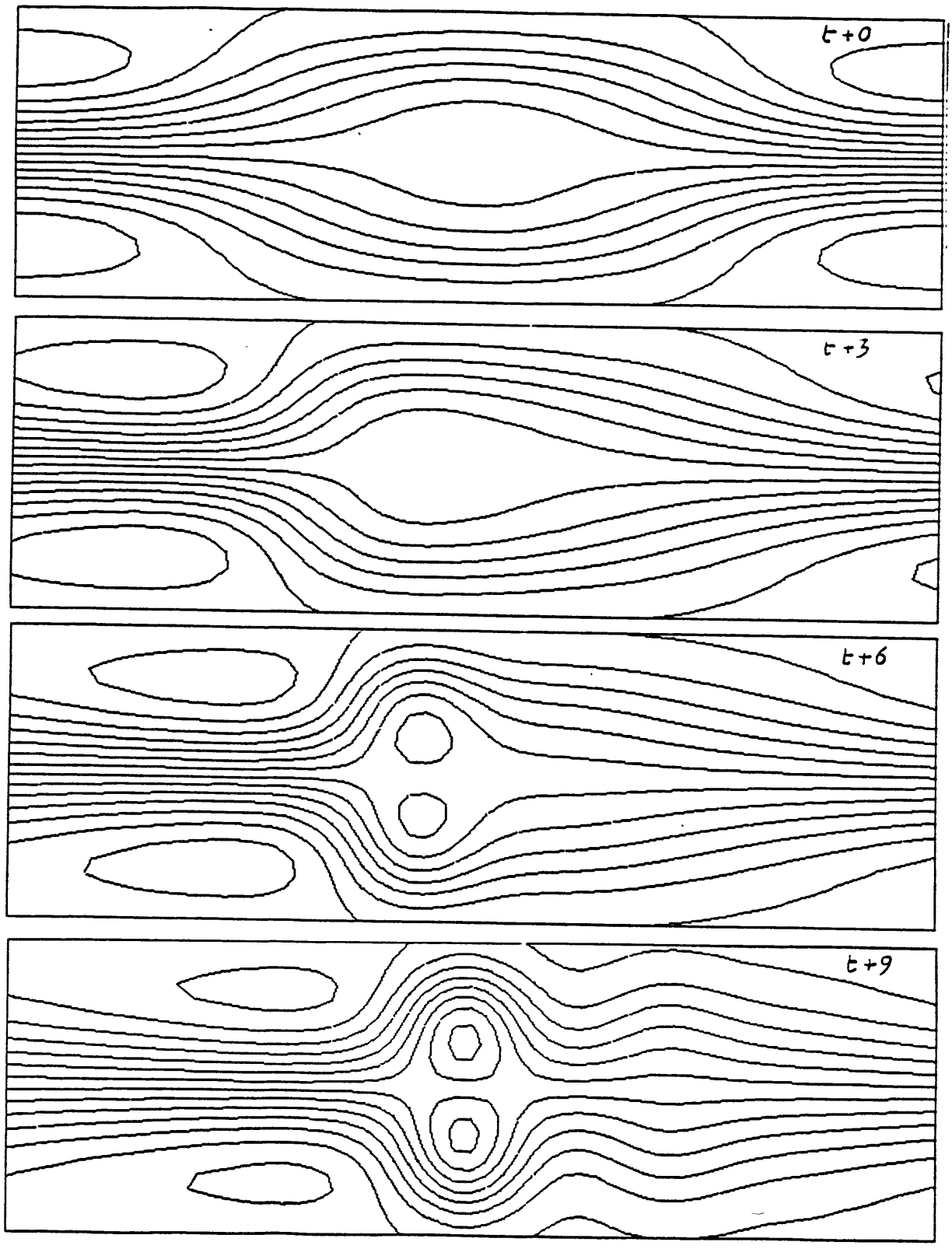

Fig. (V,1)

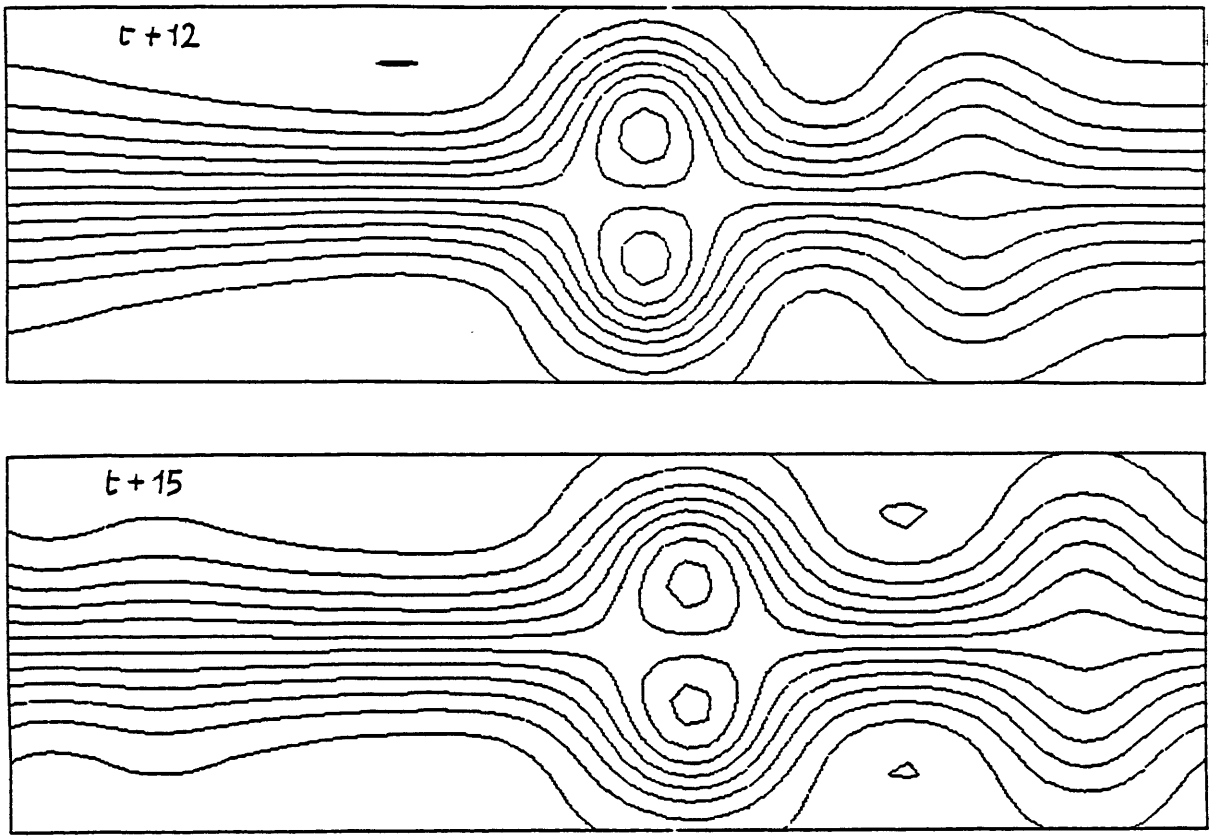

Fig. (V,1)

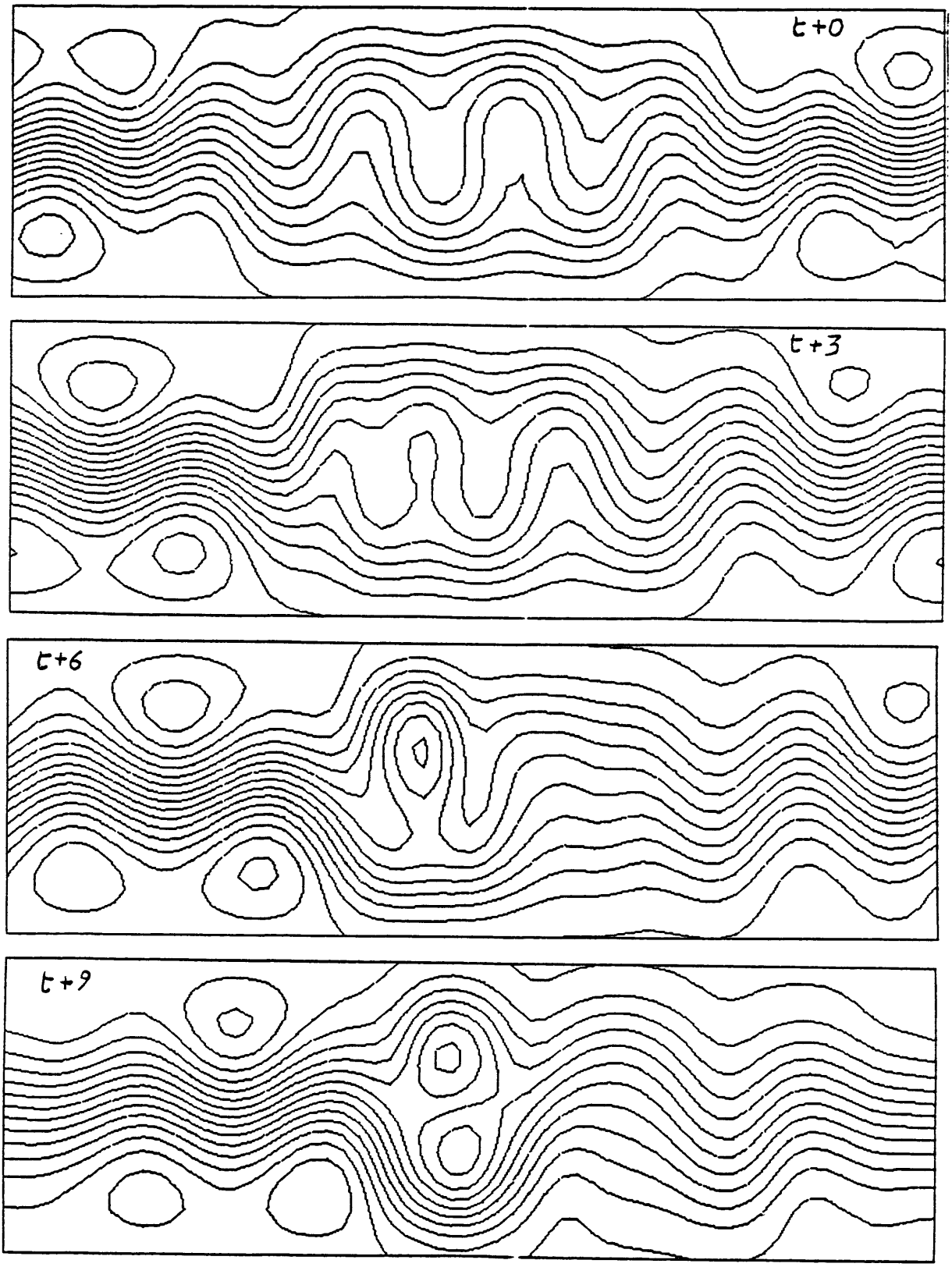

Fig. (V,2)

the nonlinear interaction with the other normal modes.

One interesting characteristic of these time evolutions is that a strong zonal flow is observed upstream to the splitting region, together with strong meridional motion on the western side of the block. This feature is consistent with point d) of Rex's definition.

More generally, numerical experiments along the same line show that:

a) The evolution of (V,1) into the block configuration is also observed when randomly generated perturbations (of the kind described in Chapter III) are superimposed to (V,1);

b) the block formation described above is not affected by friction or by the presence of a baroclinically unstable zonal wind, since growing perturbations have little effect on the KdV dynamics of mode

c) the steepening of the wave proceeds faster and the amplitude attained by the pulse is larger when the initial amplitude is larger;

d) if the initial amplitude of the wave is not large enough the steepening process does not occur. In fact, in order for the wave to steepen, the nonlinearity must be initially larger than dispersion. From (II,18) we see that the condition is satisfied when

$$\frac{\delta_{222}}{2} A_2{}^2 > \varepsilon_{2n2} u_n A_{2xx}$$

In general, for a sinusoidal initial condition with east-west wavenumber K and amplitude B, the condition for the steepening to occur is

$$|B| > \frac{2\varepsilon_{2n2} u_n}{\delta_{222}} K^2 \approx \frac{2\langle \bar{u}\phi_2{}^2 \rangle}{\langle V_y \phi_2{}^3 e^{z/2} \rangle} K^2 \approx 3K^2 \qquad (V,2)$$

This condition is satisfied by long waves, especially wavenumber one. Shorter waves basically follow a linear dynamics with phase speed given by the linear dispersion relationship (balance between tendency and dispersion).

Since the initial steepening is dominated by tendency and nonlinearity, the same evolution, at least during the first stages, should be observed also when the eigenvalue K_2, which determines the sign of Ω in (II,19), is negative. In the integration depicted in Figure (V,3) we changed the sign of K_2 ($K_2 = -.2$) leaving the other parameters unchanged.(1) The interesting point is that only one high amplitude pulse forms as the result of the initial steepening, despite the fact that the equilibrium solution is now a cnoidal wave [see section (II,b)] (to make sure that we are not in the parameter regime of a single soliton, we checked the sign of Ω using (II,19,a) and the phase speed measured from the experiment). Basically, almost all of the energy initially present "fills" only one pulse of the infinite wave, being consequently kept in that coherent shape by nonlinearity. Note that (at least) a second pulse of weaker amplitude is clearly recognizable at t = 9 and t = 12 days. The

---

(1)Strictly speaking, we should have defined a new zonal wind $\bar{u}$ such that K_2 is negative and compute again all the coefficients of appendix C. However, the other important coefficient in the dynamics of ϕ_2, δ_{222}, is not sensitive on the definition of the mean wind.

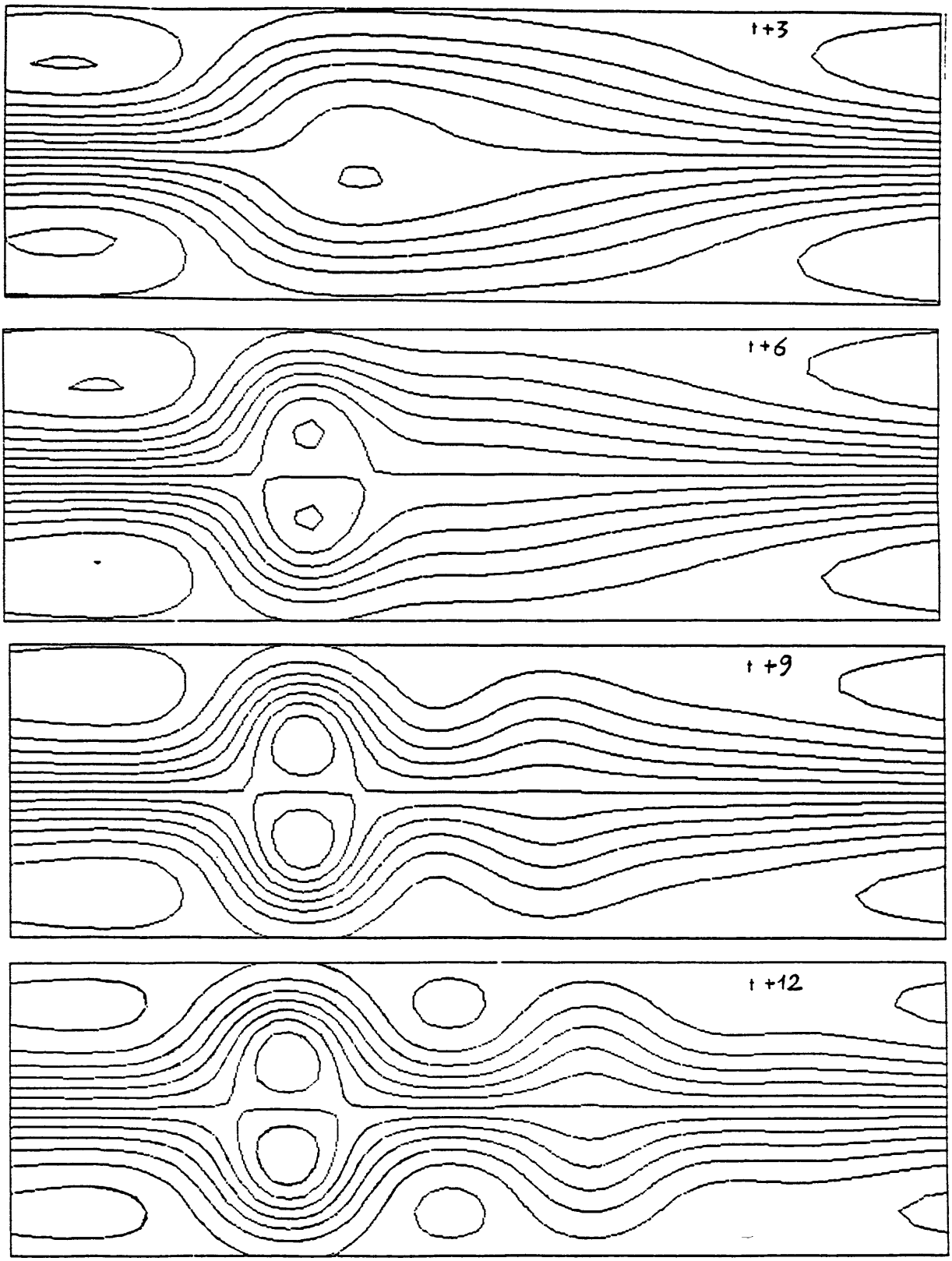

Fig. (V,3)

second pulse is not part of the same cnoidal wave as the primary pulse but it behaves independently, as can be seen from the fact that the primary pulse is slowly regressing while the second pulse is progressing. These partial realizations of a cnoidal wave behave like isolated solitons, since they survive after collisions.

From these considerations[1] the fact emerges that a necessary and sufficient condition for the coherent structure to form in our truncated model is the pre-existence of a (zonal) wavenumber one component of mode ϕ_2 having a large enough amplitude and meridionally confined by the turning points of the zonal wind. The question now is how energy can be injected into this component. At this stage we can only make some speculations.

So far we have considered a model with a flat bottom. After Charney and Eliassen (1949) no doubt was raised about the essential role played by topography in forcing the long wave components of the time-averaged northerm hemisphere circulation. Immediate evidence comes from inspection of the southern hemisphere: the minor interaction of the southern circumpolar vortex with topography results in enhanced symmetry.

One possibility is that the wavenumber one component grows via baroclinic conversion of zonal available potential energy to eddy energy. In the truncated model zonal wavenumber one is stable by ordinary baroclinic instability [see diagram (III,2)] so

---

[1]And from a long series of frustrating attempts to get the soliton in another way.

that conversion cannot occur spontaneously (in a continuous model this is not necessarily true). However, topography can "catalyze" baroclinic instability at long scales through the form-drag relationship (Charney-Straus, 1980). Moreover, an input of kinetic energy into long scales comes from direct topographic forcing, that is, conversion of zonal kinetic energy to eddy kinetic energy through the term $u\partial_x h$.

In order for these mechanisms to be relevant, the bidimensional Fourier decomposition of the northern hemisphere topography must have a strong wavenumber one component in the east-west as well as north-south direction. The geographical distribution land-ocean-land-ocean is asymmetric, since the Asian continent is larger than the American one. This gives rise to a wavenumber one component in the Fourier representation of the topography around a latitude circle. Furthermore, the largest Asian mountain chain, the Himalayas, is located to the south of the mid-latitude jet stream, so that its contribution to the meridional Fourier spectrum of the topography will have a strong wavenumber one component also in the north-south direction.

An important aspect of this interpretation is that the geographical position for the formation of the coherent structure can be fixed by the phase of the long wave which is forced by the topography.

The incorporation of topography into the present model will be the subject of future research.

Discussion and Conclusions

In this study we have proposed a nonlinear theory of atmospheric Rossby waves superimposed on westerly winds with meridional shear.

The underlying physical idea is that the self-interaction of the wave is responsible for the steepening that ultimately leads to a localized, coherent structure whose persistence is typically $\geq$ 10 days. We speculated that some cases of Atlantic blocking may be modeled by these structures.

We now explain, by using a very simple example, what we mean by "self-interaction." Let us suppose we construct a (very) low-order model of a barotropic atmosphere by truncating the Fourier representation of the streamfunction in terms of some complete, orthonormal basis $\{\phi_n\}$. Hence, we write:

$$\psi = \sum_{n=1}^{\infty} A_n(x,t)\phi_n(y) \approx A_1\phi_1$$

We then project the advection of relative vorticity upon ϕ_1:

$$J(\psi,\nabla^2\psi) \approx \langle J(A_1\phi_1, A_{1_{xx}}\phi_1 + A_1\phi_{1_{yy}}) \cdot \phi_1 \rangle \phi_1$$

where the brackets stand for the scalar product. By neglecting the boundary contributions of ϕ_1 we obtain, after some straightforward algebra, the self-interaction:

$$J(\psi,\nabla^2\psi) \approx (A_1{}^2)_x \langle \phi_{1_{yyy}} \phi_1{}^2 \rangle \phi_1$$

The scalar product at the right-hand side is basically the δ parameter that we have encountered over and over in this study. It can be noted that the self-interaction is identically zero when sine and cosine are taken as Fourier components. Also, only asymmetric (in y) waves can self-interact, since $\langle \phi_{1_{yyy}} \phi_1{}^2 \rangle$ vanishes for symmetric functions. Speaking in qualitative terms, we may say that the north-south mean shear modifies the meridional structure of the waves embedded in it (with respect to the ordinary sinusoidal function), so that the waves self-interact.

The point that deserves further discussion is the degree of applicability of the theory here proposed to the real atmosphere. We have seen in Chapter I that an isolated coherent structure exists only if the mean wind, upon which the structure is superimposed, satisfies certain constraints. In fact, (I,19) is an asymptotic solution of the governing equation if its y-z structure is a bound state of the Schrödinger equation (I,14) and if the associated eigenvalue is small and positive. While the positiveness of the eigenvalue is necessary to satisfy the upstream boundary condition (I,2,b), that is, the requirement of the solution being an isolated pulse, the smallness is required only because we assumed small nonlinearity and small dispersion. From the analysis of Chapter I we cannot say anything about the eigenvectors whose corresponding eigenvalues are $\geq O(1)$ and positive. In those cases the nonlinearity cannot be assumed small and the linear problem itself becomes

meaningless. We conclude that the requirement of small eigenvalue is only a sufficient condition.

In Chapter II we removed the constraint that the solution be isolated and we presented an approximation that also allows for large eigenvalues. The only hypothesis we made was that there exists a finite number of bound states of (I,14) and, in particular, that the y-z structure of the coherent solution (ϕ_2) be among them. However, we already pointed out that the normal modes associated with positive eigenvalues $\geq O(1)$ do not represent the meridional structure of any of the solutions of the potential vorticity equations. Again, K_2 small enough is a sufficient condition that tells us when the basis defined by the normal modes of (I,14) is the natural one upon which to project our coherent solution.

We have seen in Chapter V that wavenumber one component evolves into a single high amplitude pulse also if $K_2 < 0$, so that the requirement of positive eigenvalue can be abandoned in practice without losing physical realism. This assumes special importance because it renders the solutions of (II,19) applicable to blocking independently of the sign of the coefficients.(1)

In conclusion, we have found only sufficient conditions that tell us when the dynamics predicted by our model is going to be

---

(1)In fact, the sign of the parameter δ appearing in (II,19) is not cause of concern since, for an antisymmetric normal mode, it is always positive.

meaningful: for a given $\bar{u}(y,z)$ the recipe tells us that if there is a bound state of the linear problem (I,14) asymmetric in y, and if the corresponding eigenvalue is small enough, then the KdV dynamics here described should be observed.

It is interesting to determine the parameter range in which the above conditions are satisfied. Let us specify the north-south profile of a mid-latitude jet as in (I,8,b) [see also figure (I,1,a)] and let us fix its vertical profile as in Fig. (I,1,b). We still have the possibility of varying three parameters: the minimum wind speed U_0, the half-width of the jet y_0, and its maximum wind speed which enters the definition of β.

In diagram 2,a the eigenvalue K_2 as function of U_0 and y_0 is plotted for $\beta = 1/3$. In the region of the U_0-y_0 plane towards larger values of U_0 and y_0 the numerical algorithm described in section (I,c) failed to converge, meaning that ϕ_2 is not bounded for those parameter values. There are, however, plenty of possibilities for realistic values of the jet width. The behavior when the jet velocity decreases is interesting: Figure 2,b shows that when β increases (weaker jet) the allowed region of the parameter space shrinks. A weaker mid-latitude jet can be identified with a summer situation during which blocking is less frequently observed.

Although the parameter range, in which we know that a solution exists, looks realistic, it must be noted that the mean zonal wind may be barotropically unstable, since $\beta - \bar{u}_{yy}$ changes sign in the domain. This characteristic is necessary in order to achieve the meridional confinement of the waves.

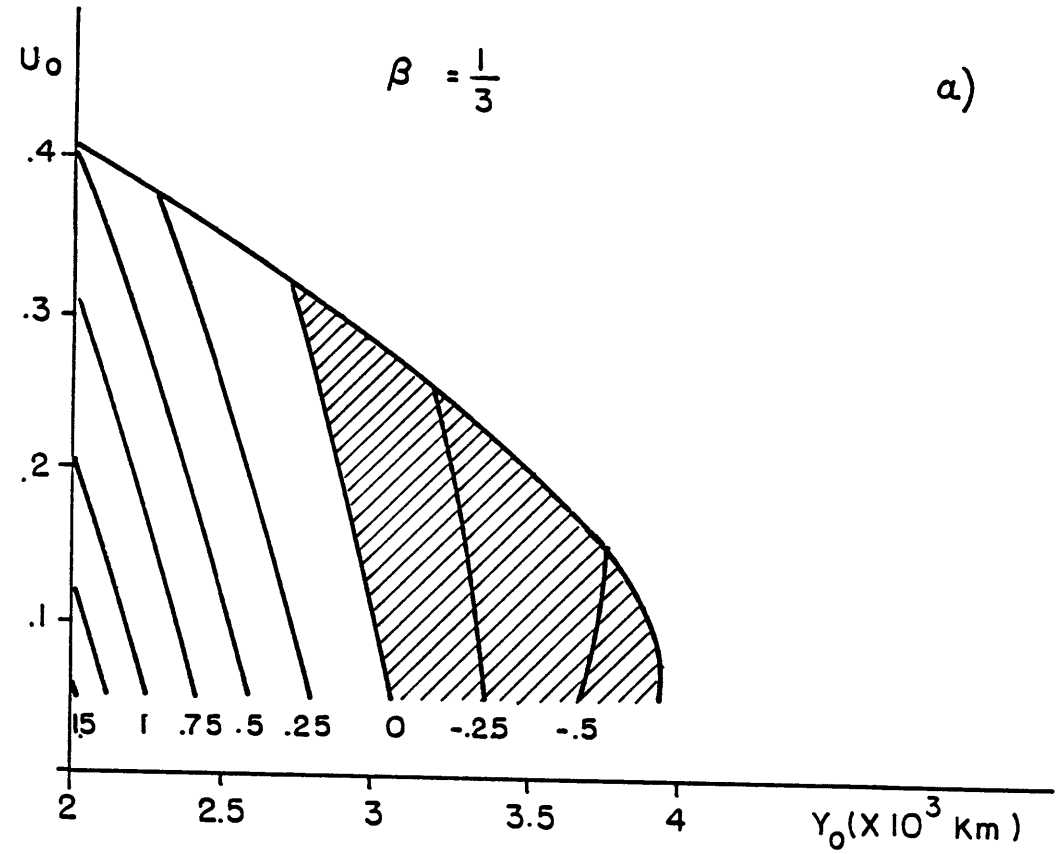
U_o
$\beta = \frac{1}{3}$
a)
.4
.3
.2
.1
1.5
1
.75
.5
.25
0
-.25
-.5
2
2.5
3
3.5
4
Y_o(X 10^3 Km)

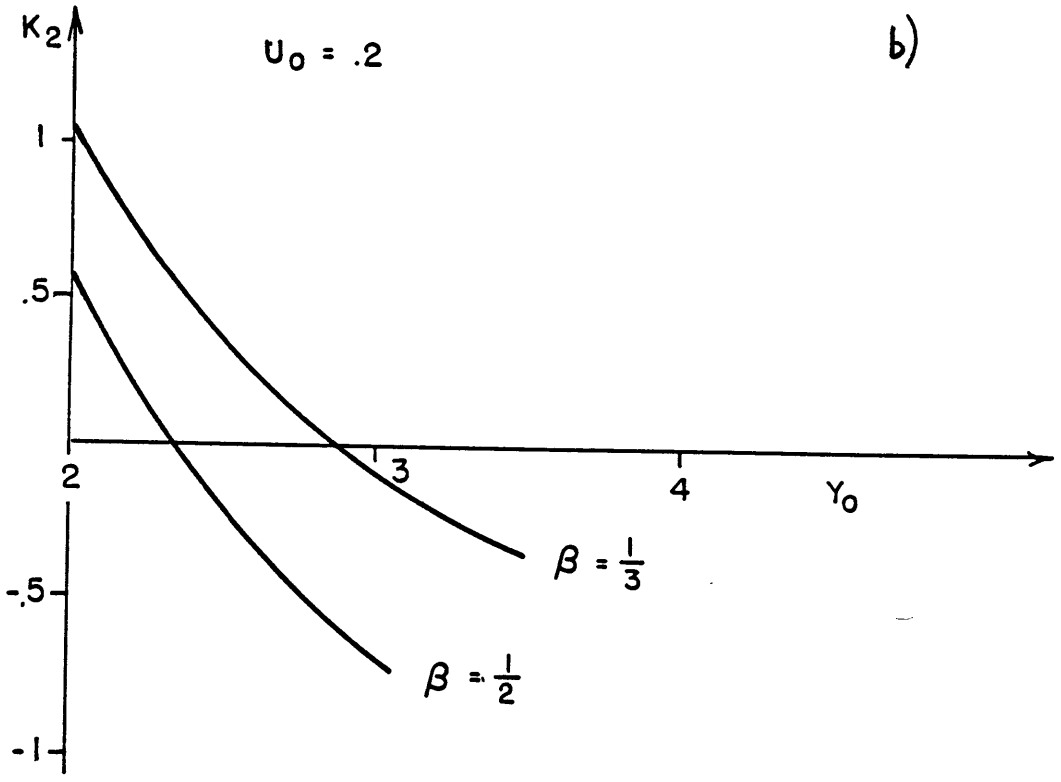
K_2
$U_o = .2$
b)
1
.5
-.5
-1
2
3
4
Y_o
$\beta = \frac{1}{3}$
$\beta = \frac{1}{2}$

Fig. 2

Is it reasonable to expect a barotropically unstable zonal wind to persist for a long enough time in the atmosphere? In the numerical experiments described in Chapter III we allowed for some readjustment of the zonal wind; however, the meridional resolution was too coarse to resolve such instability. The "fine structure" of the mean shear, which is responsible for the meridional confinement, was left untouched; hence, the experiments cannot provide the answer to the present question. According to the analysis of Chapter I, the mean shear must be computed in the region upstream from the block development. In the real atmosphere, such a region can be identified with the Atlantic storm track, which is dominated by baroclinic instability. One of the characteristics of the baroclinic instability of a jet is that the momentum flux, created by the growing perturbations, is upgradient of the mean momentum distribution (Stone, 1969; Simmons and Hoskins, 1980). Thus, westerly momentum is injected into the jet stream so that some degree of barotropic instability seems possible. However, we point out that in our model this problem has to do more with the mechanism of meridional confinement than with the effect of nonlinearity.

The other problem of the theory presented here is the severe truncation employed. Although it looks good for the stationary coherent structure, the neglected continuous part of the spectrum may be important especially during the transient that leads to the establishment of the block. Again, this question is basically related to the applicability of this theory to the real atmosphere. The spectral model described in Chapter II cannot be extended to the

continuum of the spectrum: these results should be verified by using a grid point model in which particular care is given to the resolution of the meridional profile of the mean shear. However, our feeling is that this problem is not a crucial one, since the same solution can also be obtained by solving the potential vorticity equation in the asymptotic limit of weak nonlinearity and weak dispersion.

In conclusion, we think that this theory removes the most fundamental objections (in particular structural instability and the modelling of the vertical structure) raised about the applicability of coherent structure models to the baroclinic atmosphere.

Appendix A

The lower boundary condition is $w = 0$ at $z = 0$. From the thermodynamic equation:

$$J(\psi,\psi_z) = 0 \qquad z = 0$$

it follows:

$$\psi_z = G(\psi)$$

Thus:

$$\bar{\psi}_z + \psi'_z = G(\bar{\psi}) + \frac{dG}{d\bar{\psi}}\psi' + \frac{1}{2}\frac{d^2G}{d\bar{\psi}^2}(\psi')^2$$

From the equality $\bar{\psi}_z = G(\bar{\psi})$ we get:

$$\frac{dG}{d\bar{\psi}} = \frac{\bar{u}_z}{\bar{u}} \qquad z = 0$$

$$\frac{d^2G}{d\bar{\psi}^2} = -\frac{1}{\bar{u}}\partial_y\left(\frac{1}{\bar{u}}\bar{u}_z\right) \qquad z = 0$$

With $\bar{u}$ given by (I,8,a), $d^nG/d\bar{\psi}^n = 0$ for $n > 1$. Performing the substitution $\psi' = \psi^* e^{z/2}$, the lower boundary condition becomes:

$$\psi^*_z = \left(\frac{\bar{u}_z(y,0)}{\bar{u}(y,0)} - \frac{1}{2}\right)\psi^* \quad \text{at} \quad z = 0$$

exactly.

Appendix B

a) Spectral decomposition of $\partial_y(\overline{\psi_x' q'})$

Using (II,4) and the definition of q' we get:

$$\partial_y(\overline{\psi_x' q'}) = \partial_y\Big[\overline{e^z A_{n_x}\phi_n(A_{m_{xx}}\phi_m + A_m\phi_{m_{yy}} + A_m\phi_{m_{zz}} - \frac{1}{4}A_m\phi_m)}\Big] =$$

$$= e^z\Big[\overline{A_{n_x}A_m}\partial_y(\frac{1}{4}\phi_n\phi_m) + \overline{A_{n_x}A_{m_{xx}}}\partial_y(\phi_n\phi_m) - \overline{A_{n_x}A_m}\,K_m\partial_y(\phi_n\phi_m)$$

$$+ \overline{A_{n_x}A_m}\,\partial_y(V\phi_n\phi_m)\Big]$$

where (II,2) has been used. The only term that survives after x-average is

$$- e^{z/2}\Big[\overline{A_{n_x}A_m}\,K_m\,e^{z/2}\partial_y(\phi_n\phi_m)\Big]$$

Projecting this term upon the i^{th} component of $\{\phi_n\}$ we get:

$$e^{z/2}\gamma_{inm}K_m\,\overline{A_{n_x}A_m}$$

where the tensor γ is defined as

$$\gamma_{inm} = \langle e^{z/2}\phi_i(\phi_n\phi_m)_y\rangle$$

b) Spectral decomposition of the nonlinear term $J(\psi',q')$

$$J(\psi',q') = e^{z}J(A_n\phi_n, A_{m_{xx}}\phi_m + A_m\phi_{m_{yy}} + A_m\phi_{m_{zz}} - \frac{1}{4}A_m\phi_m) =$$

$$= e^{z}\phi_{n_y}\phi_m(A_{m_x}A_{n_{xx}} - A_nA_{m_{xxx}}) + e^{z}A_{n_x}A_m[\phi_n(\phi_{m_{yyy}} + \phi_{m_{zzy}}) -$$

$$- \phi_{m_y}(\phi_{n_{yy}} + \phi_{n_{zz}})]$$

By using the definition of $\{\phi_n\}$, the last term at the r.h.s. of the previous relation becomes:

$$e^{z}A_{n_x}A_m[V_y\phi_n\phi_m + (K_n - K_m)\phi_{m_y}\phi_n]$$

The i^{th} component of the nonlinear term is

$$e^{z/2}[\gamma_{mni}(A_nA_{m_{xxx}} - A_{m_x}A_{n_{xx}}) + \gamma_{nmi}(K_m - K_n)A_{n_x}A_m + \delta_{inm}A_{n_x}A_m]$$

where

$$\delta_{inm} = \langle e^{z/2}V_y\phi_i\phi_n\phi_m\rangle$$

and where γ_{inm} is defined in a).

c) The spectral decomposition of $\partial_{yy}(\overline{\psi_x'q'})$ is similar to that of $\partial_y(\overline{\psi_x'q'})$ derived in a). The result is

$$e^{z/2}\varepsilon'_{inm}K_m\overline{A_{n_x}A_m}$$

where

$$\varepsilon'_{inm} = \langle e^{z/2}\phi_{i_{yy}}\phi_n\phi_m\rangle$$

d) It is easy to prove that i^{th} component of the tendency of the eddy potential vorticity is:

$$e^{z/2}[\dot{A}_{i_{xx}} + (\alpha_{in} - \zeta_{in})\dot{A}_n]$$

where

$$\zeta_{in} = \langle \phi_{i_y} \phi_{n_y} \rangle \ , \ \alpha_{in} = \langle \phi_i (\phi_{n_{zz}} - \frac{1}{4} \phi_n) \rangle$$

ζ_{ii} and α_{ii} play the role respectively of the square of the meridional and vertical wavenumber of ϕ_i.

Similarly, the i^{th} component of $\dot{u}_{yy} + \dot{u}_{zz} - \dot{u}_z$ is

$$e^{z/2}(\alpha_{in} - \zeta_{in})\dot{u}_n$$

as is clear from the definition of u in terms of the elements of the basis $\{\phi_n\}$.

Appendix C

$$\zeta_{ij} = \begin{bmatrix} .25 & 0 & -.02 \\ 0 & 1. & 0 \\ -.02 & 0 & .35 \end{bmatrix}$$

$$\alpha_{ij} = \begin{bmatrix} -.35 & 0 & -.45 \\ 0 & -.3 & 0 \\ -.45 & 0 & -3.5 \end{bmatrix}$$

$$K_i = [-.67,\ .23,\ 2.8]$$

$$\varepsilon_{ij1} = \begin{bmatrix} .6 & 0 & .1 \\ 0 & .48 & 0 \\ .1 & 0 & .45 \end{bmatrix} \qquad \delta_{ij1} = \begin{bmatrix} 0 & .09 & 0 \\ .09 & 0 & .04 \\ 0 & .04 & 0 \end{bmatrix}$$

$$\varepsilon_{ij2} = \begin{bmatrix} 0 & .48 & 0 \\ .48 & 0 & 0 \\ 0 & 0 & 0 \end{bmatrix} \qquad \delta_{ij2} = \begin{bmatrix} .09 & 0 & .04 \\ 0 & .34 & 0 \\ .04 & 0 & .08 \end{bmatrix}$$

$$\varepsilon_{ij3} = \begin{bmatrix} .1 & 0 & .45 \\ 0 & 0 & 0 \\ .45 & 0 & .2 \end{bmatrix} \qquad \delta_{ij3} = \begin{bmatrix} 0 & .04 & 0 \\ .04 & 0 & .08 \\ 0 & .08 & 0 \end{bmatrix}$$

$$\gamma_{ij1} = \begin{bmatrix} 0 & .2 & 0 \\ -.4 & 0 & 0 \\ 0 & 0 & 0 \end{bmatrix} \qquad \varepsilon'_{ij1} = \begin{bmatrix} .17 & 0 & .01 \\ 0 & .53 & 0 \\ 0 & 0 & .15 \end{bmatrix}$$

$$\gamma_{ij2} = \begin{bmatrix} .2 & 0 & 0 \\ 0 & 0 & 0 \\ 0 & 0 & .15 \end{bmatrix} \qquad \varepsilon'_{ij2} = \begin{bmatrix} 0 & .12 & 0 \\ .53 & 0 & 0 \\ 0 & 0 & 0 \end{bmatrix}$$

$$\gamma_{ij3} = \begin{bmatrix} 0 & 0 & 0 \\ 0 & 0 & -.3 \\ 0 & .15 & 0 \end{bmatrix} \qquad \varepsilon'_{ij3} = \begin{bmatrix} .01 & 0 & .15 \\ 0 & 0 & 0 \\ .15 & 0 & .06 \end{bmatrix}$$

Appendix D

We briefly describe the characteristics of the numerical model used in the experiments described in the text.

The model integrates forward in time the model equations (II,13) and (II,14) to which frictional terms have been added. We include both Newtonian cooling and linear drag. The linear drag ($\dot{u} + \ldots = -\nu u$, $\dot{v} + \ldots = -\nu v$), which gives a contribution to the vorticity equation equal to $-\nu\nabla^2\psi$, has, in our formulation, the same effect as Ekman pumping acting at the lower boundary.

In the equation governing the time evolution of the zonal wind $u(y,z,t)$ we allow for thermal forcing and momentum driving in the form:

$$(\zeta_{in} - \alpha_{in})\dot{u}_n + \varepsilon'_{inm}K_n\overline{A_{n_x}A_m} = -\nu\zeta_{in}(u_n - u_n^d) + \mu\alpha_{in}(u_n - u_n^h)$$

where u_n^d is the momentum driving and u_n^h the thermal forcing associated with different heating. No external forcing is considered in the eddy equation.

The variables $A_n(x,t)$ appearing in (II,13) and (II,14) are decomposed in Fourier components around the latitude circle:

$$A_n(x,t) = \sum_{j=1}^{JM}\left[a_{nj}(t)\ \sin\frac{2\pi jx}{L_x} + b_{nj}(t)\ \cos\frac{2\pi jx}{L_x}\right]$$

In all the numerical integrations performed we used $L_x = 30$ (30,000 km) and JM = 16.

As a time integration scheme we used a centered one (leapfrog) in which computational instability was eliminated by performing a three time step average every 20 time steps, reinitializing the integration with a forward time derivative.

Bibliography

Arnold, V. I., 1965. Condition for nonlinear stability of stationary plane curvilinear flows of an ideal fluid. Soviet Math. Dokl. 6, 773-777.

Blumen, W., 1968. On the stability of quasigeostrophic flow. J. Atmos. Sci. 25, 929-931.

Charney, J. G., and A. Eliassen, 1949. A numerical method for predicting the perturbations of the middle-latitude westerlies. Tellus, 1, 38-54.

Charney, J. G., 1971. Geostrophic turbulence. J. Atmos. Sci., 28, 1087-1095.

Charney, J. G., and D. Straus, 1980. Form drag instability, multiple equilibria and propagating planetary waves in baroclinic orographically forced, planetary wave systems. J. Atmos. Sci., 37, 1157-1176.

Charney, J. G., et al., 1981. Comparison of a barotropic blocking theory with observations. J. Atmos. Sci., 38, 762-769.

Courant-Friedrichs. Supersonic flow and shock waves. Pure and Applied Mathematics, Vol. I, 1948. Interscience Publishers, New York.

Dole, M. R., 1982. Persistent anomalies of the extra-tropical northern hemisphere wintertime circulation. Ph.D. Thesis, Dept. of Meteorology, Massachusetts Institute of Technology, Cambridge, Mass.

Flierl, G. R., 1978. Models of vertical structure and the calibration of two-layer models. Dyn. Atmos. Oceans, 2, 341-381.

Flierl, G. R., 1979. Baroclinic solitary waves with radial symmetry. Dyn. Atmos. Oceans, 3, 15-38.

Flierl, G. R., et al., 1983. The physical significance of modons: Laboratory experiments and general integral constraints. Dyn. Atmos. Oceans, 7, 233-266.

Gill, A. E., 1974. The stability of planetary waves on an infinite beta plane. Geophys. Fl. Dyn., 6, 29-47.

Green, J. S. A., 1976. The weather during July 1976: some dynamical considerations on the drought. Weather, 32, 120-128.

Hansen, A. R., and T. C. Chen, 1982. A spectral energetics analysis of atmospheric blocking. Mon. Wea. Rev., 110, 1146-1165.

Hansen, A. R., and A. Sutera, 1983. A comparison of the spectral energy and enstrophy budgets of blocking versus nonblocking periods. Tellus, 35 (August number).

Holton, J. R., 1972. An introduction to Dynamic Meteorology. Academic Press, pp. 394.

Hoskins, B. J., I. James and C. White, 1983. The shape propagation and mean-flow interaction of large-scale weather systems. J. Atmos. Sci., 40, 1595-1612.

Illari, L., 1982. Diagnostic study of a warm blocking anticyclone. Ph.D. Thesis, Atmospheric Physics group, Department of physics, Imperial College of Science and Technology, London.

Julian, R. P., et al., 1970. On the spectral distribution of large-scale atmospheric kinetic energy. J. Atmos. Sci., 27, 376-387.

Landau, L., and Lifchitz, 1969. Mecanique. Editions MIR, 120 pp.

Lindzen, R. S., 1971. Atmospheric tides. Mathematical problems in the geophysical sciences. Lectures in Applied Math., 14, Amer. Math. Soc., 293-310.

Long, R. R., 1964. Solitary waves in the westerlies. J. Atmos. Sci., 21, 197-200.

Lorenz, E. N., 1963. The mechanics of vacillation. J. Atmos. Sci., 20, 448-464.

Lorenz, E. N., 1971. Barotropic instability of Rossby wave motion. J. Atmos. Sci., 29, 258-264.

Malanotte-Rizzoli, P., 1980. Solitary Rossby waves over variable relief and their stability. Part II: numerical experiments. Dyn. Atmos. Oceans, 4, 261-294.

Malanotte-Rizzoli, P., 1982. Planetary waves in geophysical flows. Advances in Geophysics, 24, Academic Press, 147-224.

Malanotte-Rizzoli, P., 1984. Boundary forced nonlinear planetary radiation. J. Phys. Ocean., 14, 1032-1040.

McWilliams, J. C., 1980. An application of equivalent modons to atmospheric blocking. Dyn. Atmos. Oceans, 5, 43-66.

O'Conner, F., 1963. The weather and circulation of January 1963. Mon. Wea. Rev., 91, 209-218.

Patoine, A., and T. Warn, 1982. The interaction of long, quasi-stationary baroclinic waves with topography. J. Atmos. Sci., 39, 1018-1025.

Pierrehumbert, R. T., and P. Malguzzi, 1984. Forced coherent structures and local multiple equilibria in a barotropic atmosphere. J. Atmos. Sci., 41, 246-257.

Rex, D. D., 1950a. Blocking action in the middle troposphere and its effects on regional climate. I. An aerological study of blocking. Tellus, 2, 196-211.

Scott, A. C., et al., 1973. The soliton: a new concept in applied science. Proceedings of the IEEE, 61, 1443-1483.

Shutts, G. L., 1983. The propagation of eddies in diffluent jet streams: eddy vorticity forcing of "blocking" flow fields. Q. J. Roy. Met. Soc., 109.

Simmons, A. J., and B. J. Hoskins, 1980. Barotropic influences on the growth and decay of nonlinear baroclinic waves. J. Atmos. Sci., 1679-1684.

Stone, P. H., 1969. The meridional structure of baroclinic waves. J. Atmos. Sci., 376-389.

Sumner, E. J., 1954. A study of blocking in the Atlantic-European sector of the Northern Hemisphere. Q. J. Roy. Met. Soc., 80, 402-416.

Tung, K. K., and R. S. Lindzen, 1979b. A theory of stationary long waves. Part II. Resonant Rossby waves on the presence of realistic vertical shears. Mon. Wea. Rev., 107, 735-750.

Zabusky, N. J., and M. D. Kruskal, 1965. Interaction of "solitons" in a collisionless plasma and the recurrence of initial states. Physical Review Letters, 15, 6, 240-243.

Figure Captions

Fig. 1 Three cases of Atlantic blocking showing dipolar structure: a) after Sumner, 1954; b) after Hansen and Chen, 1982; c) after O'Conner, 1963.

Fig. (I,1) a) Meridional profile of the mean wind U(y). b) Vertical profile of the mean wind Z(z).

Fig. (I,2) "Potential" of the Schrödinger eq. (I,14) computed from the zonal wind shown in Fig. (I,1).

Fig. (I,3) y-z structure ($\phi_2 e^{z/2}$) associated with the coherent solution (I,19).

Fig. (I,4) Geopotential ψ' at 500 mb corresponding to (I,19). C.I.=.1 (40 m). The length of the zonal domain is 10,000 km.

Fig. (II,1) First three eigenfunctions ϕ_1, ϕ_2, and ϕ_3 (normalized) of the Schrödinger eq. (I,14).

Fig. (II,2) Eigenfunctions of (I,14) ordered by modal lines.

Fig. (II,3) a) Total streamfunction pattern at 500 mb given by (II,21). C.I. = .25 (100 m). The zonal and meridional dimensions of the domain are 30,000 km × 6,000 km. b) Anomaly pattern ψ' at 500 mb. C.I. = .25.

Fig. (II,4) Dispersion relation (phase speed versus amplitude) of the coherent solution (II,21) in a periodic domain of length $L_x = 30$ (30,000 km) and in an infinite domain.

Fig. (II,5) Example of cnoidal wave solution of equation (II,19) computed for $\Omega = -.2$, $\delta = .34$.

Fig. (III,1) Eigenmode ϕ_4 (normalized) of equation (I,19) having one horizontal and one vertical modal line. The corresponding eigenvalue is $K_4 = 3.8$.

Fig. (III,2) Imaginary part of the phase speed c of baroclinically unstable waves with antisymmetric meridional structures (ϕ_2 and ϕ_4) as function of the zonal wavenumber and of the mean wind vertical shear. The arrows on the x-axes indicate the position of zonal wavenumbers 5, 6, and 7.

Fig. (III,3) Same as Fig. (III,2) but for the real part of c.

Fig. (III,4) Same as Fig. (III,2) but for perturbations having symmetric meridional structure (ϕ_1 and ϕ_3).

Fig. (III,5) Same as Fig. (III,4) but for the real part of c.

Fig. (III,6) Time evolution of the 500 mb streamfunction field of the coherent structure (III,21) "perturbed" by the introduction of the fourth mode ϕ_4. The baroclinic component of the zonal wind is $u_3 = .1$, in the stable region of diagram (III,2). The pattern at t = 10 days, t = 20 days, and t = 30 days is reported. C.I. = .25.

Fig. (III,7) Same as Fig. (III,6) but with $u_3 = .2$.

Fig. (III,8) Vertical integral of area averaged kinetic energy. The solid line represents the mean spectrum for all blocking days during the 1978-1979 winter (after Hansen and Sutera, 1983). The thin line is the kinetic energy spectrum generated by a computer random number generator on which a K^{-3} law is imposed for $K \geq 6$. The total kinetic energy is normalized to one (1.35×10^6 J/m^2) and the total potential energy is .40 ($.54 \times 10^6$ J/m^2).

Fig. (III,9) ϕ_2-component of the streamfunction field at 500 mb, respectively at t = 5, 6, 7, and 8 days of the instability experiment with $E_0 = .5$, $u_3(0) = .2$. C.I. = .25.

Fig. (III,10) Same as Fig. (III,9) but for the total streamfunction pattern at 500 mb. C.I. = .25.

Fig. (III,11) Time evolution of the modulus of the Rossby wave $\phi_2 e^{z/2} \sin(2\pi 4x/L_x)$, respectively unperturbed (solid line), perturbed with an initial perturbation having $E_0 = .25$ (dotted line), $E_0 = .5$ (dashed line), and $E_0 = .75$ (thin line).

Fig. (III,12) Phase of the first three Fourier components of A_2 plotted versus time for the instability experiment $E_0 = .5$, $u_3(0) = .25$. The thin, sloping lines give the time evolution of the same components of a coherent structure with phase speed c = .1.

Fig. (III,13) Same as Fig. (III,12) but for the stability experiment with $E_0 = .75$, $u_3(0) = .25$.

Fig. (IV,1) Kinetic energy (dimensionless) of solution (II,21) versus time when dissipation is present. Curve I: Newtonian cooling with $\mu = (14 \text{ days})^{-1}$. Curve II: linear drag with $\nu = (14 \text{ days})^{-1}$.

Fig. (IV,2) Eddy forcing of potential vorticity due to monochromatic transient eddies with zonal wavenumbers $2\pi n/L_x$, n = 1, . . ., 5. The forcing is antisymmetric around x = 0. The units are arbitrary.

Fig. (IV,3) a) Same as Fig. (IV,2) but for short, transient eddies (n = 6, 8, 10, 12, 14, and 16). The dashed line is the sech^2 profile of the coherent structure. b) Eddy forcing due to short eddies superimposed to the coherent structure in the x-y plane.

Fig. (IV,4) "Modified flow" $\widehat{A_2^{(2)}}$ normalized to one. For reference, the profile of the zero-order solution is also reported.

Fig. (IV,5) Effect of eddy forcing on the coherent structure. a) 500 mb streamfunction pattern at t = 10 days. The initial condition was (II,21) plus a random perturbation with $E_0 = .75$. The dissipation parameters ar $\mu = \nu =$ $(14 \text{ days})^{-1}$. C.I. = .25. b) Same as a) but without initial perturbation.

Fig. (IV,6) a) Time-mean streamfunction pattern computed from t = 3 to t = 10 days for the experiment described in section (IV,e). C.I. = .25. b) After O'Conner, 1963.

Fig. (IV,7) a) Eddy forcing $\widehat{J(\psi'',q'')}$ superimposed on the mean potential vorticity at 250 mb. C.I. = $2\text{x}10^{-10}\text{sec}^{-2}$. The time-mean was computed from t = 3 to t = 10 days of the experiment described in (IV,e). b) Same as a) but for the July 1976 drought over the British Isles (after Illari, 1982). C.I. = $2\text{x}10^{-10}\text{sec}^{-2}$. The solid lines are the "trough" and "ridge" lines of the mean potential vorticity. The pattern is computed at 300 mb.

Fig. (V,1) 500 mb total streamfunction pattern at t = 0, 3, 6, 9, 12, and 15 days. The initial condition is given by equation (V,1). C.I. = .25.

Fig. (V,2) 500 mb total streamfunction pattern at t = 0, 3, 6, and 9 days. The initial condition is given by (V,1) plus a ϕ_1-type wave with zonal wavenumber 6. C.I. = .25.

Fig. (V,3) Same as (V,1) but with $K_2 = -.2$.

Fig. 2 a) Eigenvalue K_2 as function of U_0 and y_0 plotted for $\beta = 1/3$. b) K_2 versus y_0 for $U_0 = .2$ and $\beta = 1/3$, $1/2$, respectively.

Table Caption

Table (III,I). Persistence times (circled numbers). The row marked "E_0" contains the dimensionless kinetic energy of the initial perturbation. The row marked "TKE(0)" contains the dimensional kinetic energy of the initial perturbation plus coherent structure. The columns marked "$u_3(0)$" and "e.f.t." contain respectively the initial vertical shear component of the mean zonal wind and the corresponding e-folding time (in days) of the most unstable wavenumber (which is reported between parentheses) given by diagram (III,4). The time-mean kinetic energy computed during each experiment is written below the persistence time.